Combined inhibition of BET proteins and PI3Kα reallocates BRD4 to transcriptional regulatory elements of BH3-only proteins and triggers mitochondrial apoptosis

Dissertation

zur Erlangung des Doktorgrades

der Naturwissenschaften

vorgelegt beim Fachbereich

Biochemie, Chemie und Pharmazie

der Goethe-Universität

Frankfurt am Main

von

Cathinka Boedicker

aus Frankfurt

Frankfurt am Main, 2019

Vom Fachbereich Biochemie, Chemie und Pharmazie (FB14) der Goethe-Universität Frankfurt am Main als Dissertation angenommen.

Dekan: Prof. Dr. Clemens Glaubitz

1. Gutachter: Prof. Dr. Rolf Marschalek
2. Gutachter: Prof. Dr. Simone Fulda

Datum der Disputation: noch offen

Table of contents

List of abbreviations

AIF	Apoptosis inducing factor
AML	Acute myeloid leukemia
APS	Ammonium persulafte
ARMS	Alveolar rhabdomyosarcoma
ATCC	American Type Culture Collection
ATP	Adenosine triphosphate
BAD	BCL-2-Antagonist of Cell Death
BCL-2	B-cell lymphoma protein-2
BCL2-A1	BCL-2-related protein A1
BCL2L1	BCL-2-like protein 1
BCR	B cell receptor
BD	Bromodomain
BET	Bromodomain and extra-terminal
BH3	BCL-2 homology 3
BIM	BCL-2 Interacting Mediator Of Cell Death
BMF	Bcl2 Modifying Factor
BRCT	BRCA1 C-terminal
BRD4	Bromodomain containing protein 4
BSA	Bovine serum albumin
CDK9	Cyclin-dependent kinase 9
CHAPS	3-((3-cholamidopropyl) dimethylammonio)-1-propanesulfonate
CI	combination index
DISC	Death inducing signaling complex
DMEM	Dulbecco’s modified Eagle medium
DMSO	Dimethyl sulfoxide
DMT	histone demethylases
DNA	Deoxyribonucleic acid
DSIF	DRB sensitive inducible factor
DSMZ	Deutsche Sammlung von Mikroorganismen und Zellkulturen

DTT	Dithiothreitol
E	Enhancer
4EBP1	4E-binding protein 1
ECL	Enhanced chemiluminescence
e.g.	exempli gratia (latin) for example
EDTA	Ethylenediaminetetraacetate
EndoG	Endonuclease G
ERK	Extracellular Signal-regulated Kinase
ERMS	Embryonal rhabdomyosarcoma
FACS	Fluorescent activated cell sorter
FADD	Fas associated death domain protein
FasL	Fas ligand
FASR	FAS receptor
FCS	Fetal calf serum
FOXO3	Forkhead box protein O3
FOXO7	Forkhead box protein O7
GAPDH	glyceraldehyde-3-phosphate dehydrogenase
GPCR	G-protein coupled receptor
GSK3	Glycogen synthase kinase 3
H3Ser10ph	Phosphorylation of histone 3 serine 10
H4K16ac	Histone 4 lysine 16
HAT	Histone acetyltransferase
HDAC	Histone deacetylae
HEPES	Hydroxyethyl piperazinylethane sulfonic acid
Hh	Hedgehog
HMT	histone methyl transferase
HRP	Horseradish peroxidase
ICAD	Inhibitor of caspase-activated DNase
IRS1	Insulin receptor 1
KAc	Acetylated lysine
kDa	kiloDalton

LOMMP	loss of mitochondrial membrane potential
MAPK	Mitogen-activated protein kinase
MCL-1	Induced myeloid leukemia cell differentiation protein
MED1	Mediator of RNA POL II transcription subunit 1
MMP	Mitochondrial membrane permeabilization
mRNA	Messenger ribonucleic acid
mTOR	Mammalian target of rapamycin
NaCl	Natriumchloride
NADH	
NADPH	Nicotinamide adenine dinucleotide phosphate
NELF	Negative elongation factor
NFκB	Nuclear factor kappa-light-chain-enhancer of activated B-cells
NMC	NUT midline carcinoma
NPS	N-terminal cluster of phosphorylation
NUT	Nuclear protein in testis
PARP	poly(ADP-ribose)-polymerase
PAX3	Paired box 3
PBS	Phosphate buffered saline
PDK1	Pleckstrin homology (PH) domains of the serine/threonine kinases Akt and 3-phosphoinositide-dependent kinase 1
pH	Potential hydrogen
PH	Pleckstrin homology
PHD	Plant-homeodomain
PI	Propidium iodide
PI3K	Phosphatidylinositol-4,5-bisphosphate 3-kinase
PIC	Protease inhibitor cocktail

PIP3	Phosphatidylinositol-3,4,5-triphosphate
POL A	Arrested RNA POL II
POL E	Elongating RNA POL II
PRAS40	Proline-rich AKT substrate 40 kDa
PTEFB	Positive transcription elongation factor B
PWWP	Pro-Trp-Trp-Pro
qRT-PCR	Quantitative real-time polymerase chain reaction
Raptor	Regulatory associated protein of mTOR
RING	Really-interesting-new-gene
RMS	Rhabdomyosarcoma
RNA	Ribonucleic acid
ROCK I	Rho effector protein I
rpm	Rounds per minute
RPMI medium	Roswell Park Memorial Institute medium
RTK	Receptor tyrosone kinase
S6K1/2	Ribosomal protein S6 kinase 1/2
SD	Standard deviation
SDS	Sodium dodecyl sulfate
SE	Super-enhancer
SEM	Standard error of mean
SH2	Src homology 2
tBID	Truncated BID
TEMED	Tetramethylehylenediamine
TF	Transcription factor
TM	Transmembrane
TNFR	Tumor Necrosis Factor receptor
TNF-α	Tumor necrosis factor α
TRADD	TNFR associated death domain protein
WB	Western Blot

List of figures

List of tables

1 Abstract

Rhabdomyosarcoma (RMS) is the most frequent pediatric soft-tissue sarcoma comprising two major subtypes – the alveolar and the embryonal rhabdomyosarcoma. The current therapeutic regime is multimodal including surgery, radiation and chemotherapy with cytostatic drugs. Although the prognosis for RMS patients has steadily improved to a 5-year overall survival rate of 70% for ERMS and 50% for ARMS, prognosis for subgroups with primary metastases or relapsed patients is still less than 25%, highlighting the need for development of new therapies for these subgroups. Since cancer cells are addicted to their cancer promoting transcriptional program, remodeling transcription by targeting bromodomain and extraterminal (BET) proteins has emerged as compelling anticancer strategy. However, in many cancer types BET inhibition was proved cytostatic but not cytotoxic emphasizing the need for combination protocols.

In this study we identify a novel synergistic interaction of the BET inhibitor JQ1 with p110α-isoform-specific Phosphoinositid-3-Kinase (PI3K) inhibitor BYL719 (Alpelisib) to induce mitochondrial apoptosis and global reallocation of BRD4 to chromatin. At first, we showed that JQ1 single treatment had cytostatic effects at nanomolar concentrations and inhibited MYC and Hedgehog (Hh) signaling in RMS known to promote proliferation of RMS. However, JQ1 single treatment barely induced cell death in RMS cells even at concentrations of up to 20 µM (< 20% cell death). Thus, we next tested combination approaches to elicit cell death. Since we previously identified synergistic cell death induction of Hh inhibition and PI3K inhibition in RMS cells we tested JQ1 in combination with the pan-PI3K/mTOR inhibitor PI-103 and the p110α-isoform-specific PI3K inhibitor BYL719. In addition, we tested JQ1 in combination with distinct HDAC inhibitors namely JNJ-26481585, SAHA (Vorinostat), MS-275 (Entinostat) and LBH-589 (Panobinostat) since the synergistic interaction of BET and HDAC inhibition has previously been described for other tumor entities.

Interestingly the synergism of cell death induction of JQ1/BYL719 co-treatment is superior to the synergism of JQ1 with pan-PI3K/mTOR inhibitor PI-103 or the tested HDAC inhibitors as confirmed by calculation of combination index. To investigate the molecular mechanisms underlying the synergy of JQ1/BYL719 co-treatment, we performed RNA-Seq and BRD4 ChIP-Seq experiments. RNA-Seq exhibited, that JQ1/BYL719 co-treatment shifted the overall balance of BCL-2 family gene expression towards apoptosis and increased gene expression of proapoptotic *BMF*, *BCL2L11* (BIM) and *PMAIP1* (NOXA) while decreasing gene expression of antiapoptotic *BCL2L1*

(BCL-x_L). These changes were verified by qRT-PCR and Western blot. Notably, BRD4 is phosphorylated upon JQ1/BYL719 co-treatment and globally reallocates BRD4 to chromatin. This BRD4 reallocation includes enrichment of BRD4 at the super-enhancer site of *BMF*, at the super-enhancer, typical enhancer and promoter regions of *BCL2L11* (BIM) and at the *PMAIP1* (NOXA) promoter, while JQ1 alone, as expected, reduces global chromatin binding of BRD4. Integration of RNA-Seq and BRD4 ChIP-Seq data underlines the transcriptional relevance of reallocated BRD4 upon JQ1/BYL719 co-treatment. Immunopreciptation studies showed, that RMS cells are initially primed to undergo mitochondrial apoptosis since BIM is constitutively bound to antiapoptotic BCL-2, BCL-x_L and MCL-1. JQ1/BYL719 co-treatment increased BIM expression and its neutralization of antiapoptotic BCL-2, BCL-x_L and MCL-1 thereby rebalancing the ratio of pro- and antiapoptotic BCL-2 proteins in favor of apoptosis. This promotes activation of BAK and BAX resulting in caspase-dependent apoptosis. The functional relevance of proapoptotic re-balancing for the execution of JQ1/BYL719-mediated apoptosis was confirmed by individual silencing of BMF, BIM, NOXA or overexpression of BCL-2 or MCL-1, which all significantly rescued JQ1/BYL719-induced cell death. Execution of cell death by mitochondrial caspase-dependent apoptosis was veryfied by individual knockdown of BAK and BAX or caspase inhibitor *N*-Benzyloxycarbonyl-Val-Ala-Asp(O-Me) fluoromethylketone (zVAD.fmk), which all significantly rescued JQ1/BYL719-induced cell death.

In summary, combined BET and PI3Kα inhibition cooperatively induces mitochondrial apoptosis by proapoptotic re-balancing of BCL-2 family proteins accompanied by reallocation of BRD4 to transcriptional regulatory elements of BH3-only proteins.

2 Introduction

2.1 Rhabdomyosarcoma (RMS)

Rhabdomyosarcoma (RMS) belongs to the group of soft tissue sarcomas and arises from skeletal muscle precursor cells failing to differentiate into skeletal muscle cells [1], but a non-myogenic origin is discussed as well [2, 3]. It is the most frequent soft tissue sarcoma in children and adolescents less than 20 years old accounting 4-8% of all childhood malignancies and an incidence of 4.5 per one million children per year [4, 5]. Rhabdomyosarcoma is classified into two major histological subtypes, the embryonal subtype (ERMS) and the alveolar subtype (ARMS) as well as a minor pleomorphic or undifferentiated phenotype [6-8]. ERMS accounts for approximately 60 to 70% of all RMS cases and occurs more frequent in younger children mostly localized in the head and neck region or in the urogenital system while ARMS accounts approximately 20% of diagnosed RMS cases and is more frequently found in the extremities [5]. Besides the histological phenotype, ERMS and ARMS are characterized by genetic alterations [6]. Nearly two third of ERMS patients share loss of heterozygosity (LOH) at chromosome 11p15.5 leading to increased levels of insulin-like growth factor type II (IGF-II) [4, 9]. Increased IGF-II levels have been described to promote proliferation and impair differentiation of RMS cells into myoblasts thus contributing pathogenesis of ERMS [10]. Furthermore ERMS patients frequently show alterations in *NRAS*, *KRAS*, *TP53*, *NF1*, *RARA*, *CTNNB2*, *CARD11* and *PIK3CA* [11]. ARMS is genetically characterized by translocation within chromosome 2 and 13 (t(2;13)(q35;q14)) or t(1;13)(p36;q14) resulting in the chimeric fusion of *Paired Box 3 (PAX3)* or *Paired Box7 (PAX7)* and the *'forkhead' box* (*FOXO*) transcription factor *FKHR [5]. PAX3/7-FOXO* fusion proteins remodels the epigenetic landscape resulting in Bromodomain-containing protein 4 (BRD4)-dependent alteration of gene expression thereby promoting oncogenic potential of ARMS [12]. ARMS as well as ERMS frequently show insulin receptor substrate-1 (IRS1) or receptor tyrosine kinases (RTKs) activation known to stimulate PI3K signaling, thereby promoting cell growth and impairing anticancer activity of chemotherapeutics [10, 13]. Both RMS subtypes frequently show activation of hedgehog (Hh) signaling known to modulate responses to chemotherapeutics, differentiation status and motility of RMS cells [14].

ERMS patients generally have a favorable prognosis compared to ARMS patients, since ARMS patients frequently present metastasis at the time of diagnosis and suffer more often from relapses [15, 16]. Current therapeutic regime is multimodal and includes surgery, chemotherapy and radiation therapy [16]. Chemotherapy of RMS patients currently includes several combinations of chemotherapeutics including vincristine,

dactinomycin, and cyclophosphamide (VAC) or vincristine, melphalan (VM), ifosfamide and etoposide (IE) or vincristine, ifosfamide, and etoposide (VIE) [15, 16]. While combined irradiation and standard chemotherapy with VAC have improved the 5-year survival of non-metastatic ERMS patients to more than 70%, the 5-year survival of patients with metastatic ERMS accounts 65% and for ARMS only 50% [8, 16, 17]. In addition, almost 30% of RMS cases experience relapse, that result in 50-95% in progressive disease or death [8, 15, 18]. In summary, long term survival of children with metastatic ERMS or ARMS is about 25% [18]. In recent decades, the prognosis of RMS patients has rarely improved, highlighting the need for new therapies [19].

2.2 Apoptosis

Cell death can be distinguished into programmed cell death mechanisms e.g. apoptosis, necroptosis, ferroptosis, autophagy or of uncontrolled cell death, namely necrosis [20-22]. Most current therapeutic strategies aim to induce apoptosis in cancer cells [23]. Apoptosis is a tightly controlled and evolutionary conserved process of programmed cell death to eliminate single cells in multicellular organisms [24, 25]. Despite the elimination of damaged cells, apoptosis plays an important role in tissue repair, tissue formation and homeostasis as well as in immune response and during development [25]. One of most prominent examples for the relevance of apoptosis during development is the separation of fingers due to apoptosis of the cells between the digits during embryogenesis [25]. In result of the various functions of apoptosis in multicellular organisms, impaired apoptosis plays a critical role in the development of cancer and has been associated with uncontrolled proliferation, evasion and poor responses to chemotherapy [26-28]. To this end, induction of apoptosis is a compelling strategy to treat cancer [27]. Typical morphological hallmarks of apoptotic cells are membrane blebbing, cell shrinkage, chromatin condensation, nuclear and chromosomal fragmentation as well as formation of membrane-enclosed apoptotic bodies [20]. Classical apoptosis comprises two pathways – the extrinsic (death receptor) and the intrinsic (mitochondrial) pathway [23].

2.2.1 Extrinsic (death receptor) pathway

The extrinsic (death receptor) pathway is activated by binding of extracellular death ligands e.g. the CD95 ligand (FAS), TNF-related apoptosis inducing ligand (TRAIL) or tumor necrosis factor α (TNFα) to their corresponding receptors CD95 (APO1, FAS receptor), TRAIL receptor 1 and 2 or TNF receptor 1 and 2 [29-32]. All receptors contain a death domain (DD) which is required for transmitting the death signal from the surface into the cell [23, 32]. Association of the ligand to the receptor results in oligomerisation

and clustering of the receptor into the death-inducing signaling complex 1 (DISC). The DISC contains the Fas-associated death domain (FADD), which mediates interaction of the FAS receptor and caspase-8 (or -10), resulting autoproteolytic cleavage and thereby activation of caspase-8 [31, 33]. Activated caspase-8 (or -10) in turn activates downstream effector caspases, caspase-3 and -7 [29, 31, 34, 35]. Similar, stimuli of TNF ligand is transduced, despite the fact that the additional TNF-receptor associated death domain (TRADD) is required for recruitment of FADD [30].

Furthermore, caspase-8 can result in cleavage of BH3 interacting-domain death agonist (BID) into truncated BID (tBID) [35, 36]. While some cells exclusively undergo extrinsic apoptosis ("type I cells"), in "type II cells" extrinsic and intrinsic apoptosis are linked via tBID which translocates to mitochondrial membranes and induces permeabilisation of mitochondrial membranes thereby activating intrinsic (mitochondrial) apoptosis and amplifying the apoptotic signal [23, 35] (Figure 1).

2.2.2 Intrinsic (mitochondrial) pathway

The intrinsic or mitochondrial pathway is initiated upon various intracellular stress signals, including DNA damage, oxidative stress or calcium overload [37]. These cytotoxic stimuli rebalance the ratio between pro- and antiapoptotic BCL-2 proteins, which control mitochondrial outer membrane permeabilisation (MOMP). Usually MOMP is mediated by the activation of the effector BCL-2 proteins BAK and BAX, which oligomerize upon activation and form pore complexes in the outer mitochondrial membrane [38, 39]. Upon MOMP apoptotic effector molecules including cytochrome c, second mitochondria-derived activator of caspases (SMAC/DIABOLO), apoptosis inducing factor (AIF) or endonuclease G (ENDOG) are released from the mitochondrial intermembrane space into the cytosol [23, 37]. Released cytochrome c binds to the apoptotic activating factor (Apaf-1) containing the caspase-recruitment domain (CARD domain) and a ATP-mediated conformational change results in binding of caspase-9. The formed complex named "apoptosome" catalyzes self-cleavage of initiator caspase-9 into active caspase-9 fragments, which in turn activates downstream caspase-3 and -7 [23, 40]. The other effector molecules further amplify the apoptotic signal: SMAC/DIABOLO binds to inhibitor of apoptosis proteins (IAPs), that inhibit the enzymatic activity of initiator caspases [41], AIF induces nuclear condensation and fragmentation as well as further mitochondrial permeabilization and exhibits an NADH oxidase activity [42], ENDOG is another apoptotic DNase mediating nuclear condensation and fragmentation [43] (see Figure 1).

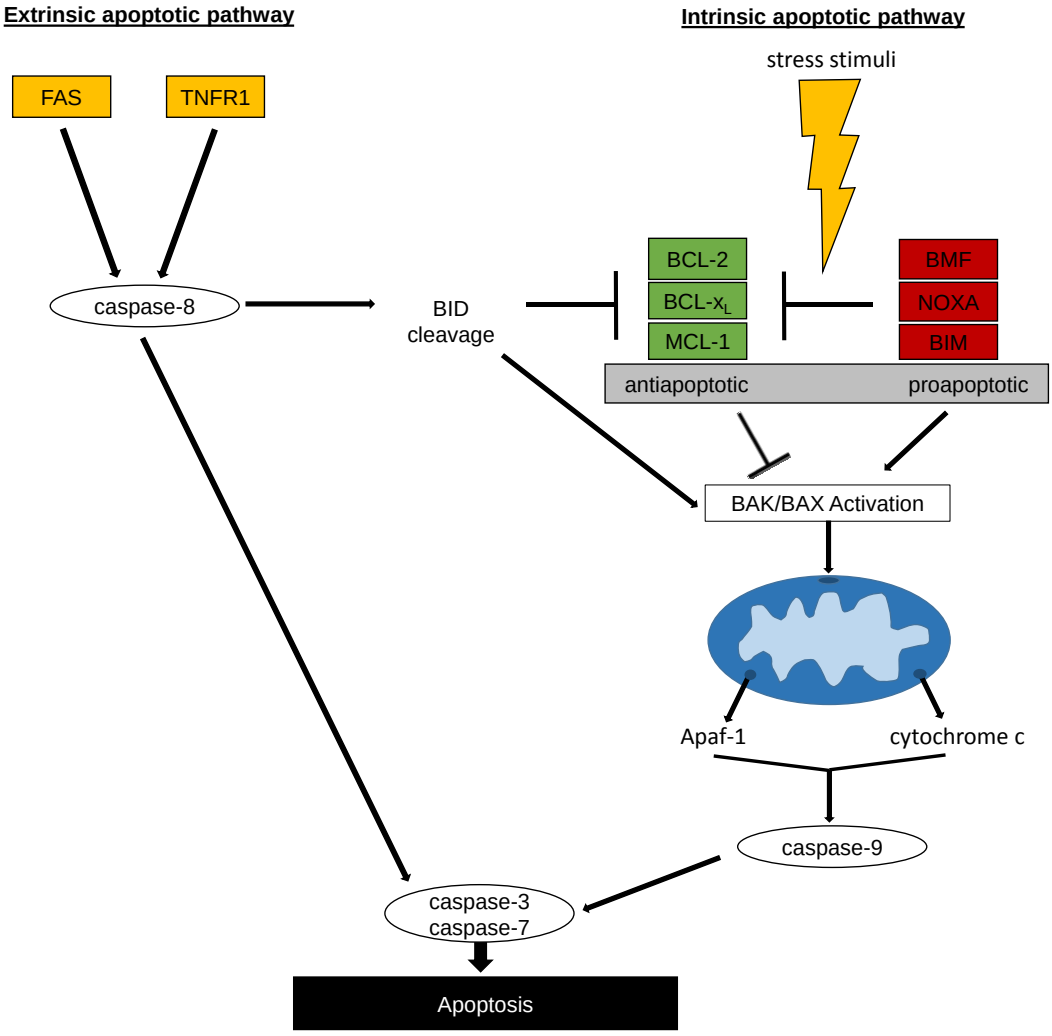

Figure 1: Apoptosis signaling pathways.
Apoptosis can be induced via two different pathways – the extrinsic (receptor) pathway and the intrinsic (mitochondrial) pathway. The extrinsic apoptotic pathway is activated upon binding of death ligands e.g. FAS ligand (FASL) to the FAS receptor (FASR), FASR trimerisation and formation of the death-inducing signal complex (DISC) which contains the FAS-associated death domain (FADD domain), that that mediates interaction and activation of caspase-8 (or -10) which in turn activates effector caspase-3 and -7. Activated caspase-8 is able to cleave BH3 interacting-domain death agonist (BID) into truncated BID (tBID), which translocates to mitochondrial membranes and induces permeabilisation of mitochondrial membranes thereby linking extrinsic (receptor) pathway to intrinsic (mitochondrial) pathway. The intrinsic apoptotic pathway is activated upon various stress stimuli reblalacing pro- and antiapoptotic proteins. This results in activation of the proapoptotic effector proteins BAK and BAX forming pores in the outer mitochondrial membrane and loss of mitochondrial membrane potential (LOMMP) as well as release of effector molecules e.g. cytochrome c and Apaf-1, which in turn activate caspase-9. Caspase-9 activates caspase-3 and -7 resulting in execution of apoptosis. See text for more details.

2.2.3 Role of BCL-2 proteins in intrinsic apoptosis

BCL-2, named according to *B-cell lymphoma-2*, was the first discovered BCL-2 protein member [44]. In B-cell lymphoma-2, translocation of *BCL-2* (t(14;18)) results increased expression of BCL-2, since BCL-2 expression is then controlled by the promoter and enhancer of immunoglobulin heavy chain on chromosome 14 [44, 45]. As overexpression of BCL-2 was shown to rescue in B-cell lymphoma from cell death, BCL-2 was identified as proto-oncogene for the first time [44]. Nowadays the BCL-2 protein family is defined as group of proteins with an evolutionary conserved sequence and structure of BCL-2 homology (BH) domains [45]. BCL-2 proteins can be divided into three distinct groups: the antiapoptotic multi-domain proteins including BCL-2, BCL-x_L, MCL-1, BCL-ω, BCL2-A1, the proapoptotic apoptosis-initiating BCL-2 homology 3 (BH3)-only proteins, including BIM, NOXA, BMF, PUMA, HRK, BIK, BAD and BID, as well as the multi-domain proapoptotic effector proteins namely BAX and BAK [46]. Antiapoptotic multi-domain BCL-2 proteins share four BH domains (BH1-4) as well as a hydrophobic transmembrane (TM) domain, facilitating insertion at the mitochondrial membrane [47]. Proapoptotic effector proteins comprise three BH3-only domains as well as the TM domain [47, 48]. The BH3-only proteins have a more diverse structure and share only homology in one BH3 motif called minimal death domain, which is necessary for binding to other BCL-2 proteins (see Figure 2) [49, 50].

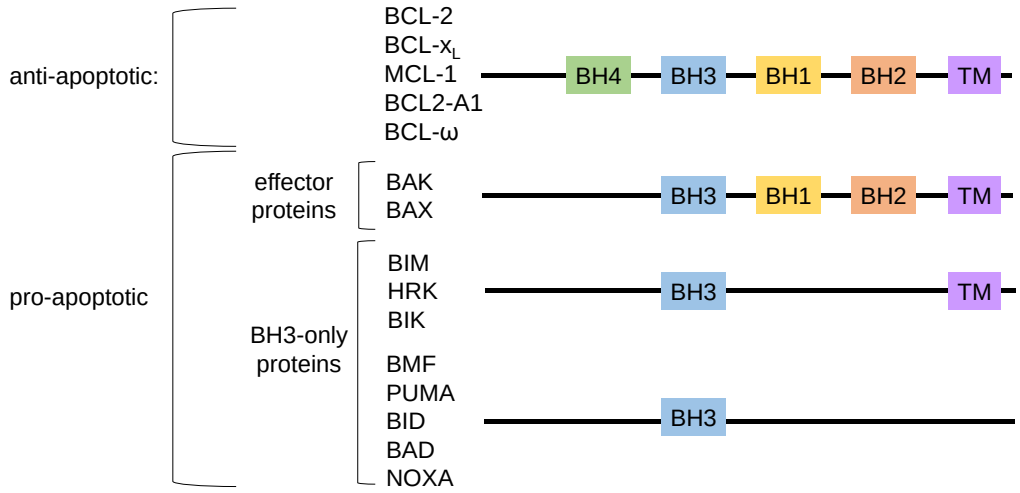

Figure 2: Prominent members of the BCL-2 family.
BCL-2 proteins can be divided into pro- and antiapoptotic BCL-2 proteins. Anti-apoptotic BCL-2 proteins e.g. BCL-2, BCL-x_L, MCL-1, BCL2-A1 and BCL-ω consist of four BCL-2 homology (BH) domains and a transmembrane domain (TM), while proapoptotic effector proteins (BAK, BAX, BOK) comprise three BH domains and a TM domain. Pro-apoptotic BH3-only proteins BIM, HRK and BIK contain only BH3 domain and a TM domain, while BMF, PUMA, BID, BAD contain only BH3 domain facilitating interaction with other BCL-2 proteins members. See text for more details. Figure is adopted from [51].

For BCL-2 proteins the ability to interact with each other is functionally important to control MOMP [50]. The proapoptotic effector proteins BAK and BAX are crucial for loss of mitochondrial membrane potential (LOMMP) since they oligomerize with each other or themselves upon activation forming pores in the outer mitochondrial membrane [38]. The antiapoptotic multi-domain proteins e.g. BCL-2, BCL-x_L and MCL-1 can prevent BAK and BAX activation by binding BAK and BAX, keeping them in an inactivated state [52-54]. BH3-only proteins including BIM, NOXA, BMF, PUMA and tBID can displace BAK and BAX from anti-apoptotic multidomain proteins thereby facilitating their activation [48, 54, 55]. BH3-only proteins show different binding affinities to antiapoptotic BCL-2 proteins [56, 57]. BIM, PUMA and tBID are able to bind to all antiapoptotic proteins whereas BIK and HRK preferably bind to BCL-x_L, BCL-ω, BCL2-A1 [58]. BAD and BMF preferably bind BCL-x_L and BCL-ω while NOXA is only bound to MCL-1 and BCL2A1 [54, 57, 59, 60]. While some BH3-only proteins function only by occupying antiapoptotic BCL-2 proteins e.g. BMF, NOXA, PUMA (sensitizers), it is suggested that other BH3-only proteins including BIM and tBID can directly activate BAK and BAX (activators) [61, 62]. In addition, abilities of BCL-2 proteins can be modulated by various stimuli in different manners: despite transcriptional regulation, BCL-2 proteins can be modulated by posttranslational modifications including phosphorylation and proteolytic activation. Phosphorylation of BCL-2 has been shown to modulate it's cytoprotective effect [63], while BAD is inactivated and degraded upon phosphorylation [64], and BIM is either promoted to bind to antiapoptotic proteins or degraded in dependence of the phosphorylation site [65]. Proteolytic cleavage and activation of BID into tBID links extrinsic and intrinsic apoptosis by binding and thereby neutralizing antiapoptotic BCL-2 proteins [23, 35]. In summary, activation of BAK and BAX is tightly controlled by the interaction of BCL-2 proteins, thereby regulating LOMMP and intrinsic (mitochondrial) apoptosis.

2.2.4 Execution of apoptosis

Extrinsic as well as intrinsic apoptosis is executed by effector caspase-3 and -7 [40, 66]. Both proteases cleave various vital proteins containing a caspase cleavage site including cell adhesion or cytoskeletal molecules, signal transducers, transcription factors, regulators of cell cycle or scaffold proteins as well as proteins involved in DNA synthesis and repair [67]. In result, proteolytic caspase cleavage either activates or inactivates substrates in favor of apoptosis. Typical morphological results of apoptosis result of proteolytic caspase activity: caspase-3 activates caspase-activated DNase (CAD) by degradation of inhibitor of caspase-activated DNase (ICAD) thereby causing DNA

fragmentation in the nucleus [68]. Simultaneously caspase-3 impairs DNA repair machinery as indicated by cleavage and inactivation of poly(ADP-ribose)-polymerase (PARP). Cleavage of nuclear lamins leads to nuclear shrinkage, which is another hallmark of apoptosis [67]. Caspase-7 in turn has been shown to be responsible for apoptotic detachment of cells [40]. Furthermore effector caspases activate Rho effector protein I (ROCK I) promoting actin–myosin contractility and thereby mediating apoptotic membrane blebbing and formation of apoptotic bodies [69]. Together caspase-3 and-7 lead to controlled decomposition of the cell into fragments enclosed into vesicles, that are removed by phagozytosis of neighboring cells [70].

2.3 Epigenetic modifications confer to transcriptional plasticity

Epigenetic modifications result in heritable changes of a phenotype without alteration in the DNA sequence [71]. Beside DNA methylation, post-translational histone modifications play a key role in transcriptional control [72-74]. Histone modifications include histone acetylation, methylation and phosphorylation. These modifications are tightly regulated by “writers” marking histones and other proteins with modifications and “erasers” removing these marks. So called “readers” recognize these modifications and translate them into a transcriptional signal [75]. “Writer” enzymes are histone acetyltransferases (HATs), histone methyl transferases (HMTs) and kinases. Histone deacetylaes (HDACs), histone demethylases (DMTs) and phosphatases remove the epigenetic marks and function as “erasers”. “Readers” of histone acetylation contain bromodomains and chromodomains, while “readers” of methylation marks comprise distinct domains including plant homeodomains (PHDs), tudor domains, PWWP (Pro-Trp-Trp-Pro) domains and malignant brain tumor domains (MBTs). Phosphorylation sites are recognized by proteins harboring 14-3-3 proteins and BRCA1 C-terminal (BRCT) domains [75]. One prominent epigenetic modification is the acetylatation of lysines of histone [76]. Histone acetylation opens the chromatin thereby facilitating access for DNA and RNA polymerases and thus promoting DNA replication and transcription [77, 78]. In cancer HDACs are frequently deregulated thereby leading to transcriptional downregulation of tumor suppressor genes or activation of oncogenes [79, 80]. Therefore, HDACs have become a prominent target in cancer therapy [81, 82]. Another approach is targeting of bromodomains, that “read” the acetylation code by binding to ε-*N*-acetylation of lysines including N-terminal histone tails [83]. By recognizing acetylation of the amino-residues of histones, BET proteins take part in transcriptional control [84, 85] promoting cellular growth, metabolism and survival [86-89].

2.4 Bromodomain and extra-terminal (BET) proteins modulate transcription

The human proteome includes 61 bromodomains present in 46 diverse nuclear and proteins [90]. Bromodomains contain four conserved left-handed α-helices (αZ, αA, αB, αC) and several loops that vary in size, surrounding a hydrophobic pocket with a conserved asparagine residue, that recognizes acetylated lysine (KAc) [91]. Structure-based alignment clustered bromodomains into eight families [92]. The Bromodomain and extra-terminal (BET) subclass II of bromodomains includes BRD2, BRD3, BRD4 and BRDT and is characterized by one bromodomain module containing two bromodomains (BD1 and BD2) simultaneously recognizing two acetylated lysine residues [92].

2.4.1 Role of BRD4 in transcriptional control

In recent years BRD4 and BRDT gained attention since they directly interact with the positive transcription elongation factor B (PTEFB), thereby being especially relevant for transcriptional control [93, 94]. Since BRDT is only present in testis, this study focuses on BRD4 having distinct functions in transcriptional control. BRD4 binds to acetylated histones at super-enhancer sites thereby creating a docking site for the CDK8-mediator complex promoting transcription [95]. Upon phosphorylation of histone 3 serine 10 (H3Ser10ph) by the kinase PIM1, a 14-3-3 protein, recognizes this phosphorylation and facilitates the acetyltransferase males absent on the first (MOF) [96, 97]. MOF acetylates H4 at promotor sites at histone 4 lysine 16 (H4K16ac), creating a new binding site for BRD4, which interacts with PTEFB [98, 99]. BRD4 and PTEFB can associate with other nuclear proteins e.g. AF4 forming transcriptional regulatory complexes such as the AF4 complex described in leukemia [100, 101]. PTEFB consists of cyclin-dependent kinase 9 (CDK9) and activator cyclin T (CycT1), which can phosphorylate RNA polymerase II (RNA POL II), controlling transcriptional elongation [100, 101]. Transcriptional elongation is required since RNA synthesis of RNA POL II is arrested after the production of the first ~50 nucleotides, because DSIF (DRB sensitive inducible factor) and NELF complex (negative elongation factor) bind and block further transcription [102, 103]. In this arrested RNA POL II state (POL A), PTEFB can phosphorylate RNA POL II-associated negative elongation factors DSIF and NELF, leading to proteasomal degradation of the NELF complex, and transformation of DSIF into an activator, thereby facilitating the transition into ‘elongating RNA POL II’ (POL E) and completing of transcription [100]. In recent years, the focus has been shifted from BRD4´s general chromatin binding activity to gene-specific binding mediated by interactions with other transcription factors and modifications of BRD4. BRD4 binds to acetylated residues of transcription factors e.g. Nuclear Factor-*κ*-light-chain-enhancer of activated B cells (NF-kB) or FOXO3a and

bridges between chromatin and chromatin remodeling complexes e.g. the histone acetyltransferase complex CBP/p300 or the histone methyltransferase NSD3 [104-107]. In result, the concerted action facilitates transcription of BRD4 target genes. Recently bromodomain-independent interaction with other transcription factors has gained attention: BRD4 can be phosphorylated by the kinase CK2 and dephosporylated by the phosphatase PP2A [108, 109]. Phosphorylation of BRD4 leads to an intramolecular conformation change allowing interaction of the bromodomains BD1 and BD2 with acetylated chromatin as well as bromodomain-independent interaction with transcription factors e.g. p53 via the N-terminal cluster of phosphorylation sites (NPS) resulting in target-specific transcription (see Figure 3) [108, 110].

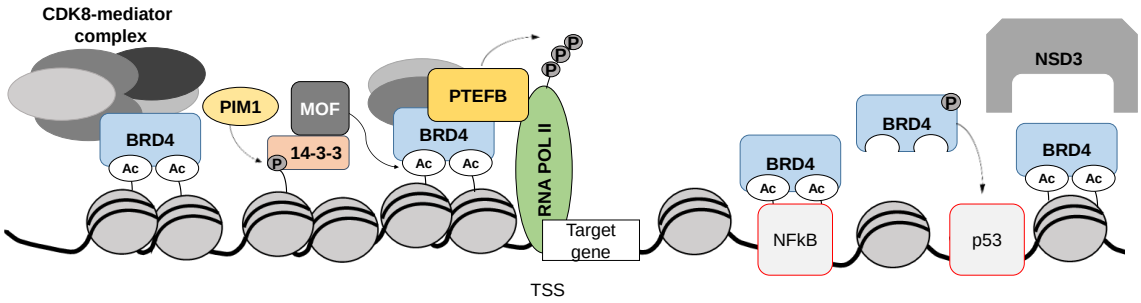

Figure 3: Role of BRD4 in transcriptional control.
BRD4 binds to acetylated (Ac) chromatin via it's two bromodomains (BD1 and BD2) thereby serving as docking site for the CDK8-mediator complex which promotes transcription. If the kinase PIM1 phosphorylates H3 at Ser10 a 14-3-3 protein recognizes this phosphorylation site which serves as docking site for the acetyltransferase MOF which in turn acetylates histones. At transcriptional start sites (TSS) BRD4 is involved in transcriptional elongation providing a docking site for PTEFB. PTEFB phosphorylates RNA Pol II-associated negative elongation factors DSIF and NELF, thereby facilitating RNA Pol II elongation. Furthermore BRD4 can bind to acetylation sites of transcription factors e.g. to NF-κB or FOXO3a, thereby stimulating transcription factor-specific gene expression. Upon phosphorylation, BRD4 changes it´s conformation allowing BD1 and BD2 binding to acetylated chromatin and recruitment of transcription factors via it´s N-terminal cluster of phosphorylation site (NPS), resulting in transcription factor-dependent gene expression. Furthermore, BRD4 can bind to acetylated chromatin and transcription factors bridging to chromatin remodeling complexes e.g. NSD3 or CBP/p300 resulting in chromatin remodeling. Figure is modified from [75, 101, 111].

2.4.2 BET proteins in cancer

Cancer arises from disease-specific transcriptional dysregulation which can be mediated either by *trans*-factors including TFs, signaling proteins, cofactors, chromatin regulators or *cis*-elements including enhancers, promoters and insulators [112]. Cancer driving TFs comprise oncogenes such as MYC or RAS as well as oncogenic TFs, generated by genomic translocations, such as BRD4-NUT fusion protein or *PAX3/7-FOXO* fusion protein, which is a typical feature of ARMS [12, 92, 113-115]. Oncogenic transcription factors such as MYC, BRD4-NUT fusion protein or *PAX3/7-FOXO* fusion protein remodel

the epigenetic landscape by establishing new enhancers and super-enhancers (SE), which are large clusters of enhancers [12]. These SEs in turn control transcription of many oncogenes modulating transcription [116, 117]. Cancer cells are addicted to these context-dependent modulations of transcription impairing cell death programs e.g. by deregulating BCL-2 protein members or promoting proliferation [112, 118]. In the context of rhabdomyosarcoma SE-regulated genes comprise *MYC* and several members of the BCL-2 protein family including *BCL2L11, BMF, PMAIP1* [12]. In conclusion, cancer cells are expected to rely more on enhancers and SEs to maintain their oncogenic transcriptional program compared to normal cells [112]. This makes disruption of enhancers and SEs an interesting strategy to treat cancer [117]. To disrupt this cancer promoting epigenetic landscape BRD4 seems to be a compelling target, since BRD4 is especially enriched at enhancers and SEs, bridging TFs to chromatin thereby facilitating TF context-dependent transcription [99, 108, 117, 118].

2.5 Small molecule inhibitors of BET domains

The highly conserved structure of the hydrophobic pocket of BET proteins was an interesting target for the development of small molecule inhibitors. In 2010 the benzotriazolodiazepine I-BET and the thienotriazolodiazepine JQ1 were published as small molecule inhibitors targeting both bromodomains of BET proteins [119, 120]. The thieno-triazolo-1,4-diazepine JQ1 contains a t-butyl ester functional group at C6 to allow side group diversity and to reduce binding affinity to the central benzodiazepine receptor [120]. Synthesis results in a racemate of (+)-JQ1 and (-)-JQ1 of which only (+)-JQ1 has been shown significant interaction with BRD4 (see Figure 4). The commercially available JQ1 consists of ≥ 98% of (+)-JQ1. By competing with acetyl lysine residues of histones, JQ1 displaces BRD4 from the chromatin and interrupts interactions of BRD4 with acetyl lysine residues of other proteins e.g. transcription factors [104, 120].

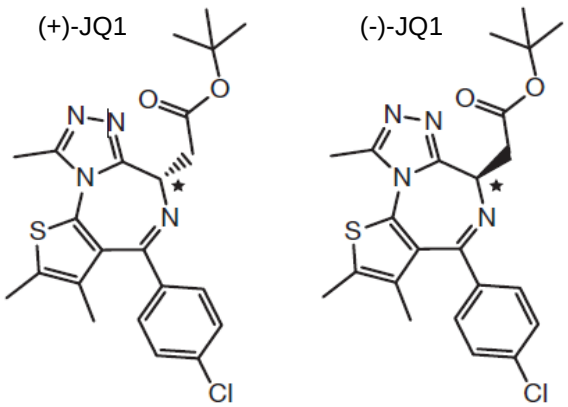

Figure 4: Structure of the small-molecule BET inhibitor JQ1.
Shown are the structures of the two JQ1 stereoisomers. The stereocentre at C6 is indicated by an asterisk. Figure is modified from [120].

The tool compound JQ1 has been shown to downregulate the protooncogene MYC which had remained to be an undruggable target for decades [121]. Furthermore, BET inhibitors including JQ1 have been shown to inhibit hedgehog (Hh) signaling, known to modulate differentiation and response to chemotherapeutics in RMS [14, 113]. In NUT midline carcinoma (NMC) cells harboring the BRD4-NUT fusion oncoprotein JQ1 showed higher antitumor efficiency *in vitro* compared to vincristine and doxorubicin that have been previously used in NMC patients [122, 123]. In addition, various *in vitro* studies in distinct cancer types show, that JQ1 rebalances BCL-2 proteins in favor of apoptosis [87, 124-126]. While single BET inhibition is sufficient to induce cell death in acute myeloid leukemia (AML) *in vitro* [127], in many cancer types single BET inhibition has proved to inhibit cell viability without inducing cell death [125, 128-130]. Additionally BET inhibition as monotherapy is limited due to several resistance mechanisms including rebound increase of BET proteins [131], compensatory upregulation of pro-survival kinases [132], compensatory upregulation of Wnt/β-catenin signaling [133] as well as hyperphosphorylation of BRD4 and interaction with mediator of RNA POL II transcription subunit 1 (MED1) [134]. However, several preclinical studies highlighted the potential of BET inhibitors in combination therapies to potentiate the cytotoxic effect or to overcome resistance to BET inhibition: these combinations included cytostatic drugs [135], HDAC inhibitors [124, 136, 137], tyrosine kinase inhibitors [129], cell cycle modulating kinase inhibitors [137], BCL-2 inhibitors [138], proteasome inhibitors [139], pan-PI3K inhibitors [104, 140] and immunomodulatory drugs [141]. Interestingly BET inhibition as well is able to overcome resistance mechanisms to PI3K inhibitors by blocking adaptive feedback loops further highlighting the potential of BET inhibitors for combination therapies [142].

2.6 Histone deacetylases (HDACs)

2.6.1 Classification and functional role cancer

HDACs belong to the “easers” of epigenetic regulators and remove acetyl groups from histones thereby repressing transcriptional activity [77, 78]. Since deregulation of HDACs is associated transcriptional downregulation of tumor suppressor genes or activation of oncogenes, HDAC inhibition has been intensively studied [56, 80-82, 143, 144]. The family of HDACs comprises four classes grouped according to sequence similarities in yeast: Class I HDACs are Rpd3-like proteins (HDAC1-4 and HDAC8), Class II includes Hda1-like proteins (HDAC4-7, HDAC9-10), Class III comprises Sir2-like proteins also called sirtuins (SIRT1-7) and Class IV only comprises HDAC11 [145]. Since HDACs remove acetyl groups by hydrolysis, they are dependent on a cofactor. HDAC classes I,

II and IV are dedpendent on a zinc ion (Zn^{2+}), whereas class III depend on nicotinamide adenine dinucleotide (NAD^{+}) [146, 147].

2.6.2 HDAC inhibitors

Due to the potential of HDAC inhibition to reactivate transcription of tumor suppressor genes and disrupt the cancer promoting transcriptional program, several HDAC inhibitors have been developed of which some already proceeded into clinics [148, 149]. In recent years several publication have shown the synergistic interaction of BET and HDAC inhibitors in distinct tumor entities [136, 150, 151]. To evaluate the potential combined HDAC and BET inhibition in RMS cells we used four distinct HDAC inhibitors including the hydroxamic acids suberanilohydroxamic acid (SAHA; Vorinostat), JNJ-26481585 (Quisinostat), LBH589 (Panobinostat) as well as the benzamide MS-275 (Entinostat). Hydroxamic acids as well as benzamids inhibit HDACs by binding to the Zn^{2+} co-factor in the catalytic domain, thus targeting HDACs of classes I, II and IV but vary in individual affinities for HDAC classes [152]. In 2006 SAHA was the first HDAC inhibitor approved by the FDA [149], followed by global approval of LBH589 in 2015 [148]. MS-275 is currently tested in clinical phase II trial in neuroendocrine tumors (NCT03211988). JNJ-26481585 is a “second-generation” HDAC-inhibitor showing higher potency compared to SAHA [153]. Up to now preclinical studies highlighted the potential of JNJ-26481585 as monotherapy as well as in combination therapies in RMS cells [56, 143, 144].

2.7 PI3K/mTOR signaling pathway

The phosphatidylinositol 3-kinase (PI3K)/AKT/mammalian target of rapamycin (mTOR) signaling pathway has been shown to regulate many cellular processes including cell survival, proliferation and differentiation [154].

2.7.1 PI3K/AKT/mTOR signaling network

PI3K signaling is usually activated downstream of RTKs and G protein coupled receptors (GPCRs) [154, 155]. Class IA PI3Ks are activated by RTKs and consist of heterodimers containing a regulatory (p85α/p85β/p55γ) and catalytic (p110α/β/δ/y) subunit. Upon RTK activation PI3K is recruited to the membrane and activated by direct interaction of the two Src homology 2 (SH2) domains of regulatory p85 subunit with the tyrosine phosphate motifs of the activated receptor (e.g. platelet-derived growth factor receptor) [156]. Alternatively PI3K can be recruited and activated by interaction of the p85 subunit with receptor-associated adaptor proteins (e.g. insulin receptor substrate 1 (IRS1)) (see Figure 5) [154, 156, 157].

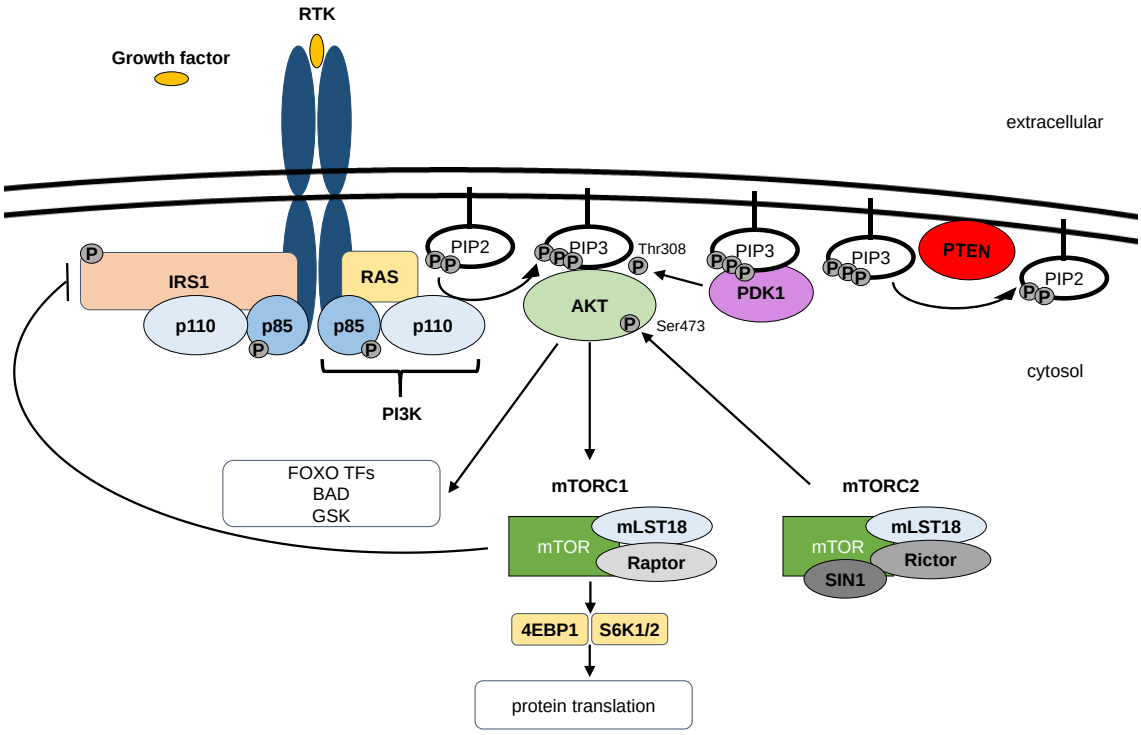

Figure 5: Scheme of PI3K/AKT/mTOR signaling.
Receptor tyrosine kinases (RTKs) are activated upon growth receptor binding which results in a conformation change of intracellular tyrosine phosphate motifs, which are then able to bind phosphatidylinositol 3-kinase (PI3K) either directly via its regulatory subunit p85, or indirectly via adaptor proteins e.g. insulin receptor substrate 1 (IRS1). In result the catalytic subunit of PI3K (p110) is activated. Alternatively to RTKs G-protein coupled receptor (GPCR) signaling as well as other small G-proteins e.g. RAS can activate PI3K signaling. Activated PI3K phosphorylates specific membrane-bound lipid molecules, i.e. phosphatidylinositol and phosphoinositide to phosphatidylinositol-3,4,5-triphosphate (PIP3). PIP3 is the second messenger facilitating downstream signaling by providing docking sites at membranes, which interact with pleckstrin homology (PH) domains of the serine/threonine kinases AKT and 3-phosphoinositide-dependent kinase 1 (PDK1). Upon membrane interaction AKT changes it´s conformation and exposes Ser473, which then can be phosphorylated by mammalian target of rapamycin (mTOR) complex 2 (mTORC2). Phosphorylated AKT regulates various transcription factors (TFs) including forkhead box (FOXO) TFs, BCL-2 proteins e.g. Bcl-2-antagonist of cell death (*BAD*), or glycogen synthase kinase 3 (GSK3), and activates mTOR complex 1 (mTORC1) signaling, which mainly controls protein synthesis via the two most prominent mTORC1 targets ribosomal protein S6 kinase 1/2 (S6K1/2) and eukaryotic translation initiation factor 4E-binding protein 1 (4EBP1). mTORC1/2 and AKT signaling are connected since mTORC2 can phosphorylate AKT at Ser473 and mTORC1 can inhibit insulin receptor substrate-1 (IRS1) promoting AKT signaling (modified from [158]).

The catalytic subunit p110 phosphorylates the membrane-bound lipid phosphoinositide phosphatidylinositol-4,5-bisphosphate (PIP2) into phosphatidylinositol-3,4,5-trisphosphate (PIP3) [159], which serves as docking site for the serine/threonine kinase AKT (147), pleckstrin homology (PH) domains and the 3-phosphoinositide-dependent kinase 1 (PDK1) [159]. Due to its close proximity PDK1 is able to phosphorylate AKT, thereby activating AKT signaling (see Figure 5) [160].

Class IA PI3Ks containing p110α, p110β or p110δ subunits can be activated by RTKs, GPCR upstream signaling or oncogenes such as the small G-protein RAS [161]. Independent of the manner of PI3K activation the second messenger PIP2 is phosphorylated to PIP3 driving all downstream cascades and mediating cellular processes [162]. PIP3 levels are controlled by the tumor suppressor phosphatase and tensin homolog (PTEN), a specific lipid phosphatase preferntilally dephosphoralating PIP3 and converts it back to PIP2 thereby controlling PI3K/AKT activation [163, 164]. Consequently loss or deactivation of PTEN promotes carcinogenesis [164-166]. The serine/threonine kinase AKT integrates all upstream signals from PI3K signaling by docking to the amino-terminal PH domain to PIP3 resulting in conformational change of AKT. Upon conformational change Thr308 and S473 are exposed for phosphorylation. PDK1 phosphorylates Thr308, while mTOR complex 2 (mTORC2) phosphorylates Ser473 [167, 168]. Phosphorylated AKT in turn phosphorylates many substrates including FOXO transcription factors, BCL-2 protein BAD and glycogen synthase kinase 3 (GSK3) resulting in regulation of cell proliferation, survival and metabolism (see Figure 5) [158, 169-171].

Class IB PI3Ks are exclusively activated by G-protein coupled receptors (GPCRs) and contain p110γ and p101 subunits. The Gβγ-subunit of trimeric G-proteins interacts with both p110γ and p101 [155].

Class II PI3Ks and Class III PI3Ks have gained less attention in tumor research. Class II PI3Ks are activated by RTKs, cytokine receptors, and integrins. The three isoforms (PI3KC2α, PI3KC2β and PI3KC2γ) consist of only one subunit preferentially phosphorylating phosphatidylinositol (PI) or phosphatidylinositol 4-phosphate (PI(4)P) and have been shown to regulate insulin signaling [172]. Class III PI3Ks comprise a single catalytic Vps34 subunit only producing Vps34 only produces Phosphatidylinositol 3-phosphate PI(3)P, which is involved in membrane trafficking [173]. Class III PI3Ks have been shown to be regulated by mammalian target of rapamycin (mTOR) signaling, starvation response and autophagy [174].

PI3K class IV comprises mammalian target of rapamycin *(*mTOR), a serine/threonine kinase, regulating cellular growth and proliferation by censoring nutrient availability, cellular energy and oxygen levels as well as mitogenic signals. mTOR exists in two distinct complexes - mTORC1 and mTORC2. The mTORC1 complex comprises the mTOR catalytic subunit, Raptor (regulatory associated protein of mTOR), PRAS40 (proline-rich AKT substrate 40 kDa) and the protein mLST8/GbL [175]. mTORC2

consists of mTOR, rapamycin insensitive companion of mTOR (rictor), mammalian stress-activated protein kinase interacting protein 1 (mSIN1), and mLST8 [176]. Prominent downstream targets of mTOR signaling are ribosomal protein S6 kinase 1 (S6K1/2) and eukaryotic translation initiation factor 4E-binding protein 1 (4EBP1), since they are involved in protein synthesis [177]. mTORC1/2 are interconnected with PI3K signaling: upon single inhibition of mTORC1, mTORC2 leads to compensatory phosphorylation of AKT at Ser473 [178, 179]. Another compensatory response to mTOR inhibition is via IRS1, which is promoting AKT signaling and is negatively regulated by mTOR (see Figure 5) [180, 181].

2.8 PI3K/AKT/mTOR signaling pathway in cancer

Cancer genomic analysis displayed that multiple components of the PI3K pathway are frequently mutated or altered in common human cancers [182]. Class I PI3K alteration including mutations of *PIK3CA* are beyond the most frequent PI3K pathway alterations driving cancer [183]. In ARMS as well as ERMS cell lines show PI3K pathway activation as indicated by high levels of phosphorylated AKT (p-AKT). In patient samples aberrant activation of PI3K pathway was found as well as activation of IRS1 and RTKs [10, 13]. In RMS AKT/mTOR activation in negatively associated with childhood survival, highlighting the potential of PI3K inhibition for treatment of RMS patients [13]. Dysregulated PI3K pathway activation occurs most frequently due to gain of function mutations or amplifications in the p110 subunit of PI3K (*PIK3CA*), mutations in the p85 subunit (*PIK3R*), AKT mutations or amplifications or due to inactivation of the PI3K antagonist *PTEN* by inactivating mutations, copy number loss or homozygous deletions [184]. Even though the mTOR gene is not frequently mutated in cancer, mTOR has been shown to be essential for PTEN-driven tumor development [185]. Since aberrant PI3K/mTOR activation impairs apoptosis and has a broad relevance in cancer [182, 186], various PI3K/mTOR inhibitors have been developed [177].

2.8.1 Small molecule dual PI3K/mTOR inhibitors

Due to their structure kinases including PI3K kinases are very appropriate for pharmacological intervention [177]. The structural similarity of p110 subunit of PI3K and the catalytic domain of mTOR facilitated development of pan-PI3K/mTOR inhibitors using a single molecule for targeting all class I p110 isoforms and mTORC1 as well as mTORC2 [187]. Pan-PI3K/mTOR inhibitors are able to effectively inhibit PI3K signaling, since potential feedback loops via mTORC1 and mTORC2 are inhibited, too [188]. The dual pan-PI3K/mTOR PI-103 belongs to the family of pyridinylfuranopyrimidines and

shows high affinity for PI3K class I and is also active in cells with PTEN deletions and mutations (see Figure 6) [189, 190]. Efficiency of PI-103 was associated with deceased AKT phosphorylation at Ser473 and G1 cell cycle arrest [191]. Preclinical data for the dual pan-PI3K/mTOR PI-103 showed potent antitumor efficiency *in vitro* and in xenograft models with aberrant PI3K activation [192]. Adverse effects of PI3K/mTOR inhibitors in patients were relatively tolerable [193]. However, in patients monotherapy with PI3K/mTOR inhibitors did not show the expected antitumor efficiency at tolerated doses in patients with PI3K pathway activation [194-196]. This may be at least in part due to adaptive feedback loops [142]. In RMS cell lines high levels of phosphorylated AKT have been reported pointing to constitutive activation of PI3K/AKT/mTOR signaling [197]. However, monotherapy with PI3K/mTOR inhibitors was shown to be limited due to compensatory MAPK-activation, which could be overcome by combination with RAS/MEK/ERK inhibitors [197]. To exploit the potential of PI3K/mTOR-inhibitors, improved selection of patients by definition of predictive biomarkers and investigation of potent combination approaches will be necessary.

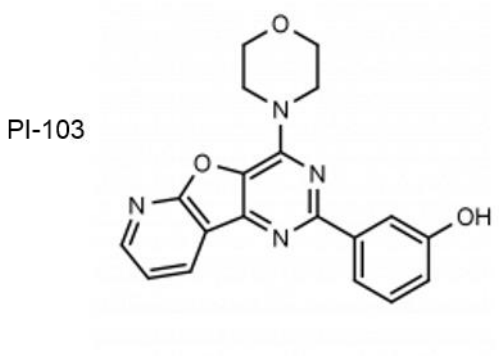

Figure 6: Structure of the small-molecule dual PI3K/mTOR inhibitor PI-103.
The chemical structure of the dual PI3K/mTOR inhibitor PI-103. PI103 is a pyridinylfuranopyrimidine inhibitor with high affinity for p110α/β/δ/γ and mTORC2.

2.8.2 PI3KA isoform-specific inhibitors

Since the 2004, *PIK3CA* mutations have been shown to activate PI3K signaling and drive cancer in many different cancer types [177, 198]. Development of p110 isoform-specific inhibitors revealed different functions of p110 isoforms in cancer. Activation of RTKs, oncogenic RAS mutations, IRS1 activation or p110α activation result in p110α-mediated increased PIP3 levels [199-202]. Inhibition of p110α was shown to be sufficient to block PI3K signaling and its downstream growth factors [203, 204]. By comparison, cancer cells harboring p110β activation, are expected to be sensitive to p110β-specific inhibitors [205]. Since increased B cell receptors (BCRs) or cytokine receptors result in p110δ-

medited increase in PIP3 levels, these cells are prone for sensitivity to p110δ-selective PI3K inhibition [206, 207]. The PI3Kα-selective inhibitor BYL719 is a proline derivate having a high affinity for p110α and was shown to have potent antitumor activity in preclinical studies [208, 209]. In clinical studies BYL719 monotherapy showed prolonged disease stabilization with tumor shrinkage in 33% of *PIK3CA*-mutant patients with oestrogen-positive breast cancer, as well as partial response in colorectal cancer [210]. Monotherapy with BYL719 showed tolerable side effects in clinical studies mainly associated with “on-target” effects of PI3K inhibition since hyperglycemia was the most frequent and dose-limiting adverse event [210-212].

BYL719

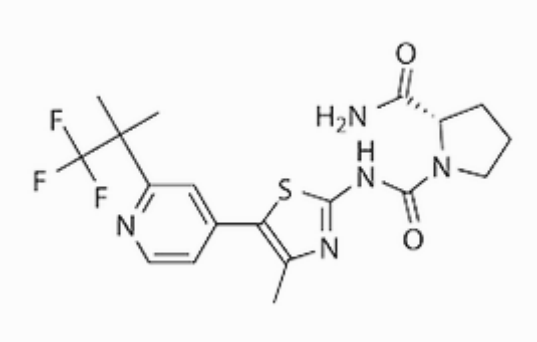

Figure 7: Small-molecule inhibitor BYL719.
The chemical structure of the selective PI3Kα inhibitor BYL719 (Alpelisib) belongs to the proline derivates.

ARMS as well as ERMS show RTK activation, known to stimulate p110α-mediated increased PIP3 levels [197]. ERMS cells additionally harbor RAS mutations, also known to activate p110α [213]. In result, p110α-specific PI3K inhibition appears to be a compelling strategy to inhibit PI3K pathway activation in RMS. However, RMS cells show compensatory expression of other isoforms upon p110α knockdown predicting a lack of clinical efficiency for monotherapeutic approaches [197]. Nevertheless, preclinical data highlight the potential of BYL719 in combination with other targeted therapies to induce apoptosis in RMS cells [208].

2.9 Rationale and aim of the study

Rhabdomyosarcoma is the most frequent soft tissue sarcoma in children and adolescents. Even though genomic and epigenomic vulnerabilities of ERMS and ARMS have been identified [183], the standard therapy still consists of surgery, radiation and combined chemotherapy with chemotherapeutics including cytostatic drugs such as vincristine, dactinomycin, cyclophosphamide, melphalan, ifosfamide and etoposide unspecifically targeting features of growing and dividing cells [15, 16]. While the prognosis of embryonal RMS without metastasis under this therapeutic regime has improved to a 5-year survival of 70%, prognosis of patients with the alveolar subtype, metastasis or relapses is still unfavorable since they frequently suffer from resistance followed by relapse [8, 11, 16, 17]. This provides a rationale for investigation of targeted combination therapies to minimize adverse effects of targeted therapies, potentiate the anticancer activity of targeted therapies and overcome resistances.

Since cancer cells show transcriptional addiction to disease-specific transcriptional programs which are frequently regulated by TFs, TFs represent highly interesting targets for treating cancer [112, 214]. In ARMS the oncogenic PAX3/7-FOXO fusion proteins was recently identified as major TF remodeling the epigenetic landscape by SEs to setup auto-regulatory loops in collaboration with master transcription factors MYOG, MYOD and MYCN conferring to RMS-specific transcriptional dysregulation [12]. In ERMS mutated TFs include *RAS* and *TP53* [11]. MEK inhibition of RAS-mutated RMS cells resulted in ERK2 release from the *MYOG* promoter thereby facilitating *MYOG* expression, which in turn established super-enhancers at genes required for late myogenic differentiation leading to reduction of cell viability and reduced tumor growth [215]. ARMS and ERMS show Hh pathway activation, leading to increased levels of the TF GLI1, which is associated with poor prognosis and modulating response to chemotherapy [14, 216]. Thus targeting major TFs in ARMS as well as ERMS is a compelling strategy to disrupt disease-promoting transcription. However, up to now development of targeted therapies for many TFs remained unsuccessful [214]. Beyond “undruggable” oncogenic TFs MYC might be the most prominent one conferring to research on BET proteins since it was speculated that the transcriptional cofactor BRD4 would be a possibility to indirectly target MYC [112]. MYC elevates transcription by facilitating RNA POL II transcriptional pause release via PTEFB recruitment [217]. Since BRD4 serves as a docking site for PTEFB, inhibition of BRD4 effectively inhibits MYC-mediated transcription [121, 218]. Due to BRD4’s distinct functions in transcriptional control BET inhibition is applicable for indirectly targeting various TFs: Besides facilitating transcriptional pause release of RNA POL II by interacting with PTEFB, BRD4 is enriched

at super-enhancer sites and interacts with TFs including FOXO proteins, PAX3/7-FOXO fusion proteins, ERG or GLI1 [12, 130, 219, 220]. Since adaptive responses are frequently regulated by enhancers and super-enhancers, BET inhibition is able to overcome adaptive feedback loops in response to targeted therapies such as MEK or PI3K inhibition [142, 221]. Vice versa MEK or PI3K inhibition was shown to overcome resistance to BET inhibition pointing to the potential of combined BET and kinase inhibition [140, 222]. In summary, BET inhibition seems to be a compelling strategy to indirectly target oncogenic driver genes in cancer including RMS [130].

RMS cell lines as well as patient samples show increased activation of the PI3K/mTOR pathway compared to normal tissue [13, 183]. In patients PI3K/mTOR activation is negatively associated with childhood survival and impairment of anticancer activity of chemotherapeutic drugs [13, 223]. However, efficiency of single inhibition of PI3K/mTOR signaling is limited due to adaptive feedback loops such as ERK activation [13, 188, 224] and in clinical trials monotherapy with PI3K/mTOR inhibitors did not show the expected antitumor efficiency [194-196]. To optimize drug efficiency and minimize toxicity PI3K isoform-specific inhibitors have been developed [225]. The PI3Kα inhibitor BYL719 showed potent antitumor efficiency in preclinical models as well as partial antitumor efficiency in clinical trials [210, 226]. However, compensatory upregulation of other PI3K isoforms and feedback loops limit the potential of PI3Kα inhibitors as monotherapeutics [197]. The potential of BYL719 for combination therapy in RMS cells was previously demonstrated, since combination of BYL719 and the MEK inhibitor MEK162 in NRAS-mutated rhabdomyosarcoma cells synergistically induced apoptosis [208]. However, ARMS cells, the more aggressive subtype, unlikely harbor RAS-mutations and were less sensitive to combined PI3Kα/MEK inhibition [208]. Since ARMS as well as ERMS frequently harbor ISR1 or RTK activation known to stimulate PI3K p110α, it would be interesting to exploit the potential of PI3Kα inhibition in a way, that in not restricted to RAS-mutated RMS [197].

In the first part of the project we aimed to evaluate the potential BET single inhibition in ARMS and ERMS as well. The anticancer efficiency of the BET inhibitor JQ1 was assessed *in vitro* by cell viability and cell death assays. As our results showed that JQ1 inhibited Hh signaling and as we previously identified synergistic induction of cell death by combined inhibition of Hh and PI3K, we tested JQ1 in combination with PI3K inhibitors [191]. Despite using the pan-PI3K/mTOR inhibitor PI-103, we wanted to exploit the vulnerability of RMS to PI3Kα inhibition and combined JQ1 with the PI3Kα inhibitor BYL719. The *in vitro* anticancer activity of the combination was determined by cell death, cell viability and clonogenic growth assay in representative ARMS and ERMS cell lines

as well as in a primary culture isolated from a patient sample. Based on cell death data, possible synergism of the drug combination was calculated with the determination of the combination index (CI) values according to the method of Chou-Talalay [227]. To further characterize drug efficiency of the combination, CAM assay, a well established *in vivo* model for drug testing, was performed using RD cells as representative RMS cell line. To elucidate the underlying molecular mechanism of JQ1/BYL719 co-treatment-mediated cell death in RMS cells, affected pathways were monitored by analyzing mRNA and protein expression. Functional relevance for cell death induction of identified proteins was confirmed either by using inhibitors, genetic silencing with siRNA or by using genetically engineered cell lines. In the second part of the project this study aimed to provide insight into the upstream mechanism of BET/PI3Kα co-inhibition. To this end RNA-Seq and BRD4 ChIP-Seq was performed focusing further analysis on BCL-2 proteins since we already confirmed that BET/PI3Kα-induced cell death is mediated by intrinsic apoptosis. Since JQ1/BYL719 co-treatment mediated global BRD4 reallocation to chromatin including enrichment at BH3-only genes, we integrated RNA-Seq and ChIP-Seq data to explore the functional relevance of BRD4 reallocation.

In summary, the overall goal of this project was to evaluate BET/PI3Kα co-inhibition as therapeutic option for RMS patients providing novel insight into the molecular underlying mechanism of JQ1/BYL719-mediated transcriptional regulation and execution of JQ1/BYL719-mediated cell death in RMS cells.

3 Materials and methods

3.1 Material

3.1.1 Cell lines

The cell lines used in this study are depicted in Table 1.

Table 1: Cell lines

Cell line	Specification	Species	Source
RH30	alveolar rhabdomyosarcoma	human	DSMZ
RD	embryonal rhabdomyosarcoma	human	ATCC
RH41	alveolar rhabdomyosarcoma	human	ATCC
RH36	embryonal rhabdomyosarcoma	human	ATCC
C2C12	non-malignant myoblasts	mouse	ATCC
CP1	embryonal rhabdomyosarcoma[1]	human	Children's Hospital Frankfurt
Phoenix (AMPHO)	2nd generation retrovirus producer cell line	human	ATCC

[1]: primary derived cell culture from a tumor sample classified as alveolar rhabdomyosarcoma harboring PAX7/FOXO3 mutation and kindly provided by M. Meister and T. Klingebiel, Children's Hospital Frankfurt,

3.1.2 Cell culture reagents

Cell culture reagents used in this study are depicted in Table 2.

Table 2: Cell culture reagents

Reagent	Supplier
Dulbecco's Modified Eagles Medium (DMEM) GlutaMAX-I	Life Technologies, Darmstadt, Germany
Dulbecco's phosphate buffered saline (PBS)	Life Technologies, Darmstadt, Germany
Fetal Calf Serum (FCS)	Life Technologies, Darmstadt, Germany
Penicillin/Streptomycin (10,000 U/ml)	Life Technologies, Darmstadt, Germany
RPMI 1640 medium, GlutaMAX-I	Life Technologies, Darmstadt, Germany
Sodium pyruvate (100 mM)	Life Technologies, Darmstadt, Germany
Trypsin/EDTA (0.05%), phenol red	Life Technologies, Darmstadt, Germany
Trypan blue	Life Technologies, Darmstadt, Germany

3.1.3 Drugs & inhibitors

Inhibitors used in this study and their mode of action are depicted in Table 3.

Table 3: Drugs and inhibitors

Inhibitor	Mode of action	Supplier
BYL719	PI3Kα inhibition	Selleckchem, München, Germany
JQ1	BET inhibition	Stefan Knapp Laboratory, Frankfurt, Germany
PI-103	dual PI3K/mTOR inhibition	Merck Millipore, Darmstadt, Germany
zVAD. fmk	Caspase inhibition	Selleck Chemicals (Houston, TX, USA)

Table 3: Drugs and inhibitors (continued)

Inhibitor	Mode of action	Supplier
JNJ-26481585 (JNJ, Quisinostat)	HDAC inhibition	Selleck Chemicals (Huston, TX, USA)
LBH589 (Panobinostat)	HDAC inhibition	Selleck Chemicals (Huston, TX, USA)
SAHA (Vorinostat)	HDAC inhibition	Selleck Chemicals (Huston, TX, USA)
MS-275 (Entinostat)	HDAC inhibition	Selleck Chemicals (Huston, TX, USA)

3.1.4 Antibodies

Primary antibodies used for Western blot analysis are depicted in Table 4. All antibodies were diluted in 2% BSA.

Table 4: Primary antibodies for Western blot analysis and histology

Target protein	Dilution	Species	Supplier
AKT	1:1000	mouse	BD Biosciences, Heidelberg, Germany
BAK	1:1000	rabbit	BD Biosciences, Heidelberg, Germany
BAX-NT	1:1000	rabbit	Millipore, Darmstadt, Germany
BCL-2	1:1000	rabbit	Abcam, Cambridge, UK
BCL-2	1:1000	mouse	BD Biosciences, Heidelberg, Germany
BCL-x_L	1:1000	rabbit	Cell Signaling, Beverly, MA, USA
BIM	1:1000	rabbit	Cell Signaling, Beverly, MA, USA
BMF	1:1000	rat	Enzo Life Sciences, Farmindale, NY, USA
BRD4	1:1000	rabbit	Biomol (Bethyl), Hamburg, Germany
cleaved caspase-3 (Asp175)	1:250-1:500	rabbit	Cell Signaling, Beverly, MA, USA
c-MYC	1:1000	rabbit	Cell Signaling, Beverly, MA, USA
phospho-Akt (Thr308)	1:1000	rabbit	Cell Signaling, Beverly, MA, USA
GAPDH	1:1000	mouse	HyTest, Turku, Finland
GLI1	1:1000	mouse	Cell Signaling, Beverly, MA, USA

Table 4: Primary antibodies for Western blot analysis and histology (continued)

Target protein	Dilution	Species	Supplier
MCL-1	1:1000	rabbit	Enzo Life Sciences, Farmindale, NY, USA
NOXA	1:1000	mouse	Enzo Life Sciences, Farmindale, NY, USA
PUMA	1:1000	rabbit	Cell Signaling, Beverly, MA, USA
phospho-BRD4 (Ser484/488)	1:1000	rabbit	Chiang Lab, UT Southwestern Medical Center, Dallas, USA
β-Actin	1:1000	mouse	Sigma Aldrich, Deisenhofen, Germany
α-Tubulin	1:1000	mouse	Calbiochem, Darmstadt, Germany

Secondary antibodies used for western blot analysis are depicted in Table 5. HPR-conjugated antibodies were diluted in 5 % SMP in PBS-T, IRDye680-conjugated antibodies were diluted in 2% BSA.

Table 5: Secondary antibodies for Western blot analysis

Antibody	Dilution	Species	Supplier
HRP-conjugated anti-mouse IgG	1:10000	goat	Santa Cruz Biotechnology, Santa Cruz, CA, USA
HRP-conjugated anti-rabbit IgG	1:10000	goat	Santa Cruz Biotechnology, Santa Cruz, CA, USA
HRP-conjugated anti-mouse IgG	1:10000	rabbit	Abcam, Cambridge, UK
HRP-conjugated anti-rabbit IgG	1:10000	rabbit	Abcam, Cambridge, UK
HRP-conjugated anti-rat IgG	1:10000	goat	Abcam, Cambridge, UK

Table 5: Secondary antibodies for Western blot analysis (continued)

Antibody	Dilution	Species	Supplier
IRDye680-conjugated anti-mouse IgG	1:5000	donkey	LI-COR Bioscience, Bad Hombung, Germany
IRDye680-conjugated anti-rabbit IgG	1:5000	donkey	LI-COR Bioscience, Bad Hombung, Germany
IRDye800-conjugated anti-mouse IgG	1:5000	donkey	LI-COR Bioscience, Bad Hombung, Germany
IRDye800-conjugated anti-rabbit IgG	1:5000	donkey	LI-COR Bioscience, Bad Hombung, Germany

Antibodies used for immunoprecipitation and chromatin immunoprecipitation are shown in Table 6.

Table 6: Antibodies for immunoprecipitation

Target protein	Amount	Species	Supplier
BAK clone AB-1	4 µg/sample	mouse	Millipore, Darmstadt, Germany
BAX clone 6A7	4 µg/sample	mouse	Sigma Aldrich, Deisenhofen, Germany
BCL-2 6C8	2 µg/sample	hamster	BD Biosciences, Heidelberg, Germany
BCL-x_L 7B2.5	2 µg/sample	mouse	Merck, darmstadt, germany
BRD4	5 µg/ 250 µg DNA	rabbit	Biomol (Bethyl), Hamburg, Germany
MCL-1	2 µg/sample	mouse	BD Biosciences, Heidelberg, Germany

3.1.5 Short-interference siRNA constructs

Short interference RNA (siRNA) constructs are shown in Table 7. Silencer® siRNA select was purchased from Invitrogen, Karlsruhe, Germany. All siRNAs were diluted to a stock concentration of 20 or 40 µM and used at a final concentration of 20 nM.

Table 7: siRNA constructs

siRNA	Target	Cat. No.
siCtrl	None	4390844
siBAK#1	BAK	s1880
siBAK#2	BAK	s1881
siBAX#1	BAX	s1888
siBAX#2	BAX	s1889
siBAX#3	BAX	s1890
siBIM#1	BIM	s195011
siBIM#2	BIM	s195012
siBIM#3	BIM	s223065
siBMF#1	BMF	s40385
siBMF#2	BMF	s40386
siBMF#3	BMF	s40387
siBRD4#1	BRD4	s23901
siBRD4#2	BRD4	s23902
siBRD4#3	BRD4	s23903
siNoxa#1	NOXA	s10709
siNoxa#2	NOXA	s10710
siNoxa#2	NOXA	s10710
siPI3Kα#1	PI3Kα	s10520
siPI3Kα#2	PI3Kα	s10521
siPI3Kα#2	PI3Kα	s10522

3.1.6 Short interference siRNA transfection with RNAiMAX

Amount of siRNA, Lipofectamine, RNAiMAX, OptiMEM, and cell concentrations is listed in Table 8.

Table 8: Preparation of siRNA transfection mix using RNAiMAX

well	siRNA for 20 nM final (Stock 20mM)	Lipofectamine RNAiMAX	OptiMEM	transfection Mix per well	Culture medium per well
	[µL]	[µL]	[µL]	[µL]	[µL]
96	0.05	0.3	5	10	90
24	0.25	1.5	25	50	450
12	0.5	2.5	50	100	900
6	1	5	100	200	1800
5cm	2	10	250	500	3500
10cm	4	20	500	1000	7000

3.1.7 Buffers

Buffers used for this study were made as following (Table 9).

Table 9: Buffers

Buffer	Ingredients
Antibody dilution buffer	0.9 % NaCl 10 mM TrisHCl pH 7.5 5 mM EDTA 1 mg/ml BSA
Blocking buffer (5 % SMP in PBS-T)	25 g milk powder in 500 ml PBS-T
Blotting buffer (1X)	11.6 g TrisBase 5.8 g Glycine 7.5 ml 10 % SDS 400 ml Methanol add 2L ddH_20

Table 9: Buffers (continued)

Buffer	**Ingredients**
CHAPS lysis buffer	10 mM HEPES pH 7.4
	150 mM NaCl
	1 % CHAPS
TritonX lysis buffer	30 mM TrisHCl
	150 mM NaCl
	10 % Glycerol
	0.5 mM PMSF
	2 mM DTT
	1 % Triton X-100
	1x PIC
RIPA lysis buffer	50 mM TrisHCl (pH 8)
	1 % NP-40
	150 mM NaCl
	2 mM MgCl2
	0.5 % Na-deoxycholate
Phosphate-buffered saline (PBS) (10X)	400 g NaCl
	10 g KCl
	10 g KH_2PO_4
	72 g Na_2HPO_4
	add 5 l ddH_2O
PBS-T (0.1%)	1x PBS
	0.1 % Tween 20
Nicoletti-Buffer	0.05% Trisodium citrate dihydrate
	pH 7.4
	0.05 % Triton X-100
	10 % Glycerol
	50 mg/ml Propium Iodide
PI solution	1 µg/ml PI in PBS
Running buffer (5X)	30.2 g TrisBase
	188 g Glycine
	100 ml 10 % SDS
	add 2 l ddH_20

Table 9: Buffers (continued)

Buffer	Ingredients
SDS loading buffer (6X)	360 mM TrisBase pH 6.8 30 % Glycerol 120 mg/ml SDS 93 mg/ml DTT 12 mg/ml bromophenol blue

3.1.8 Kits and Ready-to-use-Solutions

The kits and ready-to-use solutions are depicted in the following table.

Table 10: Kits and Ready-to-use-Solutions

Reagent/Chemical	Supplier
FACS Clean / Rinse solution	BD Biosciences, Heidelberg, Germany
FACS Flow sheath fluid	BD Biosciences, Heidelberg, Germany
FACS Shutdown solution	BD Biosciences, Heidelberg, Germany
iDeal ChIP-seq kit for histones	Diagenode, Seraing, Belgium
Lipofectamine RNAiMAX	Life Technologies, Eggenstein, Germany
pan-mouse IgG Dynabeads	Life Technologies, Eggenstein, Germany
Page Ruler Plus Prestained Protein Ladder	Thermo Scientific, Roskilde, Denmark
PEQ-Gold RNA Extraction	PEQLAB, Erlangen, Germany
Pierce BCA protein assay	Thermo Scientific, Roskilde, Denmark
Pierce ECL Western Blotting Substrate	Thermo Scientific, Roskilde, Denmark
Pierce DNase	Thermo Scientific, Roskilde, Denmark
Protein G Dynabeads	Life Technologies, Eggenstein, Germany
RevertAid First Strand cDNA synthesis kit	Thermo Scientific, Roskilde, Denmark
SUPERFIX-MRP x-ray fixer	TETENAL, Norderstedt, Germany

Table 10: Kits and Ready-to-use-Solutions (continued)

Reagent/Chemical	Supplier
Starter for x-ray developer	TETENAL, Norderstedt, Germany

3.1.9 General reagents and chemicals

The general chemicals are depicted in Table 11.

Table 11: General reagents and chemicals

Reagent/Chemical	Supplier
Albumin fraction V (BSA)	Carl Roth, Karlsruhe, Germany
Ammonium persulfate (APS)	Carl Roth, Karlsruhe, Germany
Cholamidopropyldimethyl ammonio propane sulfonate (CHAPS)	Sigma-Aldrich, Taufkirchen, Germany
Crystal violet	Carl Roth, Karlsruhe, Germany
Dimethyl sulfoxide (DMSO)	Sigma-Aldrich, Taufkirchen, Germany
Disodium hydrogen phosphate dihydrate (Na_2HPO_4)	Carl Roth, Karlsruhe, Germany
Dithiothreitol (DTT)	Millipore, Darmstadt, Germany
Ethanol	Carl Roth, Karlsruhe, Germany
Ethylene diamine tetraacetic acid (EDTA)	Carl Roth, Karlsruhe, Germany
Carbonyl cyanide-4-(trifluoromethoxy)phenylhydrazone FCCP (100 mM)	Sigma-Aldrich, Taufkirchen, Germany
Formaldehyde	Carl Roth, Karlsruhe, Germany
Glycerol Carl Roth	Carl Roth, Karlsruhe, Germany
Glycine	Carl Roth, Karlsruhe, Germany
Hydrochloric acid (HCl)	Carl Roth, Karlsruhe, Germany
Hydroxyethyl piperazinylethane sulfonic acid (HEPES)	Carl Roth, Karlsruhe, Germany

Table 11: General reagents and chemicals (continued)

Reagent/Chemical	**Supplier**
Methanol	Carl Roth, Karlsruhe, Germany
Milk powder (skimmed milk powder, SMP)	Carl Roth, Karlsruhe, Germany
Opti-MEM transfection medium	Life Technologies, Eggenstein, Germany
PMSF	Carl Roth, Karlsruhe, Germany
Potassium chloride (KCl)	Carl Roth, Karlsruhe, Germany
Potassium dihydrogen phosphate (KH_2PO_4)	Carl Roth, Karlsruhe, Germany
Protease Inhibitor Cocktail (PIC), 25x	Roche Diagnostics
Sodium chloride (NaCl)	Carl Roth, Karlsruhe, Germany
Sodium dodecyl sulfate (SDS)	Carl Roth, Karlsruhe, Germany
Sodium hydroxide (NaOH)	Carl Roth, Karlsruhe, Germany
Tetramethylethylenediamine (TEMED)	Carl Roth, Karlsruhe, Germany
TrisBase	Carl Roth, Karlsruhe, Germany
TrisHCl	Carl Roth, Karlsruhe, Germany
Triton X-100	Carl Roth, Karlsruhe, Germany
Tween-20	Carl Roth, Karlsruhe, Germany
Sodium-orthovanadate	Sigma-Aldrich, Taufkirchen, Germany

3.1.10 Fluorescent dyes for microscope and Fluorescence Activated Cell Sorter (FACS)

Fluorescent dyes used for microscope and FACS are depicted in Table 12.

Table 12: Fluorescent dyes for microscope and FACS

Dye	Supplier
Tetramethylrhodamin-methylester ($TMRM^+$)	Sigma-Aldrich, Taufkirchen, Germany
CellEvent Caspase-3/7 Green Detection Reagent	ThermoFisher Scietific, Waltham, MS, USA
Hoechst-33342	Sigma-Aldrich, Taufkirchen, Germany
Propidium iodide (PI)	Sigma-Aldrich, Taufkirchen, Germany

3.1.11 List of Primersequences for quantitative real-time polymerase chain reaction (qRT-PCR)

List of primersequences used for qRT-PCR are shown in Table 13.

Table 13: List of Primersequences

Target	Forward Primer (5'-3')	Reverse Primer (3'-5')
28S	TTGAAAATCCGGGGGAGAG	ACATTGTTCCAACATGCCAG
BCL-x_L	AGTACCTGAACCGGCACCT	GCCGTACAGTTCCACAAAGG
BIM	CATCGCGGTATTCGGTTC	GCTTTGCCATTTGGTCTTTTT
BMF	GAGACTCTCTCCTGGAGTCACC	CTGGTTGGAACACATCATCCT
c-MYC	GGGTGTTGTAAGTTCCAGTGC	TTTGTCAAACAGTACTGCTACGG
GLI1	AGCTACATCAACTCCGGCCA	GCTGCGGCGTTCAAGAGA
NOXA	GGAGATGCCTGGGAAGAAG	CCTGAGTTGAGTAGCACACTCG

3.1.12 List of genomic Primersequences for Chromatinimmunoprecipitation polymerase chain reaction (ChIP-qRT-PCR)

List of primersequences used for ChIP-qPCR are shown in Table 14.

Table 14: List of genomic Primersequences

Target	Forward Primer (5'-3')	Reverse Primer (3'-5')
BMF Promotor	CTGGAAAACAACCCGGCAAG	CGAGGAAGCCATCCATCTCC
BMF SE	GCAAGGTAACGGCTCCATCT	TGCCCAGTGGTGTGATTTGT
PMAIP1 Promotor	TGCAGGACTGTTCGTGTTCA	CTTCTTCCCAGGCATCTCCG
BCL2L11 Promotor	AGGGTAGGAGAGACAGTGCC	GGCTAACTCTCGTTTGCCGT
BCL2L11 TE	GAGTAGCTGGGTTTTCCCCC	CCTCCCCTGAAGGAGATGGA
BCL2L11 SE	CTATCTTAGCGGCTCACGCA	TAAATTCACACCCTCCGCCC
BMF Promotor	CTGGAAAACAACCCGGCAAG	CGAGGAAGCCATCCATCTCC

3.1.13 Consumables

The used consumables are in the following Table 15.

Table 15: Consumables

Consumables	Supplier
Aluminium foil	Carl Roth, Karlruhe, Germany
Cell culture dishes and flasks	Greiner Bio-One, Frickenhausen, Germany
Cell scraper	BD Biosciences, Heidelberg, Germany
Combitips	Eppendorf

Table 15: Consumables (continued)

Consumables	Supplier
Centrifuge tubes	Greiner Bio-One
Cover glass	VWR Darmstadt, Germany
Cryogenic vials	Starlab, Hamburg, Germany
Disposal bags	Carl Roth, Karlsruhe, Germany
Filter tips	Starlab, Hamburg Germany
Filter paper	Carl Roth, Karlsruhe, Germany
Hybond ECL nitrocellulose membrane	GE Healthcare, Buckinghamshire, UK
Hyperfilm ECL	GE Healthcare, Buckinghamshire, UK
Microcentrifuge tubes	Starlab, Hamburg Germany
Nitrile gloves, sterile, powder-free	Kimberly-Clark, Koblenz, Germnay
Parafilm	VWR Darmstadt, Germany
Pasteur pipettes	Carl Roth, Karlsruhe, Germany
Pipette tips	Starlab, Hamburg Germany
Round-bottom tubes	BD Biosciences, Heidelberg, Germany
Scalpels	B.Braun, Melsungen Germany
Sterile culture vials	Carl Roth, Karlsruhe, Germany
Sterile filters	Millipore, Darmstadt, Germany
Sterile pipettes	Greiner Bio-One, Frickenhausen, Germany

3.1.14 Equipment

The following table shows the used equipment (Table 16).

Table 16: Equipment

Equipment	Supplier
ARE heating magnetic stirrer	VELP Scientifica, Usmate, Italy

Table 16: Equipment (continued)

Equipment	**Supplier**
Avanti J-26 XP ultracentrifuge	Beckman Coulter
Centrifuge MIKRO 200 R	Hettich, Baden-Baden, Germany
Centrifuge ROTIXA 50 RS	Hettich, Baden-Baden, Germany
Centrifuge ROTANTA 460 R	Hettich, Baden-Baden, Germany
CO_2 incubator	SANYO, Wehr, Germany
Easypet (3)	Eppendorf, Hamburg, Germany
Electronic analytical balance EW	Kern, Balingen, Germany
Electronic precision balance 770	Kern, Balingen, Germany
FACSCanto II	BD Biosciences, Heidelberg, Germany
HeraSafe class II biological safety cabinet	Kendro, Langenselbold, Germany
ImageXpress Micro XLS system	Molecular Devices, California, USA
Infinite M100 microplate reader	Tecan, Crailsheim, Germany
Innova 4230 bacteria shaker	New Brunswick Scientific
Microcentrifuge	Benning
Microscope CKX41	Olympus, Hamburg, Germany
Mini-PROTEAN Tetra Cell electrophoresis system	Bio-Rad, Munich, Germany
Multipette plus	Eppendorf, Hamburg, Germany
QuantStudio™ 7 Flex real-time PCR System	
Vacuum pump HLC	Ditabis, Pforzheim, Germany
Vortex mixer (ZX classic; wizard X)	VELP Scientifica, Usmate, Italy
Water bath SWB20	Medingen, Arnsdorf, Germany
7900 GR fast real-time PCR system	Applied Biosystems, Darmstadt, Germany

3.1.15 Laboratory-related software

The following Software was used for data analysis (Table 17).

Table 17: Laboratory-related software

Software	Company
CalcuSyn version 2.0	Biosoft, Cambridge, UK
FACSDiva version 6.1.3	Biosciences, Heidelberg, Germany
FlowJo version 7.6.5	Tree Star, Ashland,OR, USA
Tecan i-control 1.10 Tecan	Tecan, Crailsheim, Germany
ImageJ version 1.48v	National Institutes of Health, USA
Image Studio version 2.1.10	LI-COR, Bad Homburg, Germany
ImageXpress 2015	Molecular Devices, Sunnyvale, CA, USA
Magellan Data Analysis version 7.2	Tecan, Crailsheim, Germany
MS-Office 2013	Microsoft Deutschland GmbH, Germany
Paint.NET v4.0.5.	dotPDN LLC
GraphPad Prism® (version 7.03, GraphPad Software)	GraphPad Prism, San Diego, CA, USA
ImageJ 1.43u	National Institutes of Healt, USA
QuantStudio™ Software V1.3—for QuantStudio™ 6 and 7 Flex and ViiA™ 7 Real-Time PCR Systems	ThermoFisher Scietific, Waltham, MS, USA

3.2 Methods

3.2.1 Cultivation of cells

RMS cell lines (RD, RH36, RH30, RH41, CP1) and non-malignant C2C12 cells were cultivated in DMEM GlutaMAX™-I or RPMI 1640 medium, supplemented with 10% FCS, 1 % penicillin/streptomycin and 1 mM sodium pyruvate. Since the used cell lines are adherent, they were passaged twice a week by trypsinization with 0.05% trypsin/EDTA and cultured in cell culture flasks in a humidified atmosphere at 37 °C with 5 % CO_2. Cells were stored in stocks containing 10% DMSO/media and were kept in liquid nitrogen tank at -80°C. Cells were discarded after about 30-35 passages in culture.

3.2.2 Plating of cells *in vitro*

Approximately 24 hours before treatment cells were seeded in the corresponding cell culture plate or dish in appropriate density in dependent of the timepoint of measurement. In general cells were seeded in a density of 20000 cells/cm^2 for 24 and 48 hours while 10000 cells/cm^2 were seeded for experiments with 72 hours of treatment. Deviating terms considering cell density can be depicted from the respective method. For plating all reagents were prewarmed to 37°C. To detach the cells, the consumed medium was removed, cells were washed with sterile PBS, detached with trypsin/EDTA for 5 minutes at 37 °C and trypsinization was stopped by adding at least the double amount of new culture medium compared to trypsin/EDTA. The cell suspension was used for seeding experiments. To determine the amount of viable cells a sample of the cell suspension was stained with Trypan blue and counting the number of viable cells with a Neubauer improved cell counting chamber. Dependent on well size and timepoint the cell suspension was diluted with fresh media to achieve the desired density of cells. Afterwards the cells were incubated approximately for 24 hours before treatment.

3.2.3 Treatment of cells *in vitro*

To treat the cells, treatments were diluted in prewarmed medium, consumed medium was removed and replaced with the medium containing the treatment and incubated for the indicated timeframes at 37°C and 5% CO_2.

3.2.4 Flow Cyometry measurements

3.2.4.1 Propidium iodide (PI) staining

Propidium iodide (PI) uptake in consequence of membrane permeabilization is a characteristic marker of cell death and was measured by flow cytometry analysis. For PI staining cells were seeded in 24 well plates at previously indicated densities and treated for up to 72 hours as described in 3.2.2 and 3.2.3. Next supernatants were transferred into corresponding round-bottom-tubes. The cells were trypsinzed with 200 µL trypsin/EDTA per well at 37°C followed by addition of 400 µL PBS per well. By pipetting up and down all cells were detached and the cell suspension was transferred into the corresponding round-bottom-tubes and centrifuged at 1800 rpm at 4°C for 5 minutes. The media was removed and the cells were washed with PBS and again centrifuged for 5 minutes at 4 °C and 1800 rpm. Finally, the cell pellet was resuspended in 100 µL PI solution (1 µg/µL). Cell debris was excluded from the measurement in the FSC/SSC and cell death was determined by detecting PI positive population in the PE (red) fluorescence channel.

3.2.4.2 DNA Fragmentation

DNA fragmentation is a hallmark of apoptosis. To determine DNA fragmentation, cells were seeded in 24 well plates at previously indicated densities and treated for up to 72 hours as described in 3.2.2 and 3.2.3. After treatment for the indicated time points, the supernatant of each well was transferred into a corresponding, single round-bottom-tube, centrifuged and washed once with PBS as described in 3.2.4.1. The cell pellet was resuspended in 100-200 µL `Nicoletti`-buffer´. Cells were incubated in this hypotonic buffer for at least 30 minutes at 4°C till flow cytometric measurement. The living cells were gated in the FSC/SSC and cell debris were excluded from measurement of DNA fragmentation. The living cells were analyzed for PI fluorescence intensity using the PE (red) histogram and quantification of the hypodiploid (SubG1) population.

3.2.4.3 Cell Cycle Analysis

To determine the frequency of cells per cell cycle, cells were seeded in 24 well plates at a density of 20000 cells/cm^2 and treated for the indicated timepoints and stained as previously described for DNA fragmentation in 3.2.4.2. Cell cycle analysis was performed analyzing the living population with FlowJo version 7.6.5 software and the Dean-Jett-Fox model.

3.2.4.4 Loss of mitochondrial membrane potential Tetramethylrhodamine (TMRM) Staining

Loss of mitochondrial membrane potential is a characteristic feature of mitochondrial apoptosis and was measured by flow cytometry analysis. To examine the loss of mitochondrial membrane potential (LMMP) cells were seeded in 24 well plates at a density of 20000 cells/cm^2 and treated for the indicated timepoints. As positive control six hours before measurement additional three wells were treated with FCCP (100 mM) diluted 1:1000 in media (100 µM final). Approximately 20 minutes before measurement, cells were pretreated with a final dilution of 1:200,000 of TMEM X (Stock: 1 mM) and incubated at 37°C. Next, the supernatants were transferred to corresponding round-bottom-tubes and the cells were trypsinized, suspended in PBS and the suspension with the detached cells were transferred to the corresponding round-bottom-tubes as described previously (3.2.4.1). After 5 minutes centrifugation at 1800 rpm and 4°C the cell pellet was resuspended in PBS and directly measured at the flow cytometer. The living cells were gated in the FSC/SSC and cell debris was excluded from measurement analyzing PI fluorescence intensity in the PE histogram. The left border of the PE-gate was determined measuring unstained controls, while the right gate limit was determined using FCCP positive controls. At the end of complete measuring control and positive control tubes were re-measured to assure stability of the staining during measurement.

3.2.5 Cell viability and longterm survival

The effect of the tested compounds on cell viability was assessed by analyzing the effect on metabolic activity and cell density.

3.2.5.1 MTT assay

The MTT assay measures the NADH and NADPH dependent reduction of MTT (3-(4,5-dimethylthiazol-2-yl)-2,5-diphenyltetrazoliumbromide) to formazan ((E,Z)-5-(4,5-dimethylthiazol-2-yl)-1,3-diphenylformazan) thus being an indicator of metabolic activity. For MTT assay, cells were seeded in 96 well plates at a density of 10000 cells/cm^2 and treated for 72 hours with the indicated concentrations of JQ1 and/or BYL719. After treatment the media was removed by emptying the plate on paper towels. 100 µL of MTT solution in RPMI without phenolred indicator was added and the plate was incubated for 2 to 3 hours at 37°C. Next, the precipitated formazan was dissolved by adding 100 µL of 2-propanol, resuspension with the pipette and 30 min shaking. Metabolic activity was quantified by the absorbance at 560 nm in comparision to the control using a microplate reader (Tecan sunrise with Magellan Software).

3.2.5.2 Crystal violet assay

To examine cell density cells were seeded in 24 well plates at a density of 10000 cells/cm^2 and treated for 72 hours with 1 µM JQ1, 3 µM BYL719 or the combination of 1 µM JQ1 and 3 µM BYL719. To stain the cells, the medium was removed carefully, adherent cell were washed one times with PBS and followed by 10 min incubation at room temperature with 200 µL per well of crystal violet solution, containing 0.5% crystal violet, 30% ethanol and 3% formaldehyde. Next crystal violet solution was removed by pipetting and additional washing with ddH_2O to remove remaining staining. After air-drying over night the stained plates were scanned for digitalization of results. For quantification, crystal violet was resolved by adding 200 µL 1 % SDS for 30 minutes and gentle shaking. Cell density was measured by determining the absorbance at 560 nm in comparison to the control using a microplate reader (Tecan Infinite M200).

3.2.6 Colony formation assay

To examine long term survival of RMS cells, they were seeded in 24 well plates at a density of 30000 cells/cm^2 and treated for 24 hours with the indicated concentrations of JQ1, BYL719 or the combination of JQ1 and BYL719. After treatment, the media was removed and the cells were trypsinized by adding 50 µL trypsin/EDTA/well up to 5 min incubation at 37 °C. After stopping trypsinization by adding 100 µL culture medium per well, cells were counted manually as previously described in 3.2.2. Next, 100-200 cells were reseeded per well in triplicates in a 6 well plate. After 6-8 days medium was exchanged. After 10-12 days medium was removed and the cells were washed one time with PBS followed by crystal violet staining as described previously 3.2.5.2. After the washing and drying step, 6 well plates were scanned for digitalization of results and colonies were counted manually.

3.2.7 siRNA transfection

For transient knockdown of proteins cells were transfected with Lipofectamine RNAiMAX and either non-targeting siRNA “siCtrl” or siRNAs targeting specific mRNA as listed in 3.1.5. In brief, Lipofectamine RNAiMAX and siRNA (final concentration 20 nM) were diluted separately in OptiMEM and the mixed in a 1:1 ratio as described in Table 8 by pipetting up and down, followed by 10-20 min of incubation at room temperature. Next, the transfection mix was distributed to the cell culture wells and the adjusted cell concentration was placed on top. By gently shaking the cells were distributed evenly in the cell culture plate and then incubated under cell culture conditions. Six hours after

transfection medium was exchanged to prevent from toxic effects of the Lipofectamine RNAiMAX. For confirmation of knockdown, knockdown was performed in 5 cm or 10 cm and cells were collected for Western Blotting as described in 3.2.8.

3.2.8 Harvesting and lysis of cells for Western Blotting

For Western Blotting cells were seeded in either 5 or 10 cm cell culture dishes. Cells were collected by scraping the cells from the cell culture dishes at the indicated timepoints and transferring the cells into falcon tubes. The scraped cell culture dish was washed once with PBS to remove remaining cells and the cell suspension was transferred to the falcon tube, too. After centrifugation at 4 °C, 5 minutes and 1800 rpm the supernatant was removed, the cell pellet was resuspended in 1 mL PBS and transferred to a 1.5 mL tube. After another centrifugation step at 4 °C, 5 minutes and 1800 rpm cell pellets were lysed on ice for 20 min with TritonX lysis or, to check for nuclear proteins, in RIPA lysis buffer (see Table 9). In order to remove the debris, lysates were then centrifuged for 25 minutes at 4 °C and 14 000 rpm and the supernatant containing the cellular proteins was transferred into a new tube which was either stored at -20°C or directly used for determination of protein concentration with Pierce BCA Protein Assay Kit followed by Western Blot analysis.

3.2.9 Protein determination

To determine proteins of whole cell lysates the Pierce BCA Protein Assay Kit was used according to the manufacturer's instructions. In brief, protein concentration was determined in relation to BSA standard curve and absorbance was measured at 550 nM at a microplate reader (Tecan sunrise with Magellan Software).

3.2.10 SDS-polyacrylamidegel elctrophoresis (PAGE) and Western Blot analysis

The polyacrylamide gels consisted of a 5 % stacking gel and a resolving gel containing 10 %, 12 % or 15 % polyacrylamide in regard to the size of the proteins that were aimed to be detected. The 5 % stacking gel consisted of 5 % polyacrylamide, 125 mM TrisHCl pH 6.8, 0.1 % SDS, 0.1 % APS, 0.1 % TEMED, the resolving gels of 10 %, 12 % or 15 % polyacrylamide, 250 mM TrisHCl pH 8.8, 0.1 % SDS, 0.1 % APS, 0.04 % TEMED. For the SDS-PAGE 50 µg of protein sample (150 to 300 µg protein for detection of BMF) were diluted in 1x SDS Loading Dye (see Table 9) and adjusted with ddH_2O to an equal volume, followed by 5 minutes denaturation at 96°C. For SDS-PAGE of the stacking gel a constant voltage of 80 – 100 V, for the resolving gel a constant voltage of 100 – 140 V

was used. Duration of electrophoresis was chosen in regard to the size of the gel and the intended separation of proteins sizes, which was indicated by protein size marker (Page Ruler Plus Prestained Protein Ladder). After separation, proteins were transferred to a nitrocellulose membrane using a semi-dry system. Thus, nitrocellulose membrane and Whatman-papers were soaked in blotting buffer (see Table 9) and nitrocellulose membrane and resolving gel were put between two Whatman-papers on each side and placed into the semi-dry system. Transfer of proteins was performed with constant amperage (1 mA per cm² nitrocellulose membrane) for 1 h 30 min. After blotting, the nitrocellulose membrane was removed from the semi-dry system and shortly washed in PBS-T followed by 1 h blocking in 5 % milk/PBS-T to reduce unspecific antibody binding. Afterwards the nitrocellulose membrane was washed three times in PBS-T to remove remaining milk before protein detection (see 3.2.11).

3.2.11 Protein detection

After blocking and washing the membrane was incubated with primary antibody diluted in 2% BSA/PBS-T at 4 °C overnight on an orbital shaker. The next day the primary antibody solution was removed and stored at -20°C for further use. The membrane was washed three times for approximately 5 minutes with PBS-T. Afterwards the membrane was incubated with the secondary antibody/5% milk depending on the host of the primary antibody for 1 hour at room temperature. Next, the membrane was washed three times in PBS-T for 5 min. Detection of horseradish peroxidase (HRP)-conjugated secondary antibodies enhanced chemiluminescence (ECL) was performed following the manufacturer's protocol. In brief, ECL solution premixes were mixed in a 1:1 ratio and incubated with the membrane for 1 min. The membrane was placed into a X-Ray developer cassette. In a foto laboratory a film was placed onto the membrane, incubated for 1 to 60 min dependent on the signal intensity and put into developing solution. Next, the film was washed and fixed in fixation solution. For digitalization the film was washed, dried and scanned. IRDye-labelled secondary antibodies were detected at 680 or 800 nM using the infrared Odyssey imaging system. Before reusing the membrane for the detection of the next protein, the membrane was shortly washed three times. For detection of several proteins, primary antibodies of different hosts were chosen in order to avoid overlapping of signals.

3.2.12 Immunoprecipitation (IP) of activated BAK or BAX

For immunoprecipitation of active BAK and BAX three to five 15 cm dishes were seeded with 20000 cells per cm^2 and treated with 1 µM JQ1 and 3 µM BYL719 for 24 hours.

Then the cells were harvested and lysed as described in 3.2.8 and 3.2.9 except for the fact that CHAPS buffer (see Table 9) was used instead of TritonX or RIPA buffer. For the input 50 µg of protein sample were diluted in ddH_2O and 1x Loading Dye prepared in a total volume of 15 µL. For the IP samples 500 µg of protein were incubated with either 0.5 µg anti-BAK or 8 µg anti-BAX conformation specific antibody (see Table 6) and 10 µl pan mouse IgG Dynabeads on a rotational wheel together over night. The next day the beads were washed three times with CHAPS buffer using a magnetic rack binding the beads to the tube thus facilitating that only the supernatant is removed. Next, the beads were mixed with 15 µL 1x Loading Dye and incubated at 96°C for 5 min. Afterwards the tubes were again placed into the magnetic rack remove the IP sample without beads for Western Blot analysis. Then activated BAK or BAX as well as loading control (see Table 4) of input and IP were analyzed by Western Blotting.

3.2.13 Co-Immunoprecipitation (Co-IP) of BCL-2, BCL-x_L and MCL-1

Co-Immunoprecipitation (Co-IP) of BCL-2, BCL-x_L and MCL-1 was performed similar to IP of activated BAK and BAX as described in 3.2.12 using suitable antibodies and magnetic beads for the targeted proteins. In brief, after lysis with CHAPS buffer (Table 9) 1000-2000 µg protein lysate were incubated overnight at 4°C with 2 µg/ml mouse anti-MCL-1 antibody, anti-BCL-x_L antibody and 10 µl pan-mouse IgG Dynabeads or hamster anti-BCL-2 antibody or 10 µl pan-mouse IgG Dynabeads (see Table 6). The precipitate was analyzed for interactions by Western blotting using rabbit anti-MCL-1, rabbit anti-BCL-, rabbit anti-BCL-x_L, mouse anti-NOXA or rabbit anti-BIM antibodies (see Table 4).

3.2.14 RNA extraction for qRT-PCR and RNA-Seq

For RNA extraction 20000 cells/cm^2 were seeded in 6 well plates and treated for 6 or 24 hours. To isolate the RNA, peqGOLD Total RNA kit was used according to manufacturer's instructions. In brief, cell culture medium was removed and 350 µL peqGOLD Total RNA lysis buffer was added. After resuspending the cells in the peqGOLD Total RNA lysis buffer, cells were transferred to a DNA removing colum, centrifuged 1 min at RT and 12000 g. The flow through was diluted in an equal volume of 70% ethanol and transferred to a PerfectBind RNA colum and centrifuged 1 min at RT and 10000 g. After washing once with RNA Washing Buffer I, washing twice with RNA Washing Buffer II each followed by 15 sec centrifugation at RT and 10000 g, the colum was dried by 2 min centrifugation at RT and 10000 g. RNA was eluted with 30 to 50 µL ddH_2O by 1 min centrifugation at 5000 g and kept on ice. For RNA-Seq samples, DNA digestion using DNase was included as additional step recommanded by the

manufacturer (see Table 10). RNA concentration was determined measuring the absorbance of 260 nM at a NanoDrop Spectrometer. Pureness of RNA was detmermined by ratio of 260 nm/280 nm as ratio for DNA contamination and 260 nm/230 nm as ration for protein contamination. For short-term storage RNA was stored at -20°C, for long-term storage at -80°C. Isolated RNA was either used for cDNA synthesis (see 3.2.15) or sent to a core facility for RNA-Seq (see 3.2.16).

3.2.15 cDNA synthesis and quantitative real-time polymerase chain reaction (qRT-PCR)

For cDNA-synthesis 300 to 1000 ng of total RNA was used within the RevertAid H Minus First Strand cDNA Synthesis and Random primers according to the manufacture's protocol. To quantify RNA expression, qRT-PCR with SYBR-green was performed in 96 well plates in triplicates on a 7900GR fast real-time PCR system or a QuantStudio 7 Flex system in 384 well plates. In brief, primers listed in Table 13 were diluted to a final concentration of 0.25 µM. Primers were premixed with ddH_2O and SYBR-green. As last step 1 µL of cDNA was added. ddH_20 served as negative control. qRT-PCR was conducted using 7900HT fast real-time PCR or QuantStudio™ Software V1.3. The following temperature steps were used: initial heating to 95°C for 10 min, 45 cycles containing 95°C for 15 sec and 60°C for 1 min, followed by final cooling step. To analyze the melting curve, an additional melting step was added to control target specificity. Automated threshold was applied with 10-times standard deviation of the background signal. For quantification the ΔΔCt method was used utilizing 28S as housekeeping reference.

3.2.16 RNA-Seq

RNA-Seq and analysis was performed at Laboratory for Epigenomics and Tumor genetics, University Hospital Cologne, Germany. "For RNA-Seq, RNA was isolated as described for quantitative real-time PCR, RNA integrity was confirmed by Bioanalyzer analysis (Agilent). Complementary DNA was prepared using SuperScript II Reverse Transcriptase (Invitrogen) according to the manufacturer's instructions. Library preparation was performed with the TrueSeq RNA Samples preparation Kit (Illumina) according to the manufacturer's instructions and sequencing was performed as 75bp paired-end sequencing on a HiSeq 4000 instrument (Illumina). Reads from fastq files were mapped against the human genome GRCh37/hg19 using STAR 2.5 with default parameters and differential gene expression was calculated using DESeq2. Three independent experiments were performed for each treatment. Overlap of differentially

expressed genes (DEGs) was created using Venn tools (http://bioinformatics.psb.ugent.be/cgi-bin/liste/Venn/calculate_venn.htpl)."[1]

ChIP-Seq and analysis was performed at Laboratory for Epigenomics and Tumor genetics, University Hospital Cologne, Germany. "For ChIP-Seq experiments, RH30 cells were treated with solvent alone, 1 µM JQ1, 3 µM BYL719 or JQ1/BYL719 for 24 hours. Three independent ChIP-Seq experiments were performed. Cells were fixed for ten minutes with 1% formaldehyde (final concentration) at RT followed by five minutes blocking with 125 mM (final concentration) at RT. Chromatin was extracted using the truChIP Chromatin Shearing Kit (Covaris, Brighton, UK) according to the manufacturer's instructions. The chromatin was sheared by sonication to a DNA fragment size of 200–600 bp and precipitated using an antibody against human BRD4 (Bethyl Laboratories, A301-985A100). ChIPs were run on the IP-Star compact system using the Auto iDeal ChIP-seq kit for histones (Diagenode, Seraing, Belgium) according to the manufacturer's direct method for ChIP preparation. ChIP-DNA was sequenced using HiSeq4000, 51-bp single-end. Reads were mapped to the hg19 genome using bwa-0.7.12 with default parameters. Peaks were called with MACS2 with the parameters "bw 500 --mfold 2 100 --broad --broad-cutoff 0.1 –bdg". Promoters were annotated as ± 3000 bp around the transcription start sides (TSS), super enhancer as well as typical enhancer annotation were extracted from Gryder et al. 2017 [12]. For visualization, all bam files were first converted to bigwig files using R/Bioconductor. Afterwards the input files were subtracted from the corresponding ChIP output files with deeptools 3.0.1 and then at least two replicates were merged using ucsc-utilities. The merged bigwig files were then converted to bedgraph files that are used for visualization with R/Bioconductor GViz package.
Gene ontology of BRD4 promoter peaks with corresponding log2 FC>I0.58I was performed using Enrichr (http://amp.pharm.mssm.edu/Enrichr/)."[1]

3.2.17 ChIP-qPCR

ChIP-qPCR was performed with 300 ng of ChIP-DNA using genomic primers listed in Table 14 and qRT-PCR with SYBR-green as described in 3.2.15. ChIP-qPCR results were normalized using the Percent Input Method: In a fist step, the input generally containing 1% of chomatin used for the ChIP is adjusted to 100%. The adjusted input

[1] Depicted from "Co-inhibition of BET proteins and PI3Kα reallocates BRD4 to transcriptional regulatory elements of BH3-only proteins and triggers mitochondrial apoptosis "

was calculated as Ct value – log2(dilution factor). In a second step, the percent input of the ChIP signal was calculated: 100 x 2^(adjusted input – Ct(IP)).

3.2.18 Immunoflourescence

3.2.18.1 PI/Hoechst Staining

For PI/Hoechst-33342 double staining cells were seeded in 96 well plates as described in 3.2.2 and treated for the indicated timepoints. The border wells of the 96 well plate were filled with PBS in order to prevent variations due to evaporation of cell culture medium. For PI/Hoechst-33342 double staining PI and Hoechst-33342 were prediluted 1:100 in PBS. The predilution was added 1:10 on top of the treatment (final concentration 1 µg/mL) and incubated for 5 to 15 min at 37°C. PI was measured using the TRITC, Hoechst-33342 using the DAPI channel at the Molecular Device Microscope. PI/Hoechst-33342 double positive stained cells indicating dead cells were counted in relation to Hoechst-33342 single positive cells indicating living cells by using automated analysis using MetaXpress Software.

3.2.18.2 Caspase activity assay

Caspase activation was measured using the CellEvent Caspase-3/7 Green Detection Reagent was used following the instructor's manual. In brief, cells were seeded in 96 well plates with a cell density of 20000 cells/cm^2. Next day they were treated for 24 hours with the indicated treatment and additional Caspase-3/7 Green Detection Reagent (final concentration 2 µM). After treatment, cells were stained with Hoechst-33342 (final concentration 1 µg/µl) and incubated for 5 to 10 minutes at 37°C. Caspase-3/7 activation was measured using FITC channel and counted in relation to Hoechst-33342 single positive cells using DAPI channel at the Molecular Device Microscope with automated analysis using MetaXpress Software.

3.2.19 Chicken chorioallantoic membrane (CAM) assay

For *in vivo* testing, CAM assay, a well established tumor model for drug testing, was performed. 1×10^6 RD cells were mixed 1:1 with matrigel and implanted onto the CAM to form tumors at day 8 of fertilization of chicken eggs. The next day a tumor was grown on the CAM and treated with JQ1 and/or BYL719 (final concentration of 1 µM) for three consecutive days. Afterwards, the CAM was fixed in 4% paraformaldehyde and cut in 3 µm sections after it was embedded in paraffin. The tumor slices were analyzed by immunohistochemistry using rabbit polyclonal anti-cleaved caspase-3 (Asp175) antibody

and hematoxylin counterstain. Active caspase-3-positive cells per tumor area were independently counted manually by two investigators.

3.2.20 Statistical analysis

To perform statistical analysis, at least three independent experiments were performed independently including duplicates or triplicates for each experiment. For comparing two different groups, Student's t-Test (equal variance, two-sample, two-sided distribution) using Microsoft Excel was used to determine significance. For comparison of several groups one-way ANOVA followed by Tukey's multiple comparisons test utilizing GraphPad Prism® was used. All *in vitro* data were expressed as mean +/- standard deviation (SD). Results of the CAM assays were expressed as mean +/- SEM. P-values indicated statistical significance: p-value ≤ 0.05 (significant, *), p-value ≤ 0.01 (very significant, **) and p-value ≤ 0.001 (highly significant, ***).

3.2.21 Calculation of Combination Index (CI)

To calculate the Combination Index (CI) value CalcuSyn software was used according to the method of the method of Chou-Talalay [227]. CI<0.9 indicates synergism, 0.9-1.1 an additive and CI>1.1 an antagonistic effect.

4 Results

4.1 BET inhibitor JQ1 reduces cell viability without inducing cell death in RMS cell lines

4.1.1 JQ1 single treatment inhibits cell viability in RMS cell lines

RMS cells have been reported to be sensitive to BET inhibition [113]. To investigate whether the BET inhibitor JQ1 affects cell viability or cell death, we performed dose response studies testing the BET inhibitor JQ1 in two ARMS (RH30, RH41) and two ERMS (RD, RH36) cell lines (Figure 8). Metabolic activity, as measured by MTT assay, was already reduced at nanomolar concentrations (0.2 µM) in a dose dependent manner in all four cell lines (Figure 8).

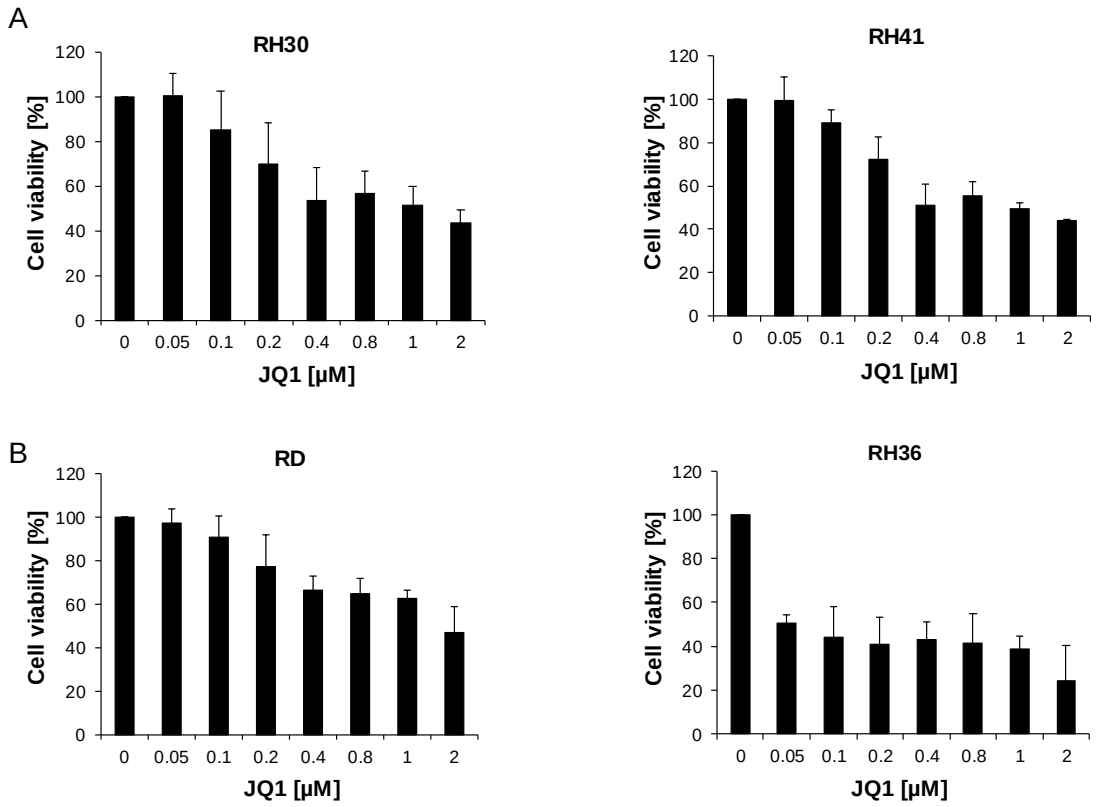

Figure 8: JQ1 inhibits cell viability in RMS cells.
RMS cell lines were treated with the indicated concentrations of JQ1 for 72 hours. Loss of viability was measured by MTT assay in ARMS (A) and ERMS (B). Data are shown as mean and SD of at least three independent experiments performed in triplicate.

4.1.2 JQ1 single treatment does not induce cell death in RMS cell lines

To assess the effect of JQ1 on cell death induction PI/Hoechst staining was performed and PI positive cells were detected. While JQ1 inhibited cell viability in nanomolar concentrations (Figure 8) it barely induced cell death at high concentrations (20 µM) (Figure 9).

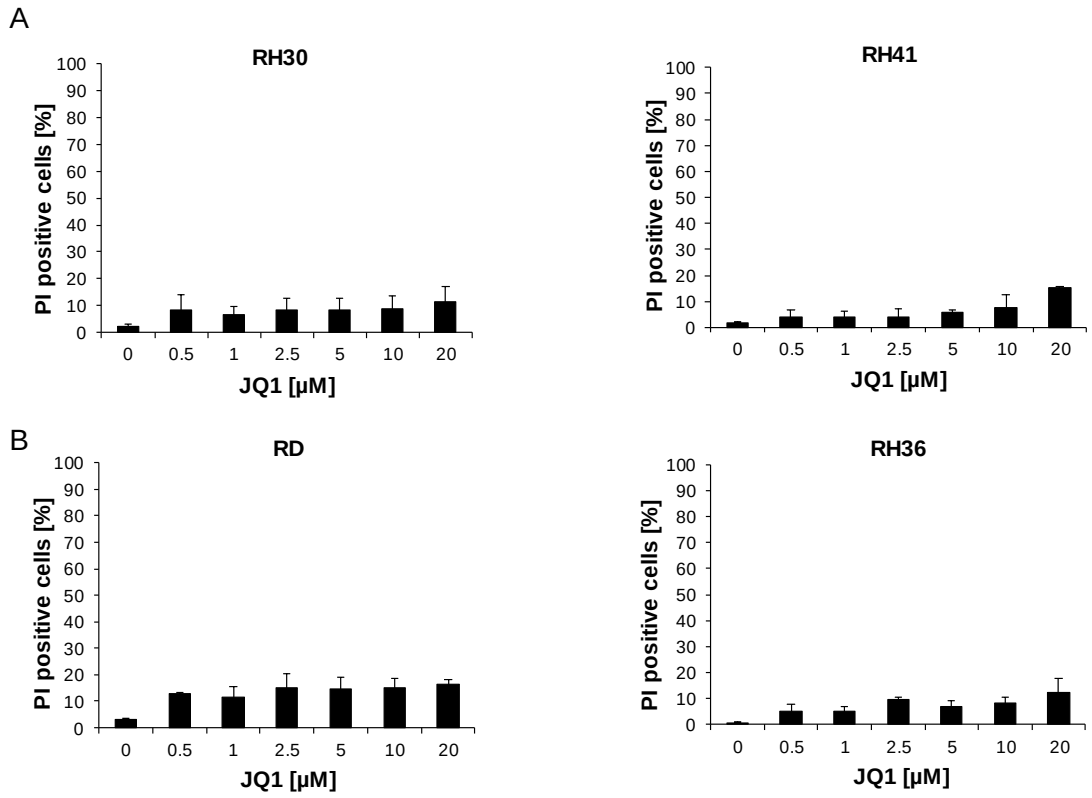

Figure 9: JQ1 single treatment does not induce cell death in RMS cells.
Cell death was determined by analysis of PI/Hoechst staining and ImageXpress Micro XLS system in ARMS (A) and ERMS (B). Data are shown as mean and SD of at least three independent experiments performed in triplicate.

4.1.3 BET inhibitor JQ1 inhibits Hh signaling

Since Hh signaling has been shown to promote the malignant phenotype of RMS [216] and JQ1 has been shown to inhibit Hh signaling in other tumor entities [130], we checked the effect of JQ1 on Hh signaling using transcription of Gli1 and Gli1 luciferase activity as readout. JQ1 inhibited transcription of Gli1 as well as Gli1 luciferase activity in RD and RH30 cells. As expected GLI1 mRNA levels were significantly reduced within six hours and GLI1 luciferase levels were significantly decreased upon JQ1 treatment after 24 hours (Figure 10).

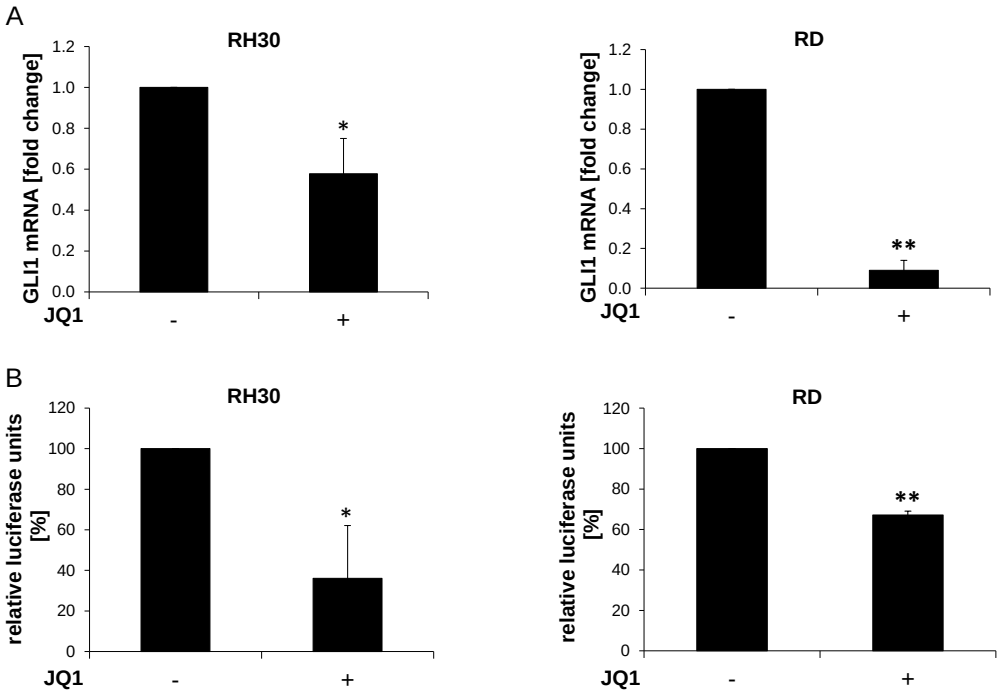

Figure 10: JQ1 single treatment inhibits Hh signaling.
(A) RH30 and RD cell were treated with 1 µM JQ1 for six hours and mRNA levels of GLI1 were analyzed by qRT-PCR and fold changes compared to untreated control are shown with mean and SD of three independent experiments performed in duplicate; *p<0.05; **p<0.01. (B) RH30 and RD cells were transfected with GLI1 luciferase reporter plasmids and treated with 1 µM of JQ1 for 24 hours. Dual-luciferase reporter assay was used to determine GLI1 transcriptional activity. Changes compared to untreated control are shown with mean and SD of three independent experiments performed in duplicate; *p<0.05; **p<0.01.

4.1.4 BET inhibitor JQ1 inhibits MYC

BET inhibitors have become a prominent tool to target the protooncogene MYC, which has remained an undruggable target for years [114]. Thus, we investigated whether JQ1 reduced MYC in RMS cells. As expected, JQ1 significantly reduced MYC mRNA within six hours and reduced protein levels as well, as shown by protein detection after 24 hours treatment (Figure 11).

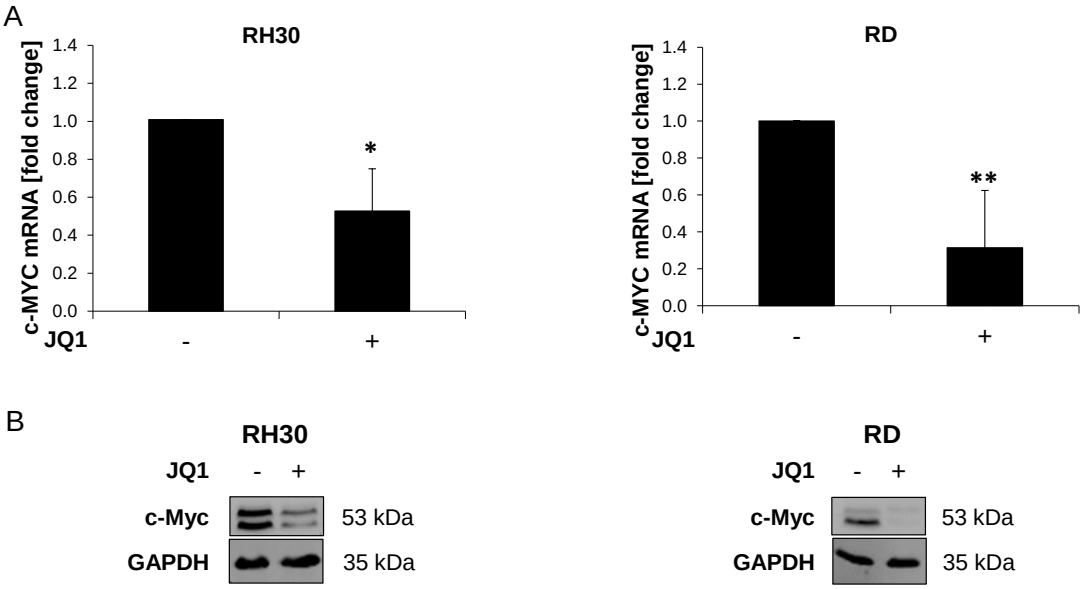

Figure 11: JQ1 single treatment inhibits MYC.
(A) RH30 and RD cell were treated with 1 µM JQ1 for six hours and mRNA levels of GLI1 were analyzed by qRT-PCR and fold changes compared to untreated control are shown with mean and SD of three independent experiments performed in duplicate; *p<0.05; **p<0.01. (B) RH30 and RD cell were treated with 1 µM JQ1 for 24 hours and protein levels of MYC were detected by Western Blotting, GAPDH served as loading control. Representative blots of two experiments are shown.

4.2 JQ1 synergizes with PI3K inhibitors to induce cell death in RMS cells

As our results showed that JQ1 inhibited Hh signaling (Figure 10) and as we previously identified synergistic induction of cell death by combined inhibition of Hh and PI3K signaling [191], we tested JQ1 in combination with PI3Kα inhibitor BYL719 (Alpelisib) and the dual pan-PI3K/mTOR inhibitor PI-103 to induce cell death.

4.2.1 JQ1 synergizes with BYL719 to induce cell death in RMS cells

We focused on BYL719 since previous studies have shown that BYL719 is more potent in combination treatment in RMS cells compared to PI-103 [208]. In order to test whether JQ1 synergizes with BYL719 to induce cells death in RMS we combined subtoxic concentrations of JQ1 and BYL719 in two ARMS (RH30, RH41) and two ERMS (RD, RH36) cell lines for 72 hours. While BYL719 single treatment induced only minor cell death (<20%), addition of JQ1 increased cell death up to 55% PI positive cells in respective of the cell line (Figure 12).

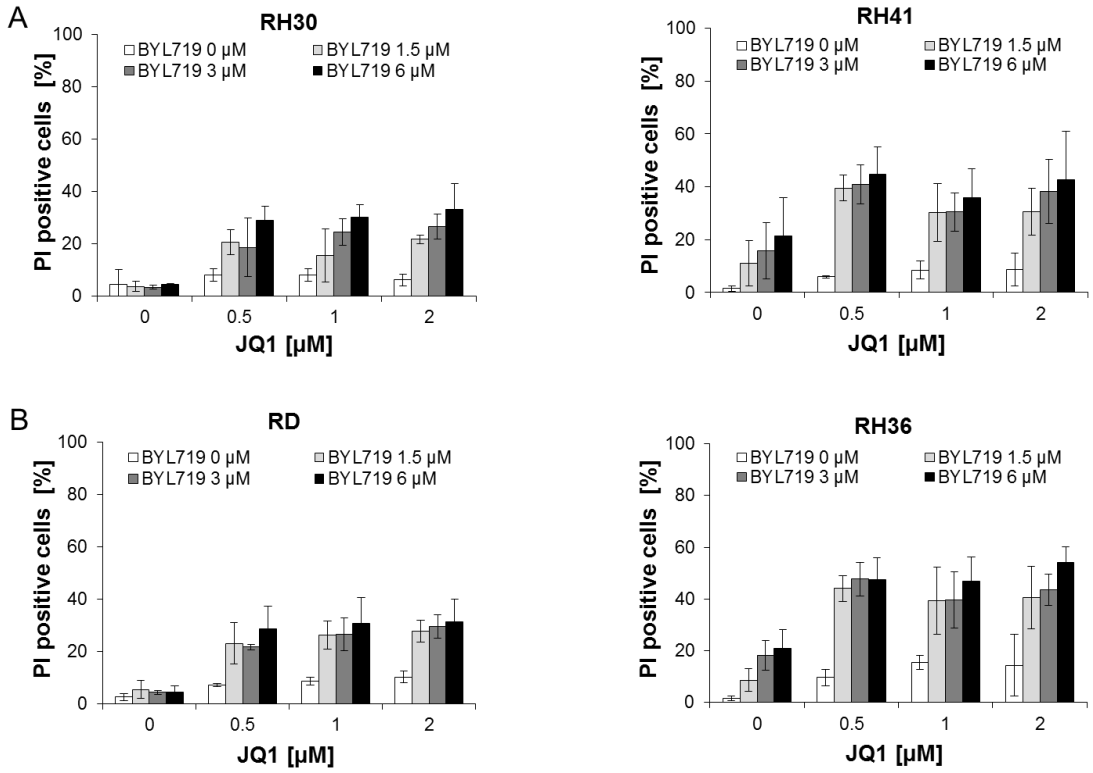

Figure 12: JQ1/BYL719 co-treatment synergistically induces cell death in RMS cells.
(A) ARMS and (B) ERMS cell lines were treated with the indicated concentrations of JQ1 and BYL719 for 72 hours. Cell death was determined by analysis of PI/Hoechst staining and ImageXpress Micro XLS system. Data are shown as mean and SD of at least three independent experiments performed in triplicate.

To confirm synergism of the combination of JQ1 and BYL719 combination index (CI) value was calculated based on the method Ting-Chao Chou using PI/Hoechst results after JQ1/BYL719 co-treatment (Table 18). CI values are considered synergistic if the value is equal or below 0.9, additive if between 0.9 and 1.1. and antagonistic if equal or greater than 1.1 [227]. All combinations used in RD, RH30 and RH36, were synergistic as indicated by CI values lower 0.9. CI values for RH41 cells could not be calculated, since the algorithm of this calculation is based on linear regression and PI positive cells did not increase continuously with increasing concentrations.

Table 18: Calculation of Combination Index Values for RMS cells treatment with JQ1/BYL719 co-treatment

	RH30			**RD**			**RH36**		
	BYL719 [µM]			**BYL719 [µM]**			**BYL719 [µM]**		
JQ1 [µM]	1.5	3	6	1.5	3	6	1.5	3	6
0.5	0.032	0.452	0.127	0.007	0.008	0.012	0.069	0.122	0.223
1	0.021	0.03	0.054	0.010	0.008	0.010	0.096	0.180	0.234
2	0.009	0.02	0.018	0.002	0.004	0.006	0.097	0.148	0.158

4.2.2 JQ1 synergizes with BYL719 to induce DNA fragmentation in RMS cells

To confirm this synergistic drug interaction by another cell death assay we analyzed DNA fragmentation, a typical hallmark of apoptosis. We focused on RH30 and RD cells for further experiments, representing the alveolar and embryonal subtype of RMS cells.

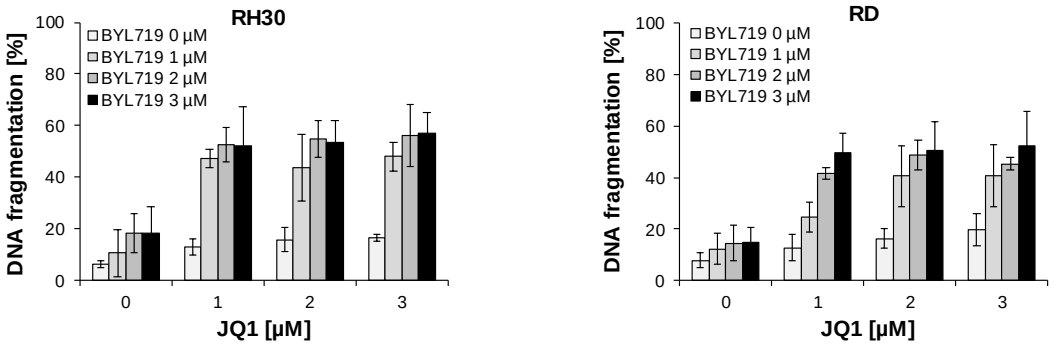

Figure 13: JQ1/BYL719 co-treatment synergistically induces DNA fragmentation in RMS cells.
Cell death was determined by flow cytometric analysis of DNA fragmentation of PI-stained nuclei. Data are shown as mean and SD of at least three independent experiments performed in triplicate.

Comparable to cell death measurement by PI/Hoechst staining, DNA fragmentation was induced in a synergistic manner by combination of JQ1 and BYL719 as confirmed by calculation of CI value (Table 19).

Table 19: Synergistic induction of DNA fragmentation by JQ1/BYL719 co-treatment

	RH30			**RD**		
	BYL719 [µM]			**BYL719 [µM]**		
JQ1 [µM]	1	2	3	1	2	3
1	0.187	0.033	0.017	0.037	0.052	0.078
2	0.074	0.036	0.031	0.053	0.044	0.074
3	0.108	0.084	0.039	0.041	0.041	0.056

4.2.3 JQ1 synergizes with PI-103 to induce cell death in RMS cells

In order to exclude that the observed synergism is restricted to the combination of JQ1 and BYL719, we tested the combination of JQ1 with the pan-PI3K/mTOR inhibitor PI-103 by assessing DNA fragmentation. Indeed, we could observe synergistic induction of DNA fragmentation upon the combination of JQ1 and PI-103 as indicated by CI values lower 0.9. As expected, the efficiency of cell death induction was minor compared to the combination of JQ1 and BYL719 highlighted by CI values higher compared to CI values of JQ1/BYL719 co-treatment (Figure 14,

Table *20* 20).

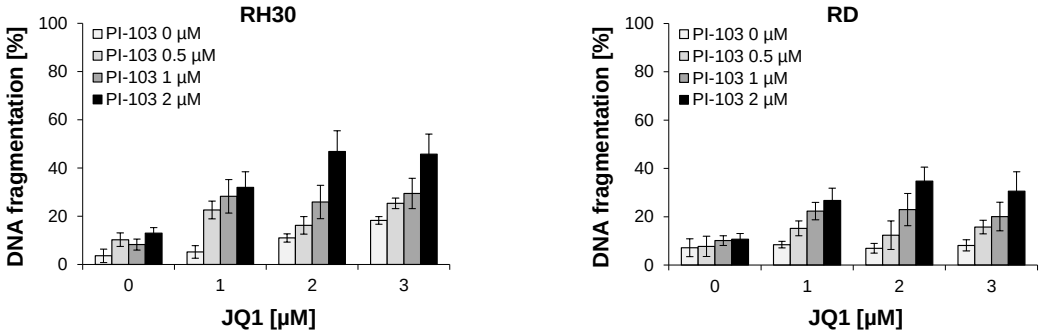

Figure 14 JQ1/PI-103 co-treatment synergistically induces DNA fragmentation in RMS cells.
Cell death was determined by flow cytometric analysis of DNA fragmentation of PI-stained nuclei. Data are shown as mean and SD of at least three independent experiments.

Table 20: Synergistic induction of DNA fragmentation by JQ1/PI-103 co-treatment

	RH30			**RD**		
	PI-103 [µM]			**PI-103 [µM]**		
JQ1 [µM]	0.5	1	2	0.5	1	2
1	0.28	0.76	0.72	0.29	0.1	0.1
2	0.21	0.46	0.6	0.27	0.21	0.1
3	0.18	0.22	0.3	0.67	0.27	0.16

4.2.4 Combination of genetic silencing of BRD4 with BYL719 or PI3K p110α with JQ1 triggers cell death in RMS cells

To exclude, that the synergistic cell death induction is caused by off target effects of the used compounds, knockdown of either BRD4 or PI3K p110α was performed, followed by treatment with either BYL719 or JQ1.

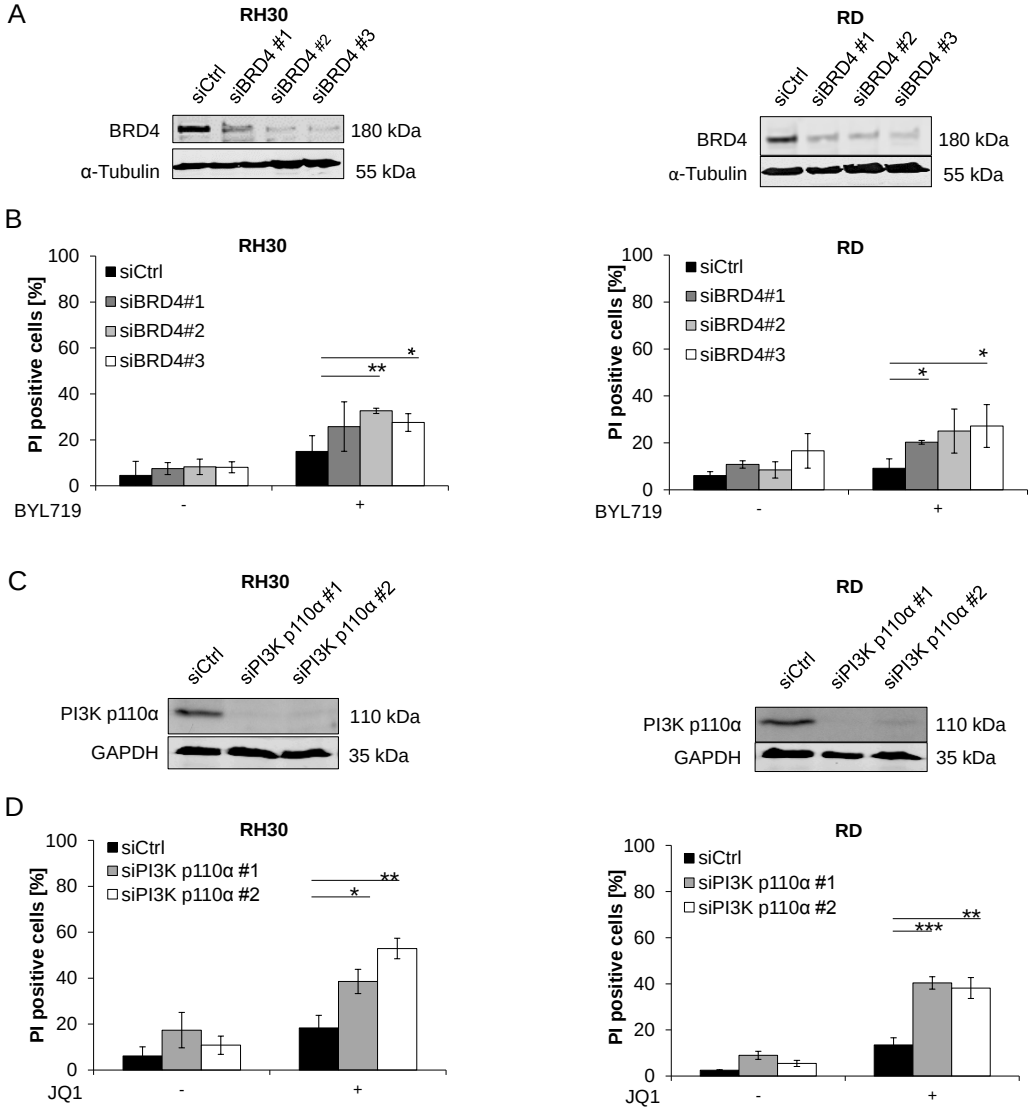

Figure 15: Combination of genetic silencing of BRD4 with BYL719 or PI3K p110α and JQ1 triggers cell death in RMS cells.
(A, B) RMS cells were transiently transfected for 24 hours with non-silencing siRNA or siRNA targeting BRD4 and then treated for 72 hours with 10 µM BYL719 or (C, D) with non-silencing siRNA or siRNA targeting PI3K p110α and then treated for 72 hours with 1 µM JQ1. (A, C) Protein levels of BRD4 were detected by Western blotting; α-Tubulin or GAPDH served as loading controls. (B, D) Cell death was determined by analysis of PI/Hoechst staining and ImageXpress Micro XLS system. Data are shown as mean and SD of at least three independent experiments performed in triplicate; *p<0.05; **p<0.01; ***p<0.001.

Combination of BRD4 knockdown with BYL719 resulted in moderate cell death induction accounting between 27 and 32% PI-positive cells in RH30 and 20 to 27% in RD cells. However, increase in PI-positive cells upon BRD4 knockdown was significant compared to treated non-silencing control in two out of three siRNA constructs (Figure 15). By comparison, knockdown of PI3K p110α followed by treatment with JQ1 resulted in more pronounced cell death induction as measured 35 or 38% PI-positive RH30 and 38 to 40% PI-positive RD cells, which was significant for both siRNA constructs in both cell lines (Figure 15).

4.2.5 JQ1/BYL719 co-treatment induces cell death in primary derived RMS cells

Next, we tested the efficiency of JQ1/BYL719 co-treatment in CP1 cells, which are RMS cells derived from a patient diagnosed with a PAX7-FOXO1 fusion gene-positive ARMS. Comparable to RMS cell lines combination of JQ1 and BYL719 induced significantly more cell death compared to either JQ1 or BYL719 single treatment.

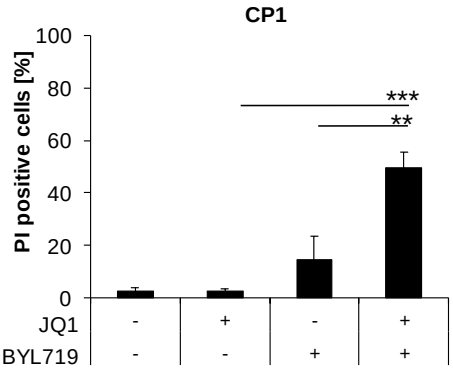

Figure 16 JQ1/BYL719 co-treatment synergistically induces cell death in primary derived RMS cells.
Primary derived CP1 RMS cells were treated with 1 µM JQ1 and 6 µM BYL719 for 72 hours. Cell death was determined by analysis of PI/Hoechst staining and ImageXpress Micro XLS system. Data are shown as mean and SD of at least three independent experiments performed in triplicate; **p<0.01; ***p<0.001.

4.2.6 Non-malignant C2C12 cells are less sensitive to JQ1/BYL719 co-treatment

Interestingly JQ1/BYL719 co-treatment induced less cell death in non-malignant C2C12 cells compared to RMS cells. Of note, the combination of JQ1 and BYL719 still induced significantly more DNA fragmentation compared to JQ1 or BYL719 single treatment. However, upon JQ1/BYL719 co-treatment only 24% of C2C12 cells showed DNA fragmentation (Figure 17) compared to 49.6% DNA fragmentation in RH30 and 53% DNA fragmentation in RD cells (Figure 13).

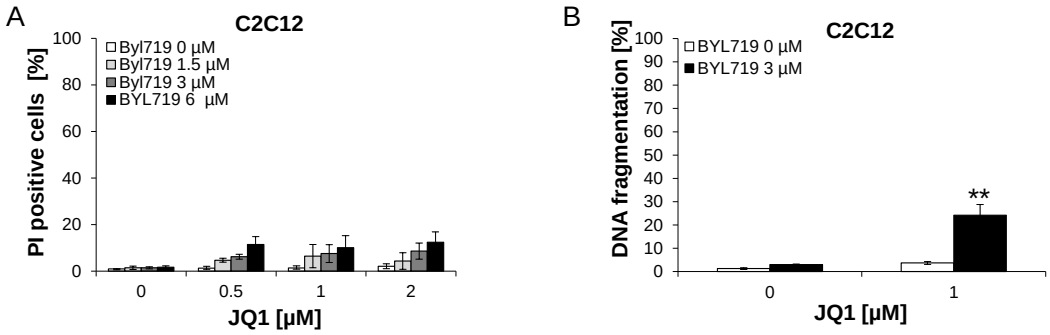

Figure 17: JQ1/BYL719 co-treatment induces minor cell death in non-malignant C2C12 cells.
Murine myoblast cells C2C12 were treated with the indicated concentrations of JQ1 and BYL719. Cell death was determined by analysis of PI/Hoechst staining and ImageXpress Micro XLS system (A) or by flow cytometric analysis of DNA fragmentation of PI-stained nuclei (B). Data are shown as mean and SD of at least three independent experiments performed in triplicate; **p<0.01.

4.2.7 JQ1/BYL719 co-treatment reduces cell density of RMS cells

Next, cell density was assessed using crystal violet staining. Cell density can be affected by detaching cells as well as by inhibition of cell proliferation. In RH30 and RD cells JQ1 and BYL719 single treatment reduced cell density. However, JQ1/BYL719 co-treatment significantly decreased cell density in comparision to JQ1 or BYL719 single treatment (Figure 18).

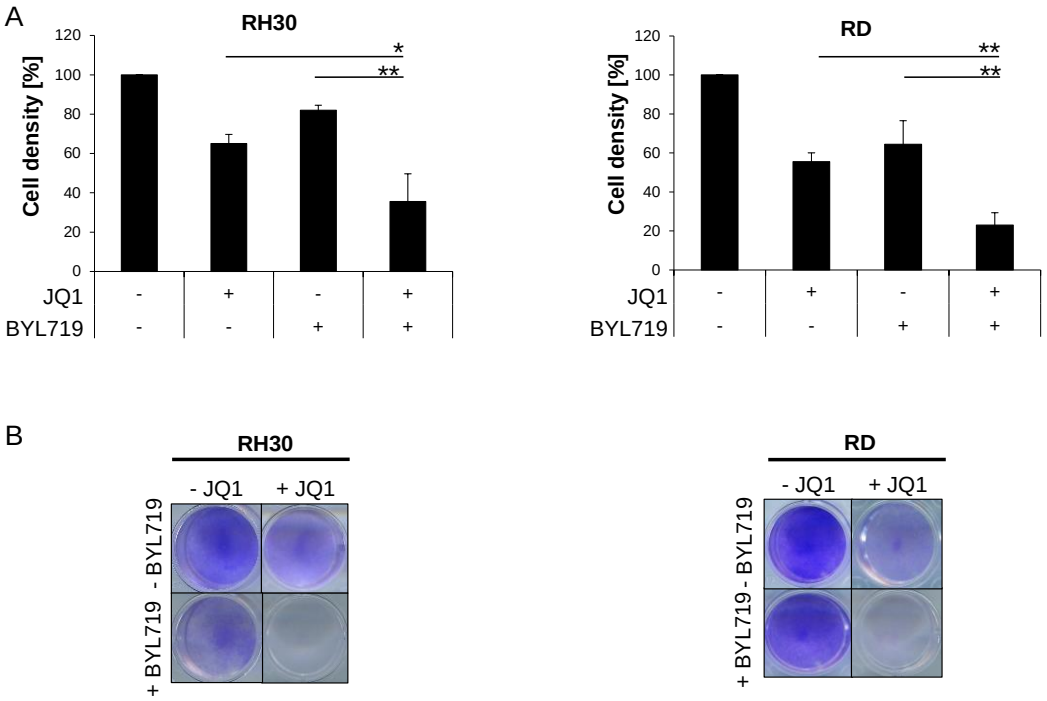

Figure 18: JQ1/BYL719 co-treatment reduces cell density of RMS cells.
(A) Cell density was measured by Crystal Violet Assay. Data are shown as mean and SD of at least three independent experiments performed in triplicate; *p<0.05; **p<0.01. (B) Representative images of crystal violet assay in RH30 and RD cells are shown.

4.2.8 JQ1/BYL719 co-treatment reduces long-term survival of RMS cells

The effects of JQ1/BYL719 co-treatment on long-term-survival was assessed by colony formation assay. Colony formation assay measures the ability of single cells to survive and attach after treatment. In RH30 cells only JQ1/BYL719 co-treatment significantly reduced long-term survival, while in RD cells JQ1 single treatment and JQ1/BYL719 co-treatment significantly reduced long-term survival, as indicated by significant reduction of colonies (Figure 19).

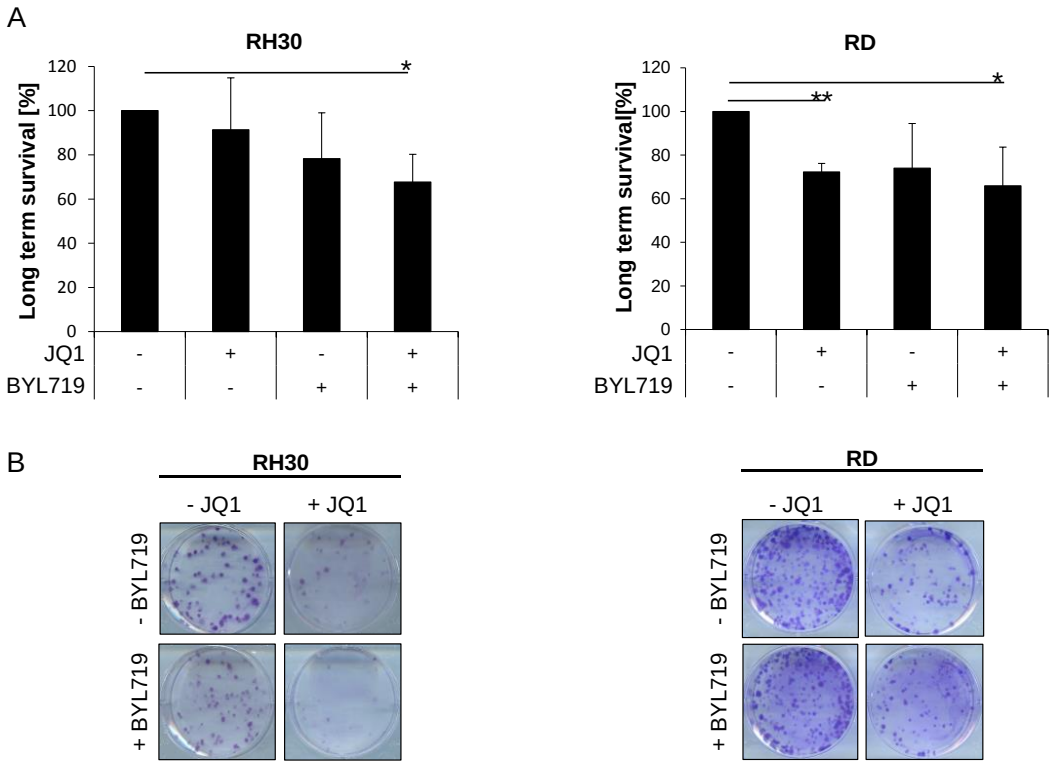

Figure 19: JQ1/BYL719 suppresses long-term survival of RH30 and RD cells. Cells were treated with 1 µM JQ1 and 10 µM BYL719 for 24 hours and colony formation was assessed after 12 days as described in 3.2.6. The number of colonies is compared to percentage of solvent-treated controls. Mean and SD of at least three independent experiments carried out in triplicates are shown; *p<0.05; **p<0.01. (B) Representative images of colony formation assay in RH30 and RD cells are shown.

4.2.9 JQ1/BYL719-mediated cell death increases over time

To further characterize molecular mechanisms of JQ1/BYL719 co-treatment induced cell death we analyzed the kinetic of cell death in RH30 and RD cells. Therefore we monitored induction of cell death determined by DNA fragmentation as typical hallmark of apoptosis after 24, 48, 72 and 96 hours. While DNA fragmentation of JQ1 or BYL719 single treatment remained comparable to control level, DNA fragmentation upon JQ1/BYL719 co-treatment increased over time till 72 hours to 47% in RH30 and to 53% RD cells. At 96 hours the DNA fragmentation increased moderately compared to 72 hours to 54% in RH30 and 54.5% in RD cells (Figure 20). Off note, we observed changes in the DNA content of cell treated with either JQ1, BYL719 or JQ1/BYL719 co-treatment in comparison to the control pointing to changes in cell cycle progression.

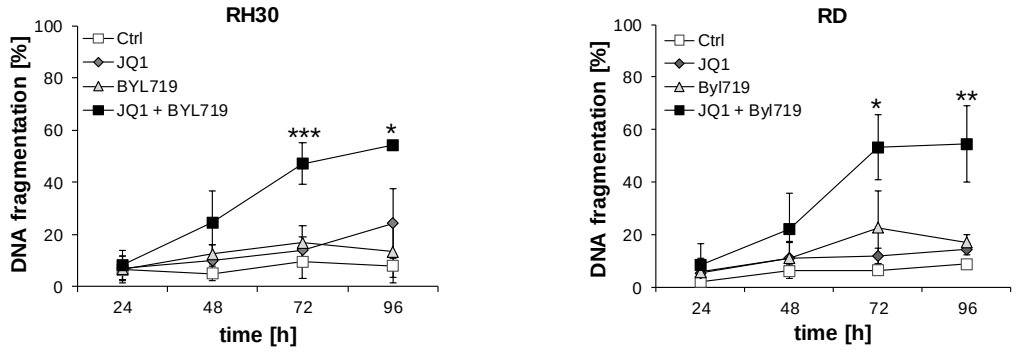

Figure 20: Kinetic of JQ1/BYL719-mediated cell death.
RMS cells were treated with 1 µM JQ1 and/or 3 µM BYL719 for the indicated time points. Apoptosis was determined by analysis of DNA fragmentation of PI-stained nuclei using flow cytometry. Data are shown as mean and SD of at least three independent experiments performed in triplicate; *p<0.05, **p<0.01, ***p<0.001

4.2.10 JQ1/BYL719 co-treatment causes G1 cell cycle arrest in RMS cells prior to cell death induction

Next, we aimed to investigate the effects of JQ1/BYL719 co-treatment on cell cycle prior to the onset of cell death. Cell cycle analysis after 24 hours of treatment with either JQ1, BYL719 or JQ1/BYL719 co-treatment revealed that single treatment with JQ1 or BYL719 alone induced G1/G0 cell cycle arrest in RH30 and RD cells. G1/G0 cell cycle arrest was further enhanced upon JQ1/BYL719 co-treatment (Figure 21).

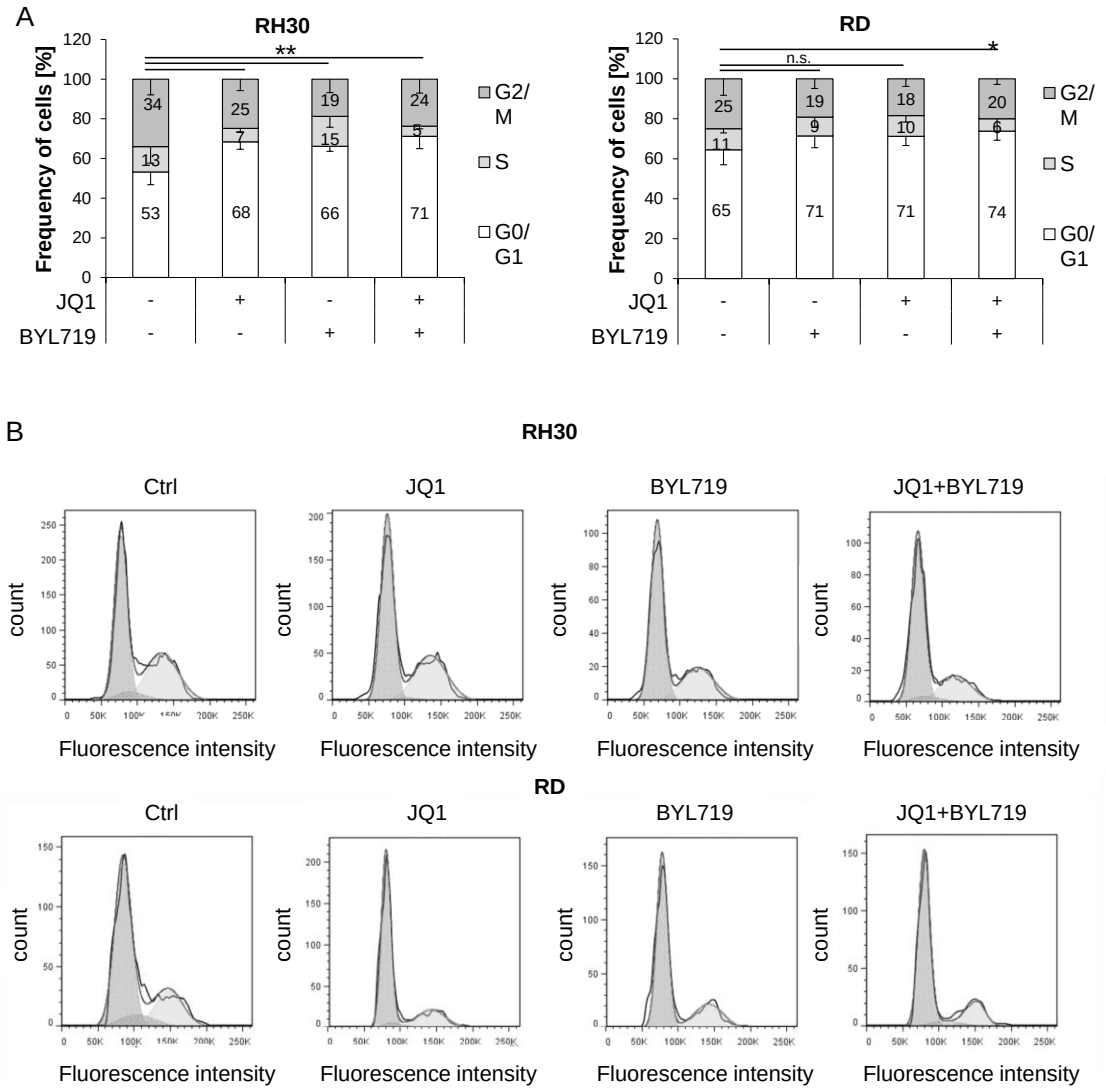

Figure 21: JQ1/BYL719 co-treatment induces G1/G0 cell cycle analysis before RMS cells undergo apoptosis.
RMS cells were treated with 1 µM JQ1 and/or 3 µM BYL719 for 24 hours. Frequency of cells per cell cycle phase was analyzed in PI-stained nuclei using flow cytometry and FlowJo software. (A) Quantitative analysis of mean and SD of at least three independent experiments performed in triplicate are shown; *p<0.05, **p<0.01, n.s. not significant comparing JQ1/BYL719-co-treated to control cells in G0/G1 phase, (B) representative histograms of frequency of cells per cell cycle phase are shown.

4.2.11 JQ1/BYL719-mediated cell death is caspase-dependent

Caspase-dependent execution of cell death is a hallmark of apoptosis. In order to investigate if JQ1/BYL719-mediated cell death is caspase-dependent, we performed caspase-3/7activity assay comparing caspase3/7 activity after treatment of RH30 and RD cells with either JQ1, BYL719 or JQ1/BYL719 co-treatment with or without the pan-caspase inhibitor zVAD.fmk. While single treatment with either JQ1 or BYL719 induced

only minor caspase activity, JQ1/BYL719 co-treatment induced pronounced caspase-3/7 activity that could be significantly rescued caspase activation by adding 50 µM of zVAD.fmk. from 39% to 6% in RH30 and in RD cells from 42% to 5% (Figure 22).

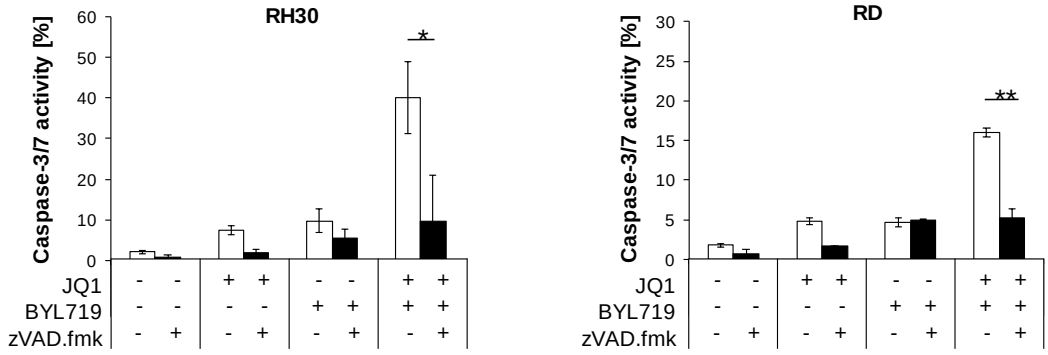

Figure 22: JQ1/BYL719 co-treatment activates caspase-3/7 in RMS cells.
RMS cells were treated with 1 µM JQ1 and/or 3 µM BYL719 in the absence and presence of 50 µM zVAD.fmk for 24 hours. Caspase-3/7 activation was detected by Cell Event Caspase-3/7 Green Detection Reagent and ImageXpress Micro XLS system Mean and SD of three experiments performed in triplicate are shown; *p<0.05; **p<0.01 comparing JQ1/BYL719-co-treated cells in the absence and presence of 50 µM zVAD.fmk.

We additionally checked if zVAD.fmk could recue RMS cells from cell death induction measured by DNA fragmentation. In line with results of caspase-3/7 activity assay addition of zVAD.fmk significantly inhibited DNA fragmentation in response to JQ1/BYL719 co-treatment as shown by reduction of DNA fragmentation from 54% to 16% in RH30 and from 52% to 17% in RD cells (Figure 23).

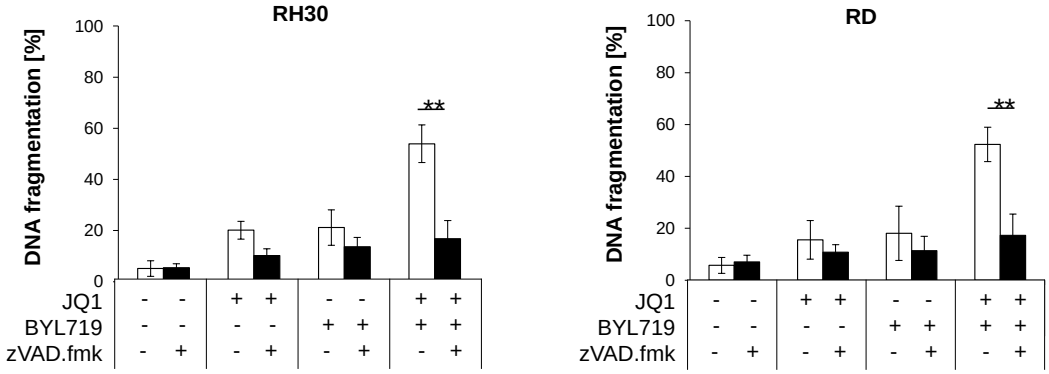

Figure 23: JQ1/BYL719 co-treatment mediated DNA fragmentation is significantly reduced upon addition of zVAD.fmk.
RMS cells were treated with 1 µM JQ1 and/or 3 µM BYL719 in the absence and presence of 50 µM zVAD.fmk for 72 hours. Apoptosis was determined analyzing DNA fragmentation of PI-stained nuclei using flow cytometry. Mean and SD of three experiments performed in triplicate are shown; *p<0.05; **p<0.01 comparing JQ1/BYL719-co-treated cells in the absence and presence of 50 µM zVAD.fmk.

4.2.12 JQ1/BYL719 co-treatment significantly induces caspase-3 activation in RD cells in CAM tumor model

Furthermore, we assessed caspase-3 activation in the CAM Assay, a well established *in vivo* model for testing of chemotherapeutics. Therefore RD cells were mixed with matrigel, implanted onto the CAM of a fertilized chicken egg and treated for three days. In result, combination of JQ1 and BYL719 induced significantly more caspase-3 positive cells in RD tumors in comparison to JQ1 or BYL719 single treatment.

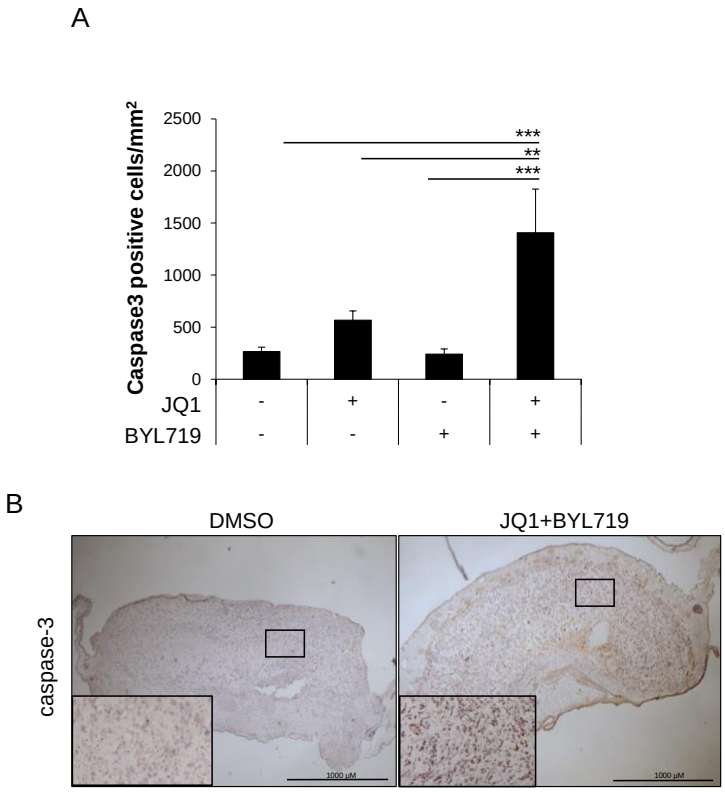

Figure 24: JQ1/BYL719 co-treatment significantly induces caspase-3 activation in RD cells in CAM tumor model.
(A) RD cells were seeded on the CAM of fertilized chicken eggs and treated with 1 µM JQ1 and/or 1 µM BYL719 for three days and caspase-3 activation was determined counting caspase-3 positive cells of paraffin sections of the CAM sections stained with cleaved caspase-3 antibody. Representative pictures and quantification of caspase-3 positive tumor cells of at least 10 tumors are shown. Mean and SEM of three independent experiments are shown; **p< 0.01, ***p< 0.001. (B) Representative pictures of RD tumor treatment with DMSO or JQ1/BYL719-cotreatment.

4.2.13 JQ1/BYL719 co-treatment induces LOMMP

Besides DNA fragmentation and caspase activation loss of mitochondrial potential is a typical feature of apoptosis. Therefore, we checked for loss of mitochondrial potential before the onset of cell death. Upon JQ1/BYL719 co-treatment slight induction of LMMP can be observed, while both single treatments show levels similar to the control. By comparison, positive control using FCCP resulted in massive LOMMP (Figure 25).

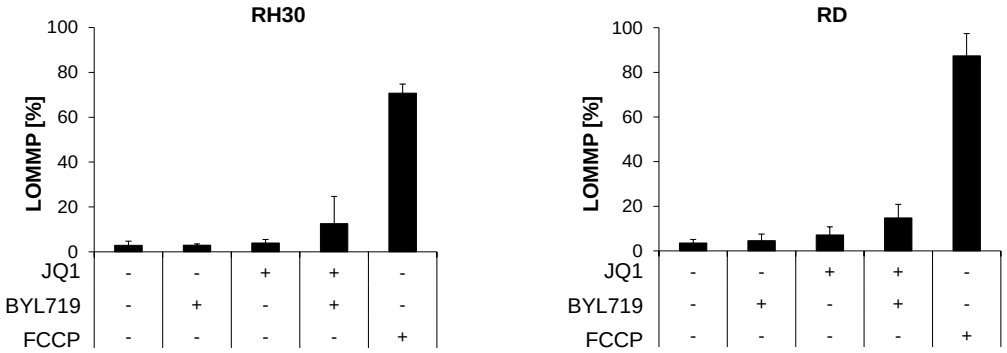

Figure 25: JQ1/BYL719 co-treatment induces loss of mitochondrial membrane potential.
RH30 and RD cells were treated with 1 µM JQ1 and/or 3 µM BYL719 for 24 hours. Loss of mitochondrial membrane potential (LOMMP) was measured by TMRM-staining and flow cytometry. 100 nM FCCP for 6 hours was used as a positive control. Mean and SD of three experiments performed in triplicate are shown.

4.3 JQ1/BYL719 co-treatment shifts the ratio of pro- and antiapoptotic BCL-2 family proteins towards apoptosis

4.3.1 RNA Sequencing of RH30 cells treated with JQ1, BYL719 or JQ1/BYL719 co-treatment reveals transcriptional changes of BCL-2 family proteins

Since we observed cooperative induction of apoptosis, we wanted to learn more about the underlying molecular mechanism. As an unbiased approach, we performed RNA-Sequencing using RH30 cells treated with either JQ1, BYL719 or JQ1/BYL719 co-treatment for 24 hours. Venn diagram of differentially expressed genes (DEG) (p-adj <0.01) as calculated using DESeq2 package revealed 1416 DEGs upon JQ1 treatment in comparison to the control while BYL719 treatment had only minor effects on gene expression inducing 101 DEGs. Upon JQ1/BYL719 co-treatment we observed 620 new DEGs neither present after JQ1 or BYL719 treatment (Figure 26). In line with our previous observation of hallmarks of apoptosis, we recognized differential gene expression of genes encoding BCL-2 proteins family members such as *BMF* and *BBC3* encoding the protein PUMA upon BYL719 and JQ1/BYL719 co-treatment. Upon JQ1 or JQ1/BYL719 co-treatment *BCL2L11* encoding BIM, *PMAIP1* encoding NOXA and *BCL2L1* encoding BCL-x_L were differentially expressed compared to the control (p-adj < 0.01) (Figure 26).

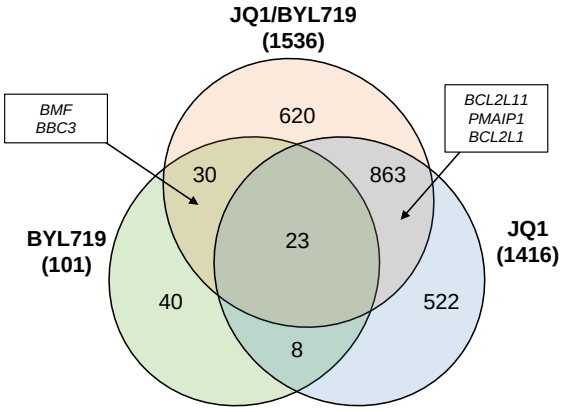

Figure 26: RNA Sequencing of RH30 cells treated with JQ1, BYL719 or JQ1/BYL719 co-treatment.
Venn diagram showing the overlap of differentially expressed genes after JQ1 and BYL719 single treatment or JQ1/BYL719 co-treatment (p-adj < 0.01) as calculated using DESeq2. RH30 cells were treated with solvent alone, 1 µM JQ1, 3 µM BYL719 or JQ1/BYL719 co-treatment for six hours and gene expression was analyzed by RNA-Seq. Experiments were performed in independent triplicates for each treatment.

4.3.2 JQ1/BYL719 co-treatment alters gene expression of pro- and antiapoptotic BCL-2 family proteins in favor of apoptosis

Next, we had a closer look at apoptosis promoting genes. JQ1 alone or in combination with BYL719 significantly increased gene expression of proapoptotic genes namely *BCL2L11* (BIM), *PMAIP1* (NOXA) and *BBC3* (PUMA), while BYL719 alone or in combination with JQ1 induced BMF and *BBC3* (PUMA) (log2FC>1) (Figure 27A). Additionally JQ1 and JQ1/BYL719 co-treatment significantly reduced levels of anti-apoptotic *BCL2L1* (BCL-x_L) (log2FC>I1I), while effects *on MCL-1, BCL2L2* and *BCL2* by JQ1, BYL719 or JQ1/BYL719 co-treatment were minor (log2FC<I1I) (Figure 27B).

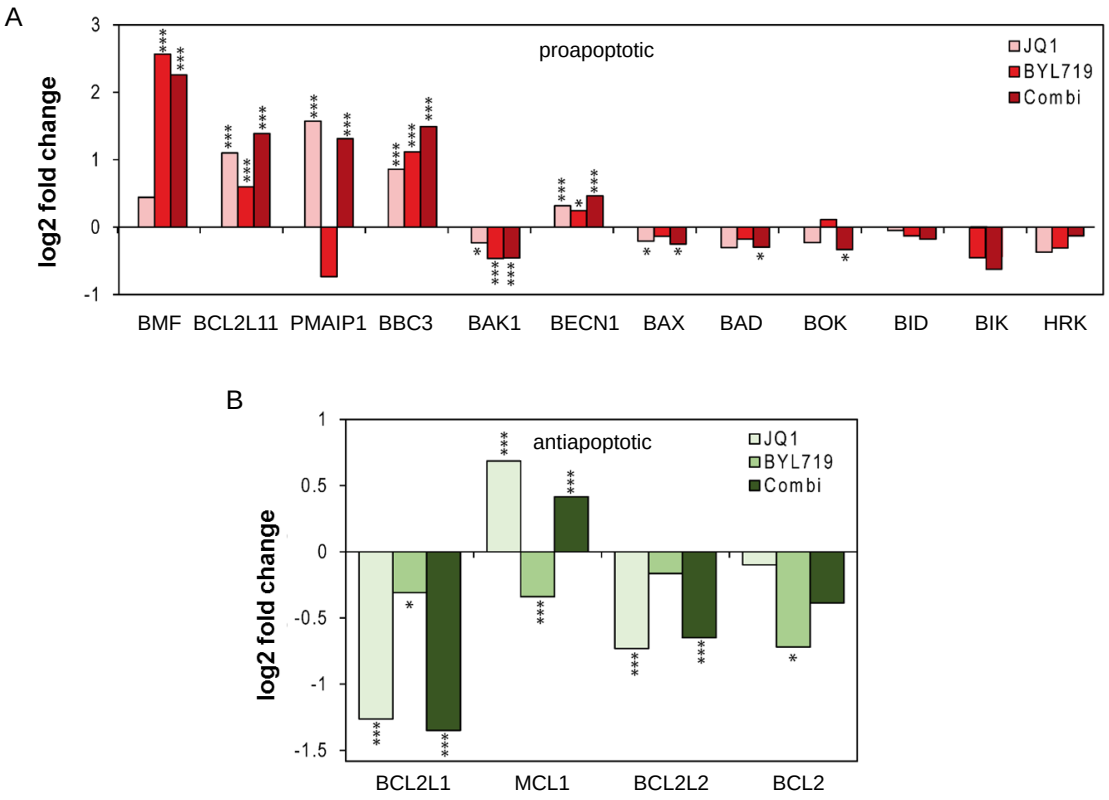

Figure 27: JQ1/BYL719 co-treatment alters gene expression of pro- and antiapoptotic BCL-2 family proteins in favor of apoptosis.
(A) Log2 fold expression levels of proapoptotic BCL-2 proteins obtained from RNA-Seq results normalized to control treatment of three independent experiments. Significance is depicted as adjusted p-value (*p<0.05; **p<0.01; ***p<0.001). (B) Log2 fold expression levels of antiapoptotic BCL-2 proteins obtained from RNA-Seq analysis normalized to control treatment of three independent experiments. Significance is depicted as adjusted p-value (*p<0.05; **p<0.01; ***p<0.001).

4.3.3 JQ1/BYL719 co-treatment shifts the overall gene expression of BCL-2 protein family members towards apoptosis

To better picture changes in the balance of pro- and antiapoptotic gene expression upon JQ1/BYL719 co-treatment, changes of overall pro- and overall antiapoptotic gene expression were visualized by boxplot, revealing a trend towards the proapoptotic side upon JQ1/BYL719 co-treatment (Figure 28).

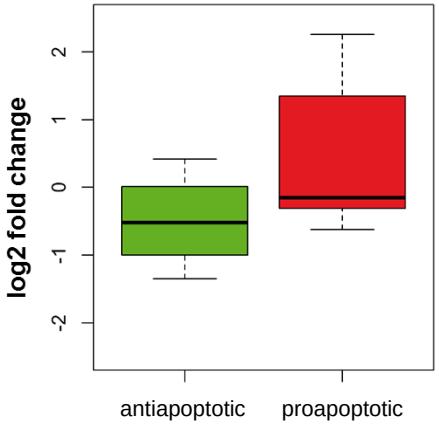

Figure 28: JQ1/BYL719 co-treatment shifts the overall gene expression of BCL-2 protein family members towards apoptosis.
Boxplots showing expression values obtained from RNA-Seq results of pro- and antiapoptotic BCL-2 proteins after JQ1/BYL719 co-treatment, normalized to control treatment.

4.3.4 JQ1/BYL719 co-treatment alters gene and protein expression of pro- and antiapoptotic BCL-2 family proteins in favor of apoptosis

In order to confirm the RNA-Seq results and to verify our observation for another cell line, we performed qRT-PCR and Western Blot analysis upon JQ1, BYL719 or JQ1/BYL719 co-treatment after 6 and 20 hours in RH30 and RD cells. Therefore we focused on pro- and antiapoptotic genes with a log2 FC>I1I. qRT-PCR confirms significant upregulation of BMF mRNA upon combination in RH30 and RD cells. Interestingly, the increase in BMF mRNA is more pronounced upon JQ1/BYL719 co-treatment compared to single treatment (Figure 29). Upon JQ1 or JQ1/BYL719 co-treatment RH30 and RD cells show upregulation of NOXA. However, this upregulation upon JQ1/BYL719 co-treatment is only significant in RH30 cells (Figure 29). For PUMA mRNA results showed a large variation and could not confirm increased PUMA mRNA levels, seen in the RNA-Seq. In line with RNA-Seq data, JQ1 or JQ1/BYL719 co-treatment upregulates gene expression of BIM mRNA accompanied by downregulation of BCL-x_L mRNA (Figure 29, Figure 30).

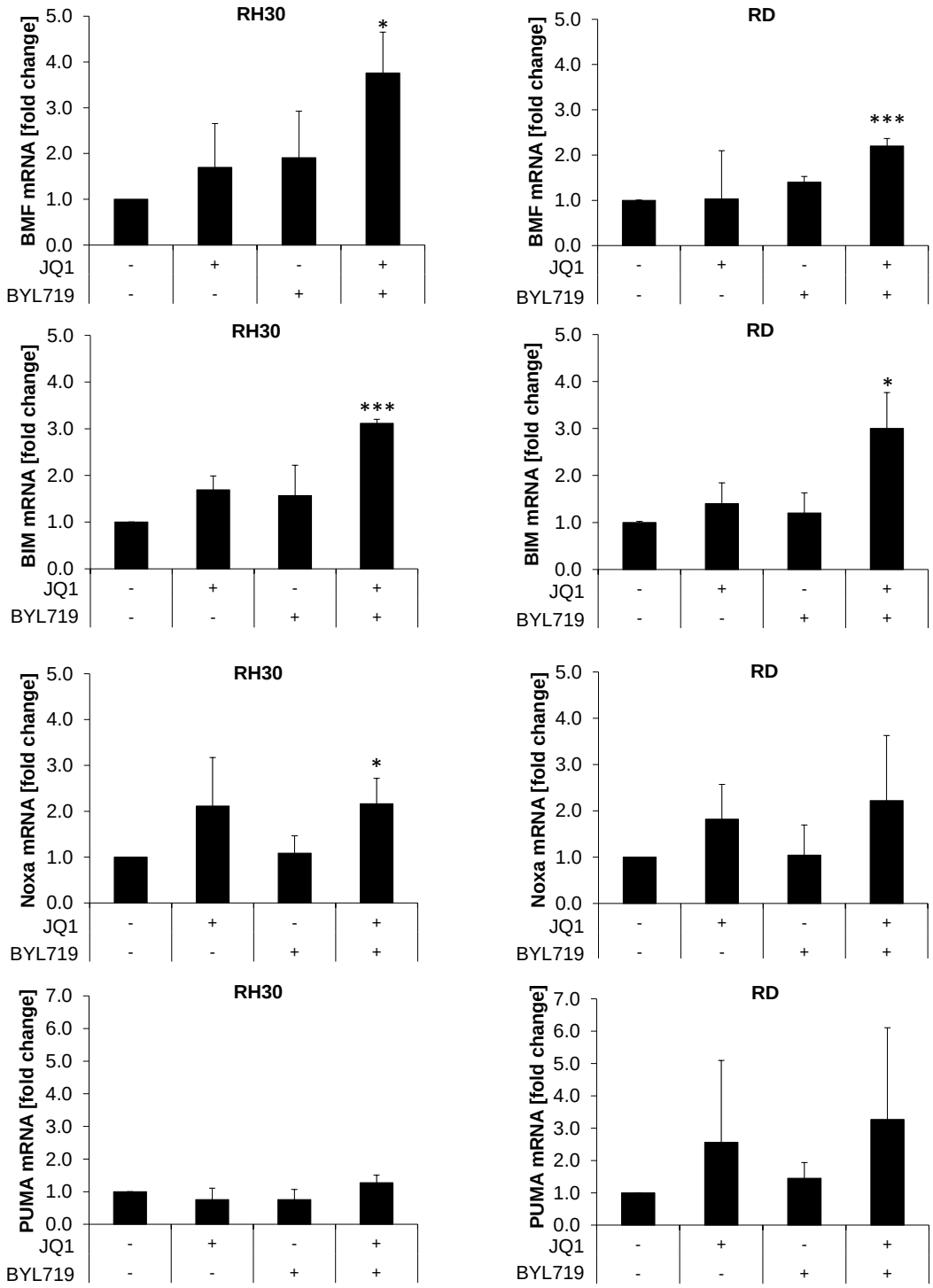

Figure 29: JQ1/BYL719 co-treatment significantly induces mRNA expression of pro-apoptotic BMF, BIM and NOXA mRNA in RH30 and RD cells.
RMS cell were treated with 1 µM JQ1 and/or 3 µM BYL719 for six hours, mRNA levels of BMF, BIM and NOXA were analyzed by qRT-PCR and fold changes compared to untreated control are shown with mean and SD of three independent experiments performed in duplicate; *p<0.05; ***p<0.001.

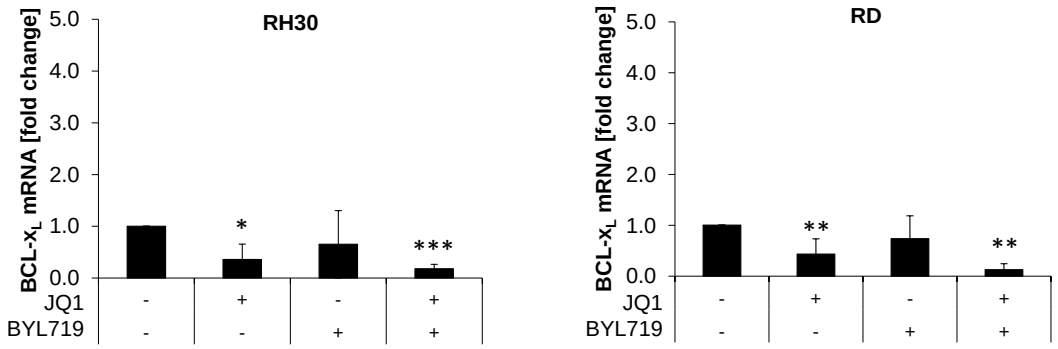

Figure 30: JQ1/BYL719 co-treatment significantly reduces mRNA expression of anti-apoptotic BCL-x_L mRNA in RH30 and RD cells.
RMS cell were treated with 1 µM JQ1 and/or 3 µM BYL719 for six hours, mRNA levels of BCL-x_L were analyzed by qRT-PCR and fold changes compared to untreated control are shown with mean and SD of three independent experiments performed in duplicate; *p<0.05; **p<0.01; ***p<0.001.

Next, we were interested how the observed transcriptional changes of BCL-2 protein members effected protein levels prior to induction of cell death. Western Blot after 20 hours treatment confirms no marked changes on protein levels of BCL-2 and MCL-1 (Figure 31). In line with transcriptional pattern, protein levels of BCL-x_L are reduced and BIM levels are increased upon treatment with JQ1 or JQ1/BYL719 co-treatment (Figure 31). Interestingly only upon JQ1/BYL719 co-treatment we observe massive induction of BMF, while constitutive BMF levels in untreated control are very low. Both, single treatments only induce low levels of BMF fitting to the qRT-PCR data (Figure 29, Figure 30, Figure 31A). Protein levels of NOXA were decreased upon JQ1/BYL719 co-treatment in RH30 and upon JQ1 or JQ1/BYL719 co-treatment after 20 hours. Since NOXA is a short-lived protein, we checked for NOXA protein levels after 6 hours of treatment. At this early time point NOXA was upregulated upon JQ1 or JQ1/BYL719 co-treatment in RH30 cells, while RD cells showed no regulation of NOXA upon treatment (Figure 31B).

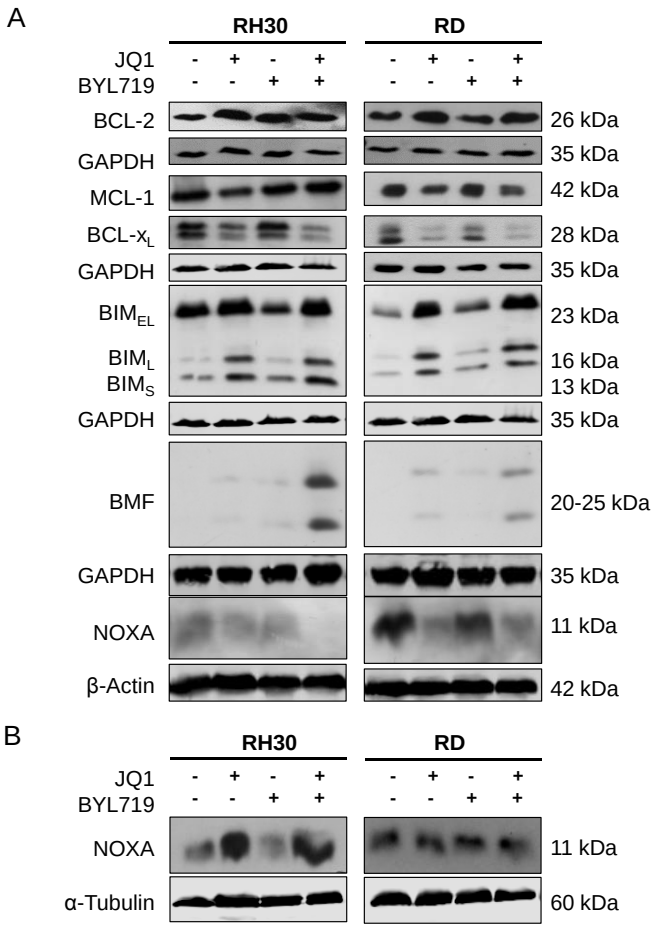

Figure 31: JQ1/BYL719 co-treatment significantly induces protein expression of pro-apoptotic BMF, BIM and NOXA mRNA in RH30 and RD cells.
RMS cells were treated with solvent alone, 1 µM JQ1, 3 µM BYL719 or JQ1/BYL719 co-treatment for 20 hours (A) or six hours (B) and protein expression was determined by Western blotting, GAPDH, β-Actin or α-Tubulin served as loading controls. Representative blots of two experiments are shown.

4.4 JQ1/BYL719 co-treatment induces reallocation of BRD4 and stimulates BRD4 enrichment at regulatory elements of BH3-only proteins

4.4.1 JQ1/BYL719 co-treatment induces reallocation of BRD4 to chromatin

To gain further insight into the upstream mechanisms resulting in JQ1/BYL719-triggered apoptosis, we performed BRD4 ChIP-Seq in RH30 cells. While JQ1 alone – as expected – reduced BRD4 binding to transcriptional start sites (TSS), addition of BYL719 reconstituted BRD4 binding to TSS to a similar level compared to the control (Figure 32).

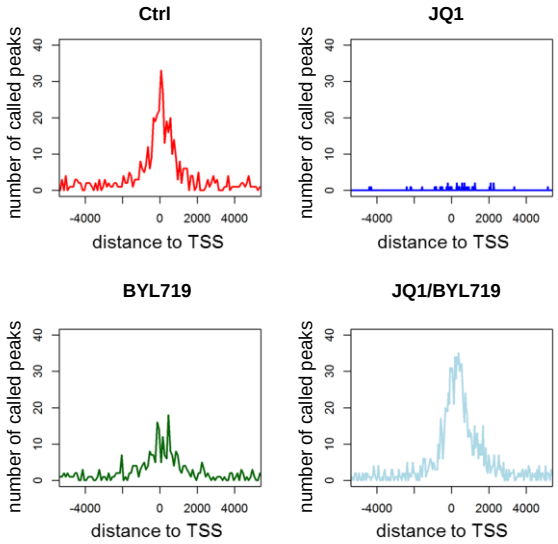

Figure 32: Distribution of BRD4 binding sites around gene transcriptional start sites after treatment with either JQ1, BYL719 or JQ1/BYL719 co-treatment.
RH30 cells were treated with solvent alone, 1 µM JQ1, 3 µM BYL719 or JQ1/BYL719 co-treatment for 24 hours followed by BRD4 ChIP-Seq performed in three independent experiments. Distribution of BRD4 binding sites around gene TSS of called peaks under untreated conditions and after treatment with 1 µM JQ1, 3 µM BYL719 or JQ1/BYL719 co-treatment for 24 hours.

More precisely, after treatment with solvent control 2031 BRD4 peaks were called. JQ1 alone reduced called BRD4 peaks from 2031 to 131 BRD4 peaks. Unexpectedly, BYL719 altered BRD4 binding to chromatin resulting in 1495 BRD4 peaks including 231 binding sites neither present in the control nor after JQ1 treatment. Upon JQ1/BYL719 co-treatment 3245 BRD4 peaks were called including 1707 new BRD4 binding sites, highlighting the reallocation of BRD4 to new binding sites (Figure 33).

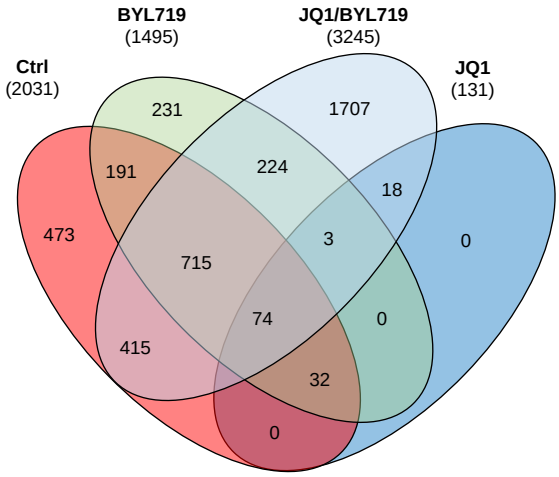

Figure 33: Overlap between called BRD4 peaks from the control and after treatment with either JQ1, BYL719 or JQ1/BYL719 co-treatment.
RH30 cells were treated with solvent alone, 1 µM JQ1, 3 µM BYL719 or JQ1/BYL719 co-treatment for 24 hours followed by BRD4 ChIP-Seq performed in three independent experiments. Venn diagram showing the overlap between called peaks from the control, JQ1, BYL719 or JQ1/BYL719 co-treatment. BRD4 ChIP-Seq peaks were counted, if they were detected in all three independent experiments per treatment.

To further investigate the reallocation of BRD4 in response to JQ1/BYL719 co-treatment, we analyzed the relative genomic distribution of BRD4 to different transcriptional regulatory elements. Interestingly, the relative distribution after JQ1/BYL719 co-treatment was similar to the pattern detected after JQ1 alone. After JQ1 or JQ1/BYL719 co-treatment more than 40% of BRD4 binding sites occurred at promoter sites compared to 22% of BRD4 binding sites at promoter sites under untreated conditions, highlighting the change in the relative genomic distribution of BRD4 binding (Figure 34). Taken together these results show, that JQ1/BYL719 co-treatment induces *de novo* BRD4 binding sites and reallocates BRD4 to chromatin (Figure 32-Figure 34).

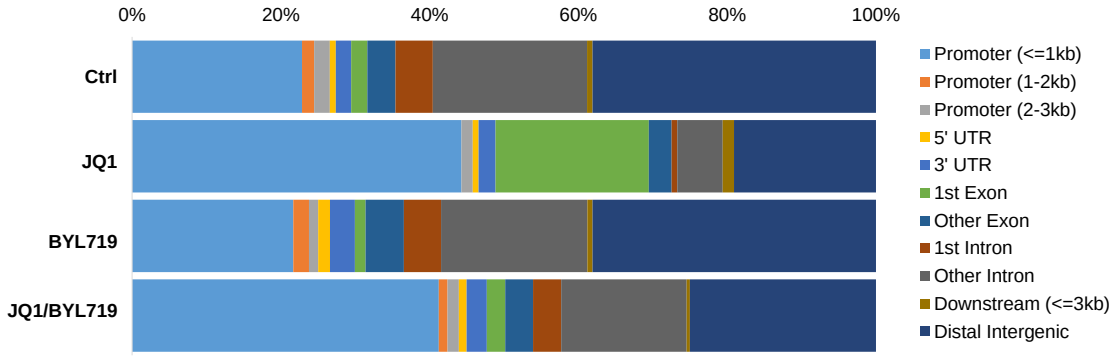

Figure 34: Relative genomic distribution of BRD4 binding sites of control cells, cells treated with JQ1, BYL719 or JQ1/BYL719 combination.
RH30 cells were treated with solvent alone, 1 µM JQ1, 3 µM BYL719 or JQ1/BYL719 co-treatment for 24 hours followed by BRD4 ChIP-Seq performed in three independent experiments. The percentage of sites in each genomic class is indicated.

4.4.2 JQ1/BYL719 co-treatment stimulates BRD4 enrichment at regulatory elements of BH3-only proteins

Next, we investigated BRD4 abundance at transcriptional regulatory elements previously described for ARMS [12], focusing on genes of BH3-only proteins *BMF*, *BCL2L11* (BIM) and *PMAIP1* (NOXA), that were transcriptionally upregulated upon JQ1/BYL719 co-treatment. JQ1/BYL719 co-treatment caused BRD4 enrichment at the super-enhancer of *BMF*, the super-enhancer, typical enhancer and promoter regions of *BCL2L11* (BIM) and the promotor of *PMAIP1* (NOXA) (Figure 35). The lack of BRD4 enrichment at other genomic regions, e.g. *PTORQ, CDH6*, *ARFGEF3* rather excludes that BRD4 enrichment is a general phenomenon but more a gene-specific phenomenon (Figure 36). Still, BRD4 was enriched at many other genomic regions that were not the focus of this study as shown by 1707 *de novo* BRD4 binding sites (Figure 33).

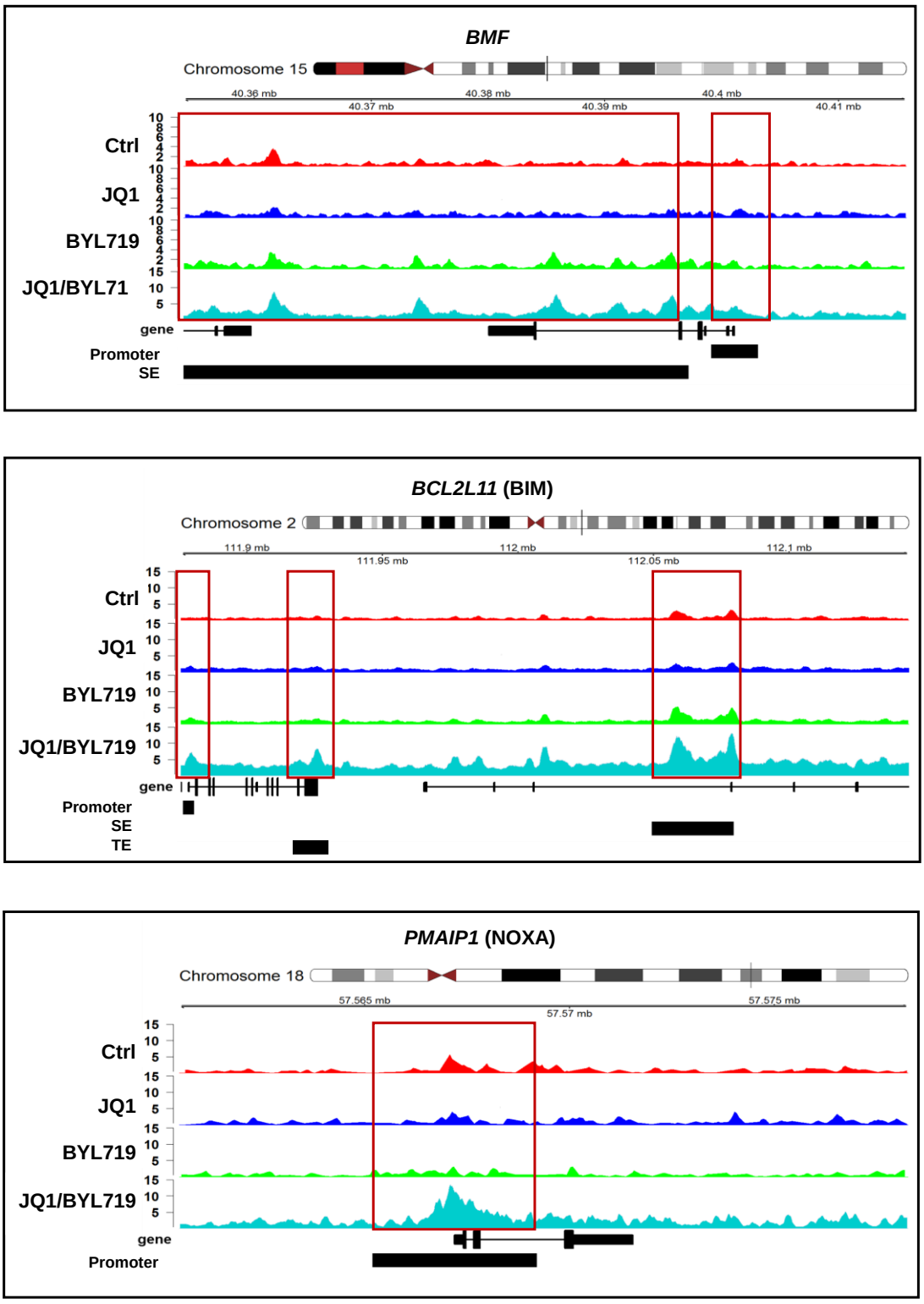

Figure 35: BRD4 reallocates to regulatory elements of BH3-only genes.
RH30 cells were treated with solvent alone, 1 µM JQ1, 3 µM BYL719 or JQ1/BYL719 co-treatment for 24 hours followed by BRD4 ChIP-Seq performed in three independent experiments. ChIP-Seq tracks depict BRD4 occupancy at indicated promoters and/or typical enhancers (TE) and/or super-enhancers (SE).

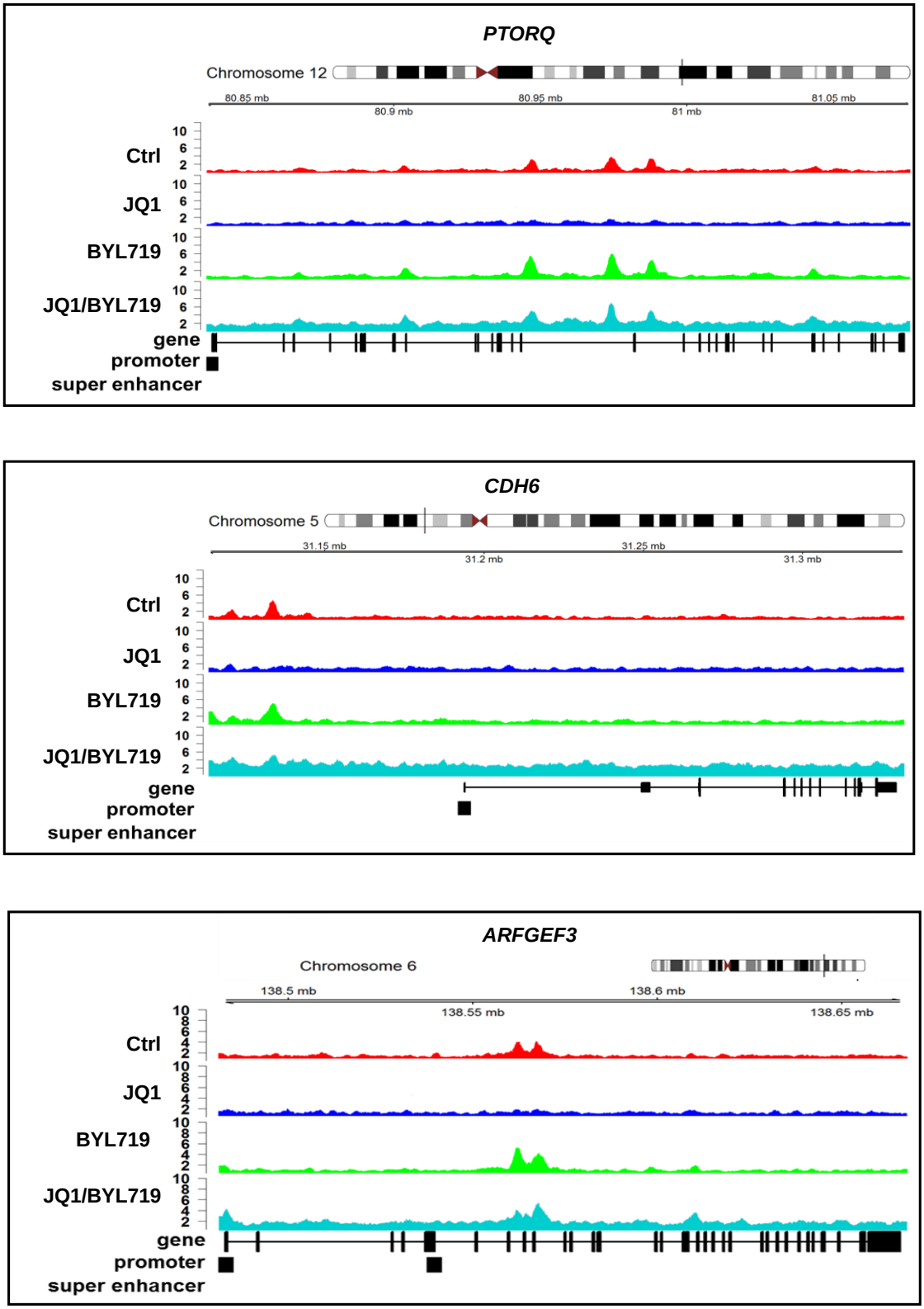

Figure 36: BRD4 does not enrich at genomic regions e.g. PTORQ, CDH6 or ARGEF3.
RH30 cells were treated with solvent alone, 1 µM JQ1, 3 µM BYL719 or JQ1/BYL719 co-treatment for 24 hours followed by BRD4 ChIP-Seq performed in three independent experiments. ChIP-Seq tracks depict BRD4 occupancy at indicated promoters.

4.4.3 JQ1/BYL719 co-treatment induces phosphorylation of BRD4 at Ser484/488

Since gene-specific chromatin binding of BRD4 has been reported to be caused by BRD4 phosphorylation at Ser484/488 [108, 110, 134], we next checked for p-BRD4$^{S484/488}$. Indeed, we observed marked increase of p-BRD4$^{S484/488}$ upon JQ1/BYL719 co-treatment, while single treatment with either JQ1 or BYL719 had only minor effects. Total BRD4 levels remained unchanged upon all conditions (Figure 37).

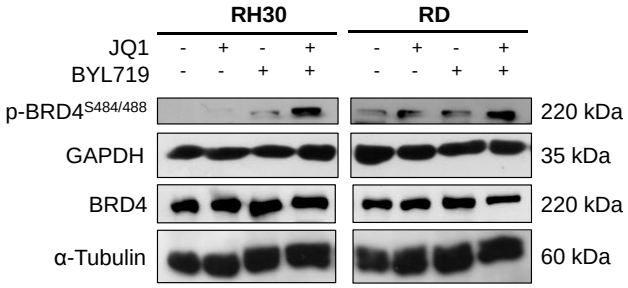

Figure 37: JQ1/BYL719 co-treatment induces phosphorylation of BRD4 at Ser484/488.
RH30 and RD cells were treated with solvent alone, 1 µM JQ1, 3 µM BYL719 or JQ1/BYL719 co-treatment for 24 hours and protein levels were detected by Western blotting; α-Tubulin or GAPDH served as loading controls.

4.4.4 BYL719 alone or JQ1/BYL719 co-treatment inhibit PI3K signaling similarly

Combination of JQ1 with PI3K inhibitors has been reported to be synergistic previously, since single treatment with PI3K inhibitors might fail due to compensatory feedback loops [228, 229]. Additionally, compensatory upregulation of other PI3K isoforms might limit the efficiency of isoform-specific inhibitors such as BYL719 [230, 231]. Therefore, we were interested if BYL719 alone succeeds to inhibit PI3K signaling and if JQ1/BYL719 co-treatment could increase this suppression. In result, both, BYL719 and JQ1/7BYL719 co-treatment resulted in similar inhibition of PI3K signaling as shown by similar reduction of p-AKT^{T308} (Figure 38).

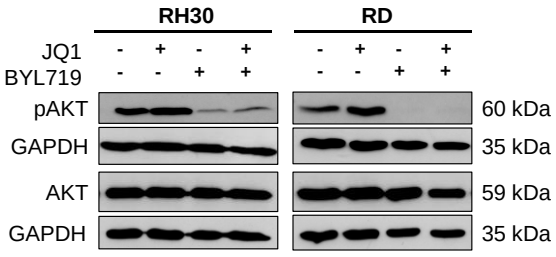

Figure 38: JQ1/BYL719 co-treatment reduces p-AKT^{T308}.
RH30 and RD cells were treated with solvent alone, 1 µM JQ1, 3 µM BYL719 or JQ1/BYL719 co-treatment for 24 hours and protein levels of p-AKT^{T308} and AKT were detected by Western blotting; GAPDH served as loading control.

4.4.5 Integration of RNA-Seq and BRD4 ChIP-Seq data

To investigate the functional relevance of BRD4 reallocation, we integrated RNA-Seq and ChIP-Seq data to link changes in BRD4 binding to altered gene expression. JQ1 treatment caused loss of 234 BRD4 peaks with corresponding changes in gene expression (log2 FC>I0.58I) in comparison to the control, while only 45 new peaks with altered gene expression emerged. Unexpectedly, BYL719 single treatment resulted in 63 new transcriptionally relevant (log2 FC>I0.58I) BRD4 binding sites. JQ1/BYL719 co-treatment resulted in 773 *de novo* BRD4 peaks with altered gene expression, while only 23 new BRD4 peaks with corresponding alterations in gene expression (log2 FC>I0.58I) disappeared. The *de novo* peaks upon JQ1/BYL719 co-treatment included proapoptotic genes such as BCL2L11 and PMAIP1 (Figure 39). Taken together this points to the generation of transcriptional relevant *de novo* BRD4 peaks.

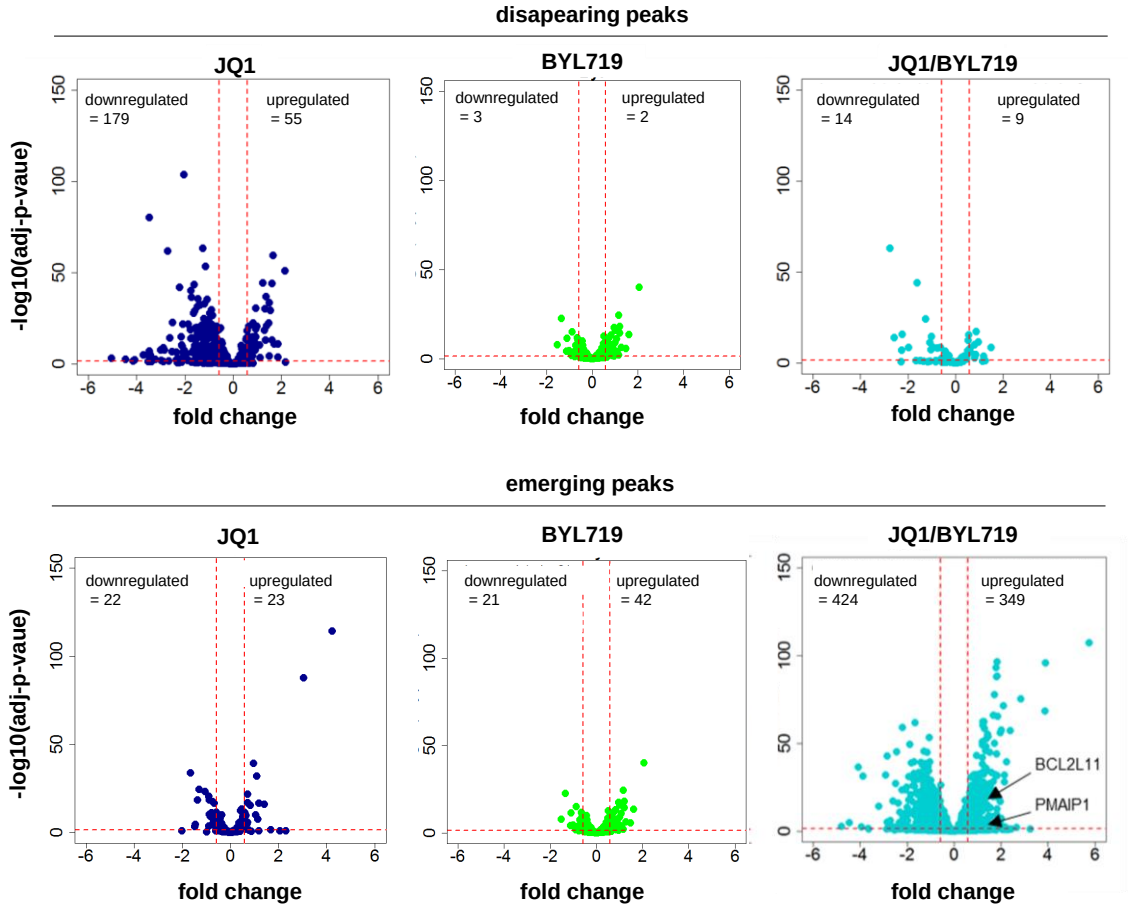

Figure 39: BRD4 binding is associated with altered gene expression.
RH30 cells were treated with solvent alone, 1 µM JQ1, 3 µM BYL719 or JQ1/BYL719 co-treatment for 24 hours followed by BRD4 ChIP-Seq performed in three independent experiments. Volcano blots of called BRD4 peaks with corresponding log2 FC>I0.58I.

4.4.6 Integration of BRD4 promotor peaks and gene expression

Since binding to the promotor of genes is directly associated with altered gene expression, we next focused on loss or gain of BRD4 promotor peaks with altered gene expression (log2 FC>I0.58I). While JQ1 treatment alone resulted in 95 and BYL719 in 70 alterations of BRD4 promotor binding with corresponding changes in gene expression (log2 FC>I0.58I), JQ1/BYL719 co-treatment resulted in 761 changes of BRD4 binding to promotor and corresponding changes in gene expression (log2 FC>I0.58I) (Figure 40).

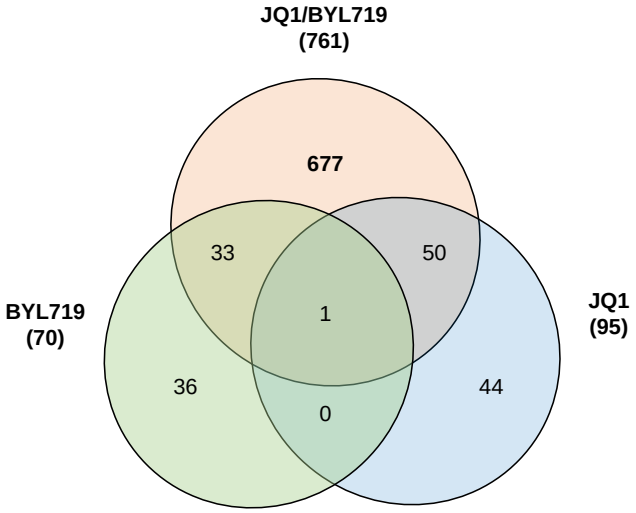

Figure 40: BRD4 promotor peaks integrated with altered gene expression.
RH30 cells were treated with solvent alone, 1 µM JQ1, 3 µM BYL719 or JQ1/BYL719 co-treatment for 24 hours followed by BRD4 ChIP-Seq performed in three independent experiments. Venn diagram showing the overlap between called peaks from the control, JQ1, BYL719 or JQ1/BYL719 co-treatment.

To gain further insight into the processes that are influenced by gene expression linked to BRD4 promotor binding, we performed Gene Ontology (GO) focusing on the category “Biological Process” as one of the three categories of gene ontology. GO analysis of genes containing BRD4 promoter peaks with corresponding log2 FC>I0.58I showed no significant enrichment of gene sets upon JQ1 or BYL719 single treatment. Only upon JQ1/BYL719 co-treatment significant enrichment of GO gene sets belonging to transcriptional regulation from RNA Pol II promoter as indicated by –log(p-adj)>2 (Figure 41). As BRD4 participates in the control of RNA Pol II, this further highlights a functional relevance of the additional BRD4 peaks after combination treatment.

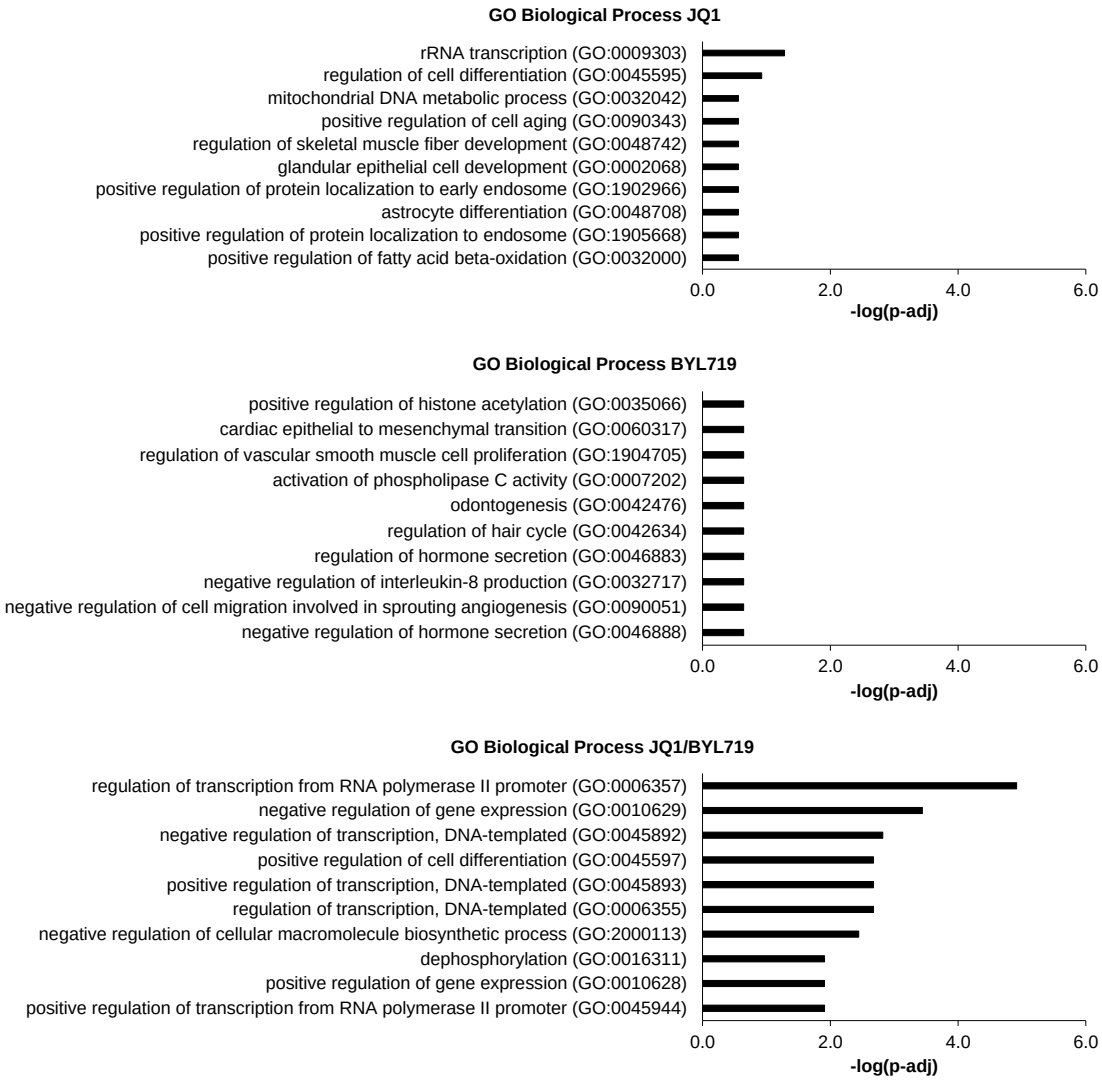

Figure 41: Gene Ontology "Molecular Function".
RH30 cells were treated with solvent alone, 1 µM JQ1, 3 µM BYL719 or JQ1/BYL719 co-treatment for 24 hours followed by BRD4 ChIP-Seq performed in three independent experiments. Bar chart showing results from GO "Molecular function".

4.5 BIM, NOXA and BMF contribute to JQ1/BYL719-induced apoptosis

To validate the functional relevance of the increase of proapoptotic proteins for JQ1/BYL719-mediated apoptosis, we performed knockdown experiments using three distinct siRNA sequences targeting mRNA of BIM, NOXA and BMF. To this end, we performed reverse knockdown targeting the respective BH3-only protein, followed by JQ1/BYL719 co-treatment. BIM and NOXA knockdown was confirmed by Western Blotting of untreated cells incubated with siRNA harvested at the time point of cell death measurement (Figure 42A, Figure 43A). siRNA against BIM reduced BIM protein levels accompanied by significant reduction of cell death for all three distinct siRNA sequences (Figure 42A+B). Knockdown of NOXA reduced NOXA protein levels although low levels of NOXA were still detectable after knockdown with all three constructs (Figure 43A). JQ1/BYL719-mediated cell death was reduced after all three siRNA constructs targeting NOXA. However, this reduction was only significant for siRNA construct #1 and #3 (Figure 43B).

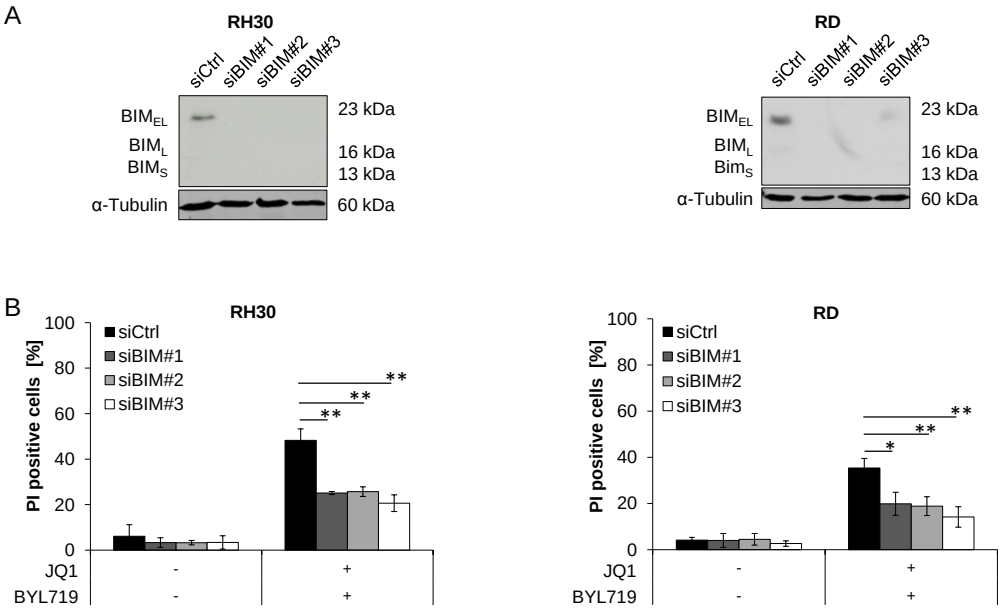

Figure 42: BIM knockdown rescues from JQ1/BYL719-mediated apoptosis.
RMS cells were transiently transfected for 24 hours with 20 nM SilencerSelect non-silencing siRNA or siRNA targeting BIM and then treated as indicated for 72 hours. (A) At the timepoint of cell death measurement protein levels were detected by Western blotting; α-Tubulin served as loading controls. (B) Cell death was determined by analysis of PI/Hoechst staining and ImageXpress Micro XLS system; mean and SD of at least three independent experiments performed in triplicate are shown; *p<0.05; **p<0.01.

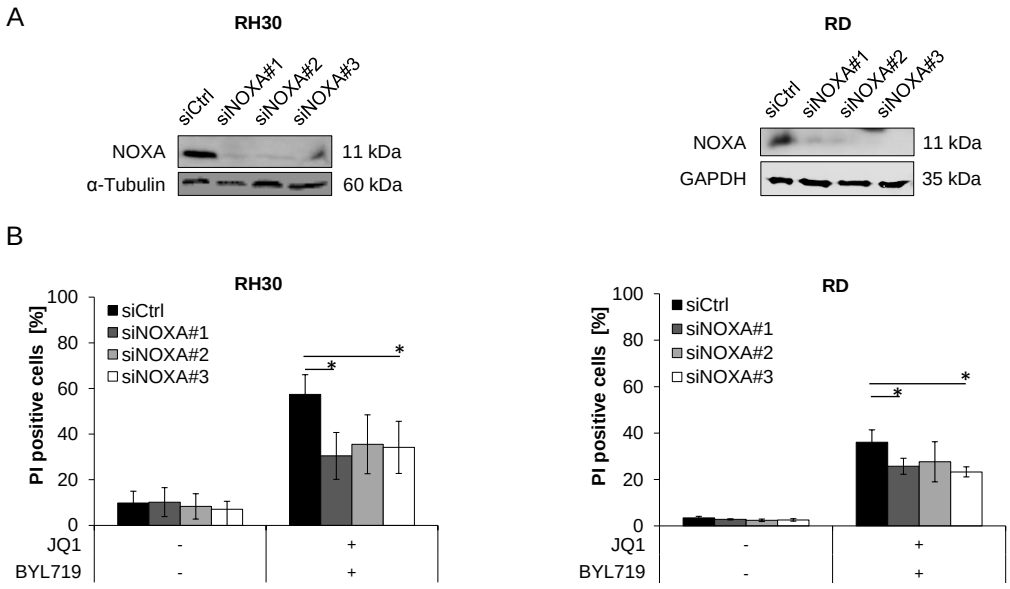

Figure 43: NOXA knockdown rescues from JQ1/BYL719-mediated apoptosis.
RMS cells were transiently transfected for 24 hours with 20 nM SilencerSelect non-silencing siRNA or siRNA targeting NOXA and then treated as indicated for 72 hours. (A) At the time point of cell death measurement, protein levels were were detected by Western blotting; α-Tubulin or GAPDH served as loading controls. (B) Cell death was determined by analysis of PI/Hoechst staining and ImageXpress Micro XLS system; mean and SD of at least three independent experiments performed in triplicate are shown; *p<0.05.

Since BMF levels are constitutively too low to be detected by Western Blotting, we performed BMF knockdown, followed by 24 hours JQ1/BYL719 co-treatment before harvesting, to check if siRNA against BMF prevents from BMF induction upon JQ1/BYL719 co-treatment (Figure 44A). Knockdown of BMF prevented RMS cells from BMF induction upon JQ1/BYL719 co-treatment and significantly reduced JQ1/BYL719-mediated cell death (Figure 44). Taken together these results indicate, that the BH3-only proteins BIM, NOXA and BMF are functionally relevant for JQ1/BYL719-mediated apoptosis.

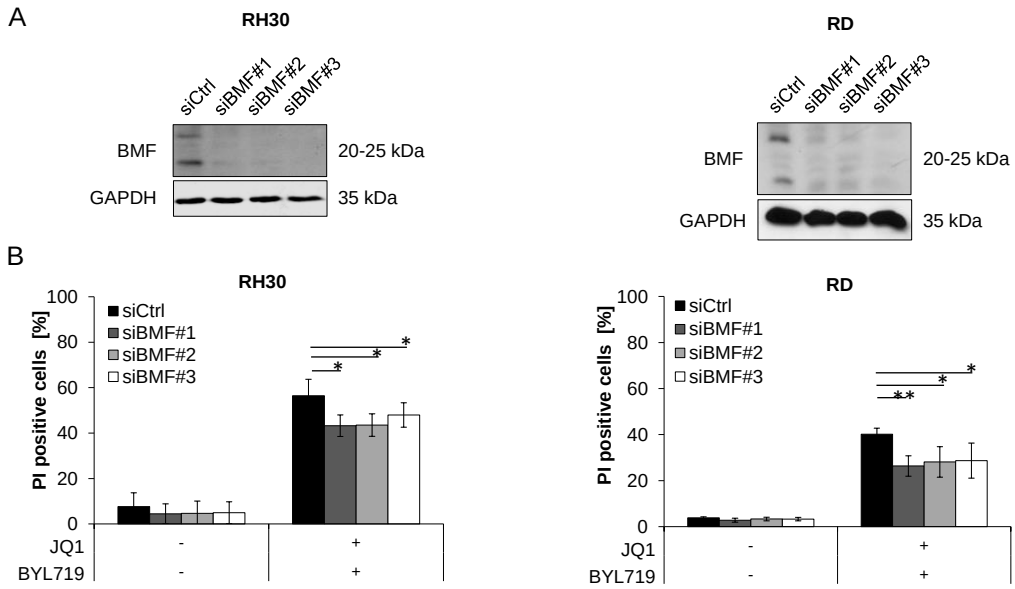

Figure 44: BMF knockdown rescues from JQ1/BYL719-mediated apoptosis.
RMS cells were transiently transfected for 24 hours with 20 nM SilencerSelect non-silencing siRNA or siRNA targeting BMF and then treated as indicated for 72 hours. (A) For Western Blot analysis of transient knockdown of BMF by siRNA, cells were reversely transfected with 20 nM SilencerSelect siRNA (Invitrogen) and the medium was exchanged six hours after transfection followed by a 24 hour JQ1/BYL719 co-treatment before harvesting, protein levels were detected by Western blotting; GAPDH served as loading controls. (B) Cell death was determined by analysis of PI/Hoechst staining and ImageXpress Micro XLS system; mean and SD of at least three independent experiments performed in triplicate are shown; *p<0.05; **p<0.01.

4.6 RMS cells are initially primed for apoptosis

Since intrinsic apoptosis is mediated by neutralization of antiapoptotic BCL-2 proteins, we next immunoprecipitated BCL-2, BCL-$_{XL}$ and MCL-1 and checked for interaction with the BH3-only proteins BIM and NOXA in RH30 and RD cells. In both cell lines BIM was already constitutively bound to BCL-2, BCL-$_{XL}$ or MCL-1, while NOXA was constitutively bound to MCL-1 revealing, that RMS cells are initially primed to undergo intrinsic apoptosis. Upon treatment with JQ1 or JQ1/BYL719 co-treatment BIM levels are increased in the input and BIM shows increased binding to BCL-2, BCL-$_{XL}$ and MCL-1 thus promoting neutralization of antiapoptotic BCL-2 proteins and thereby intrinsic apoptosis (Figure 45).

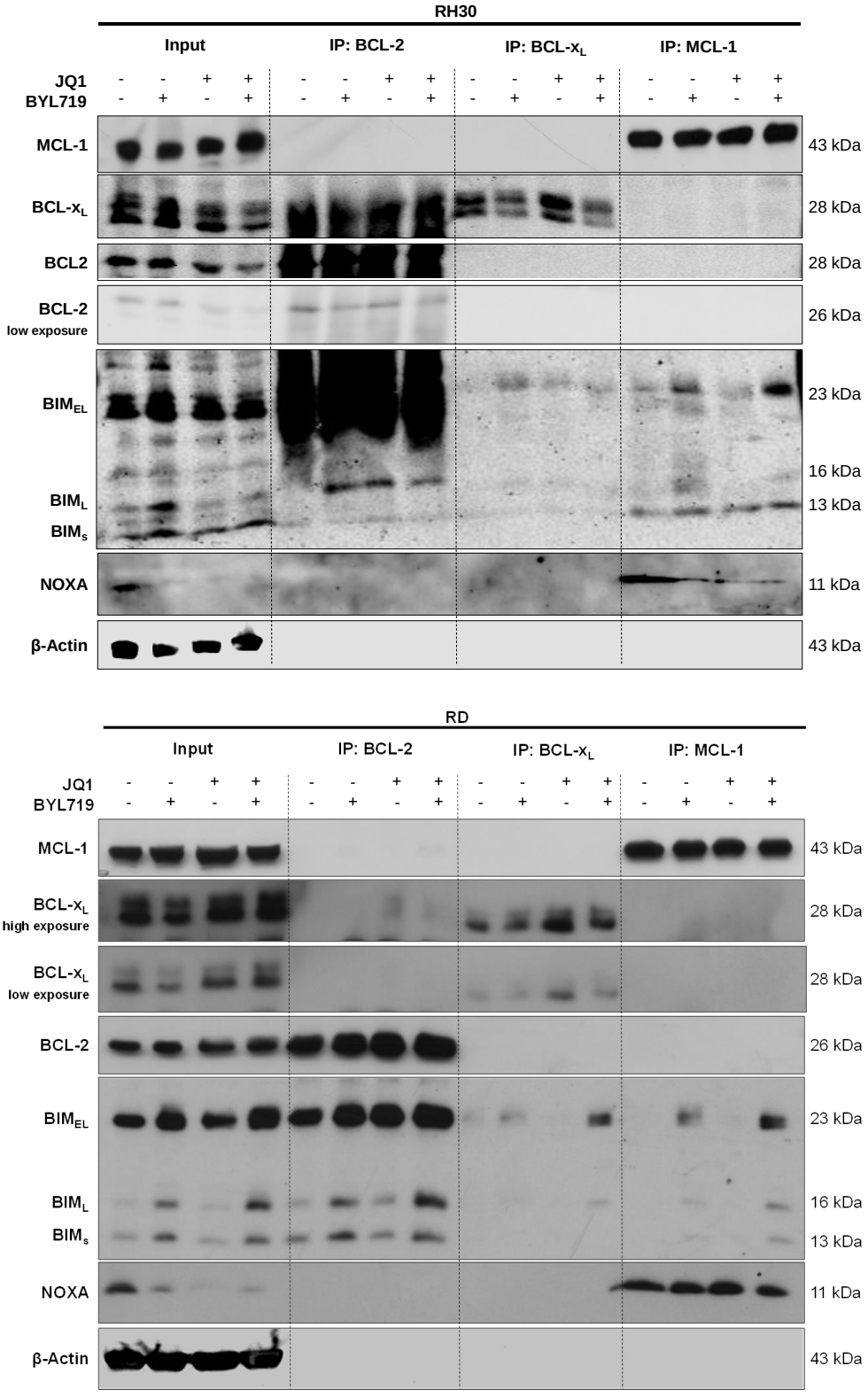

Figure 45: RMS cells are initially primed to undergo intrinsic apoptosis.
BCL-2, BCL-x_L, MCL-1 immunoprecipitation (IP) was performed and levels of BIM and NOXA in total (Input) and IPs were analyzed by Western blotting. Representative blots of two experiments are shown, β-Actin was used as loading control.

4.7 JQ1/BYL719 co-treatment stimulates activation of BAX and BAK, thereby promoting apoptosis

Activation of the two proapoptotic effector proteins BAK and BAX controlling MOMP is a typical feature of intrinsic apoptosis. Therefore, we immunoprecipitated activated BAK and BAX using conformation-specific antibodies that detect the conformational change of BAK and BAX upon their activation. While JQ1 or BYL719 single treatment had only minor effect, JQ1/BYL719 co-treatment resulted in BAK and BAK activation (Figure 46).

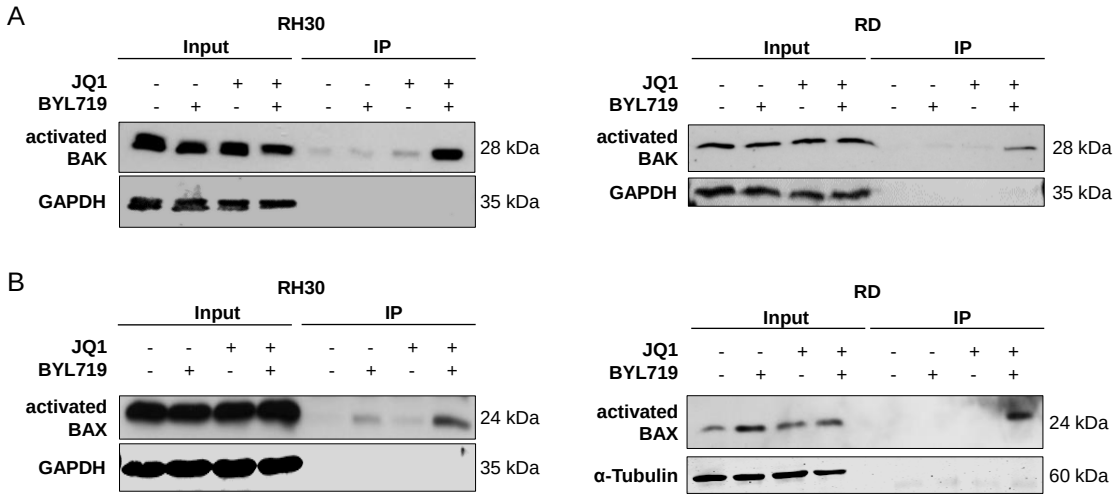

Figure 46: JQ1/BYL719 co-treatment stimulates activation of BAK and BAX.
(A, B) RMS cells were treated with 1 µM JQ1 and/or 3 µM BYL719 for 24 hours. (A) BAK or (B) BAX were immunoprecipitated using active conformation-specific antibodies and expression of active (immunoprecipitation, IP) and total (Input) BAK or BAX levels were analyzed by Western blotting, GAPDH and α-Tubulin served as loading control. Representative blots of two experiments are shown.

To assess the functional relevance of BAK and BAX for JQ1/BYL719-mediated cell death, we performed individual knockdown of either BAK or BAX using distinct siRNA sequences. Knockdown with either BAK or BAX significantly reduced JQ1/BYL719-mediated apoptosis, confirming the functional relevance of BAK and BAX for the execution of JQ1/BYL819-mediated apoptosis (Figure 47, Figure 48).

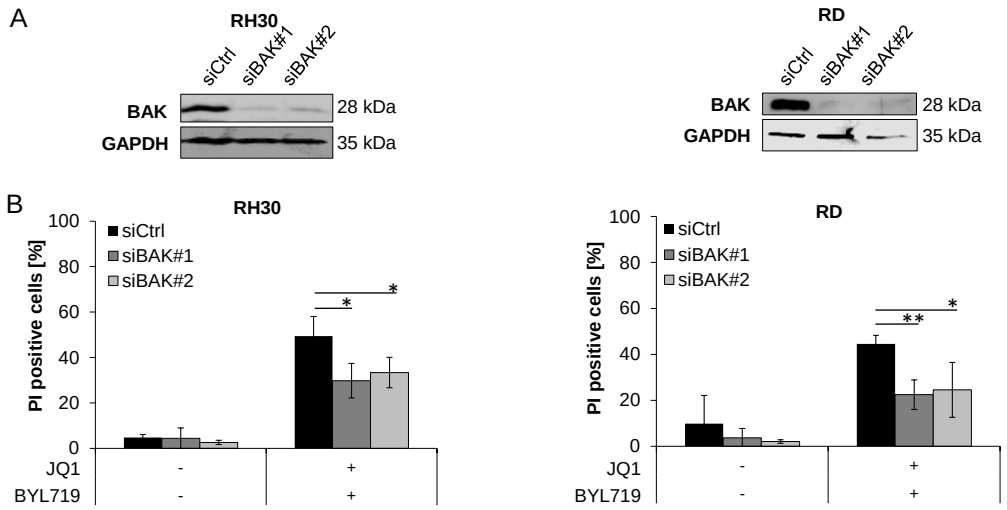

Figure 47: BAK knockdown rescues from JQ1/BYL719-mediated apoptosis.
RMS cells were transiently transfected for 24 hours with 20 nM SilencerSelect non-silencing siRNA or siRNA targeting BAK and then treated as indicated for 72 hours. (A) At the timepoint of cell death measurement, protein levels were detected by Western blotting; GAPDH served as loading controls. (B) Cell death was determined by analysis of PI/Hoechst staining and ImageXpress Micro XLS system; mean and SD of at least three independent experiments performed in triplicate are shown; *p<0.05, **p<0.01.

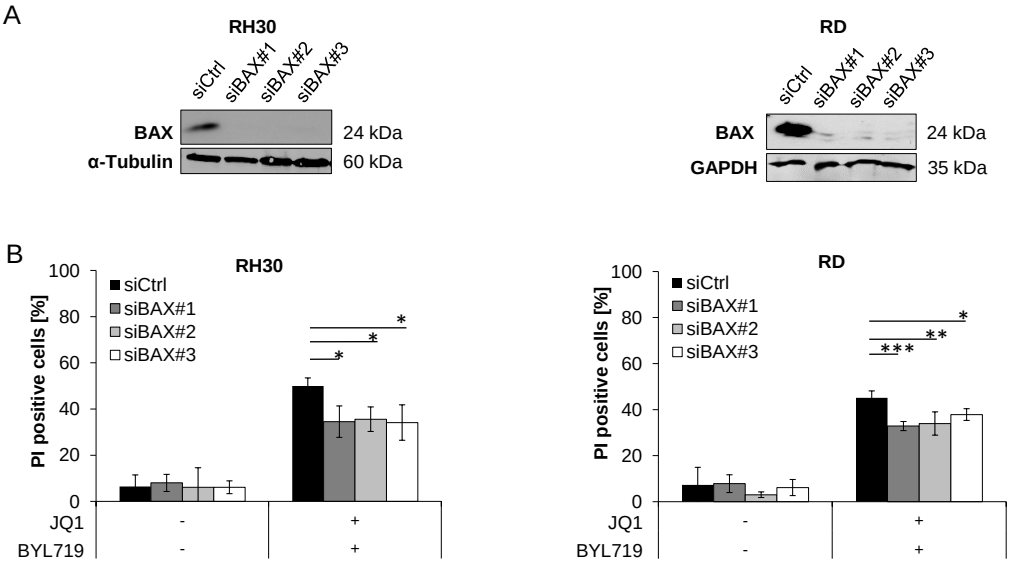

Figure 48: BAX knockdown rescues from JQ1/BYL719-mediated apoptosis.
RMS cells were transiently transfected for 24 hours with 20 nM SilencerSelect non-silencing siRNA or siRNA targeting BAX and then treated as indicated for 72 hours. (A) At the timepoint of cell death measurement, protein levels were detected by Western blotting; α-Tubulin or GAPDH served as loading controls. (B) Cell death was determined by analysis of PI/Hoechst staining and ImageXpress Micro XLS system; mean and SD of at least three independent experiments performed in triplicate are shown; *p<0.05; **p<0.01; ***p<0.001.

4.8 Overexpression of the antiapoptotic BCL-2 proteins BCL-2 and MCL-1 rescues RMS cells from JQ1/BYL719-induced apoptosis

To further investigate the functional relevance of the ratio between pro- and antiapoptotic proteins, we overexpressed murine BCL-2, MCL-1 WT or a non-degradable phospho-deficient MCL-1 mutant (MCL-1 '4A') in RH30 and RD cells. Ectopic expression of murine BCL-2, MCL-1 WT or MCL-1 '4A' was confirmed by Western blotting (Figure 49A, Figure 50A). Overexpression of murine BCL-2 reduced JQ1/BYL719-triggered apoptosis almost completely in RH30 and RD cells (Figure 49B). Comparable overexpression of MCL-1 significantly reduced JQ1/BYL719-triggered apoptosis (Figure 50B). Overexpression of non-degradable phospho-deficient MCL-1 lead to reduction of cell death similar to MCL-1 WT overexpression (Figure 50B).

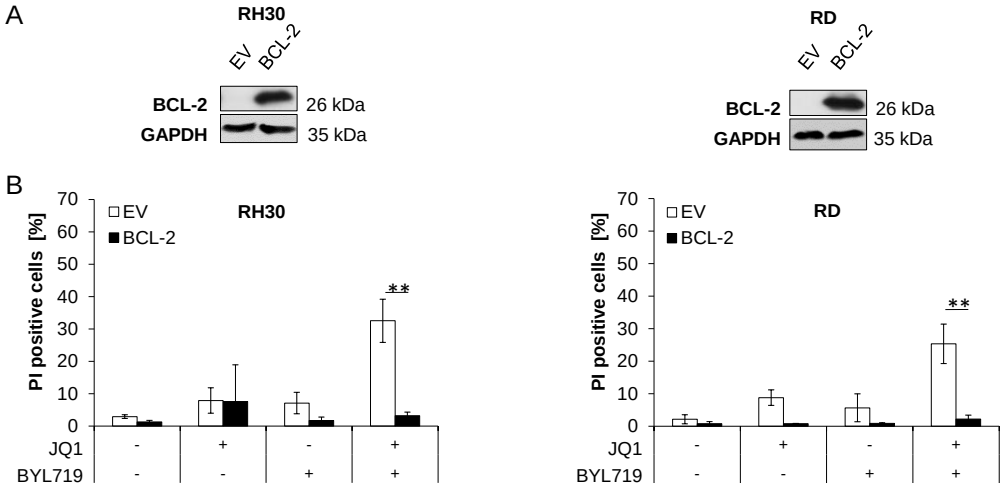

Figure 49: Overexpression of antiapoptotic BCL-2 rescues RMS cells from JQ1/BYL719-induced apoptosis.
(A, B) RMS cells were transfected with murine BCL-2 or EV. (A) Expression of murine BCL-2 was assessed by Western blotting, GAPDH served as loading control. (B) Cells were treated with 1 µM JQ1 and/or 3 µM BYL719 for 72 hours and apoptosis was determined by analysis of PI/Hoechst staining and ImageXpress Micro XLS system.

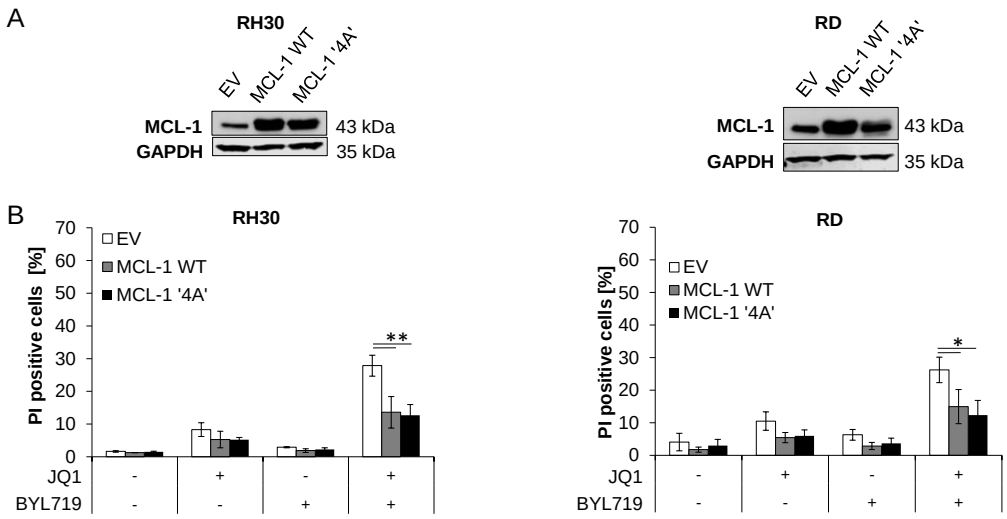

Figure 50: Overexpression of antiapoptotic MCL-1 rescues RMS cells from JQ1/BYL719-induced apoptosis.
(A, B) RMS cells were transfected with MCL-1 or non-degradable phospho-deficient MCL-1 mutant (MCL-1 '4A') or EV. (A) Expression of MCL-1 was assessed by Western blotting, GAPDH served as loading control. (B) Cells were treated with 1 µM JQ1 and/or 3 µM BYL719 for 72 hours and apoptosis was determined by analysis of PI/Hoechst staining and ImageXpress Micro XLS system.

4.9 Summary of the proposed mechanism of JQ1/BYL719-mediated BRD4 regulation and mitochondrial apoptosis.

Finally, we propose the following mechanism for JQ1/BYL719-mediated BRD4 regulation and apoptosis in RMS cells (see Figure 51). JQ1 alone inhibits BRD4 binding to chromatin and inhibits cell proliferation without inducting cell death. This may be, at least in part, due to inhibition of MYC and Hh signaling as indicated by reduced transcription of MYC and GLI1. Furthermore, JQ1 increases the priming of RMS cells for intrinsic apoptosis by downregulating transcription of *BCL2L1* and upregulation *BCL2L11* and *PMAIP1*. Addition of BYL719 increases phosphorylation of BRD4 at S484/488 and BRD4 binding to chromatin including BH3-only genes (*BMF, BCL2L11, PMAIP1*), that are transcriptionally upregulated. This rebalancing in favor of apoptosis activates BAK and BAX and thereby caspase-dependent apoptosis, since i) siRNA against BMF, BIM, NOXA, BAK or BAX, ii) overexpression of BCL-2 or MCL-1 or iii) the caspase inhibitor zVAD.fmk all rescue JQ1/BYL719-induced cell death.

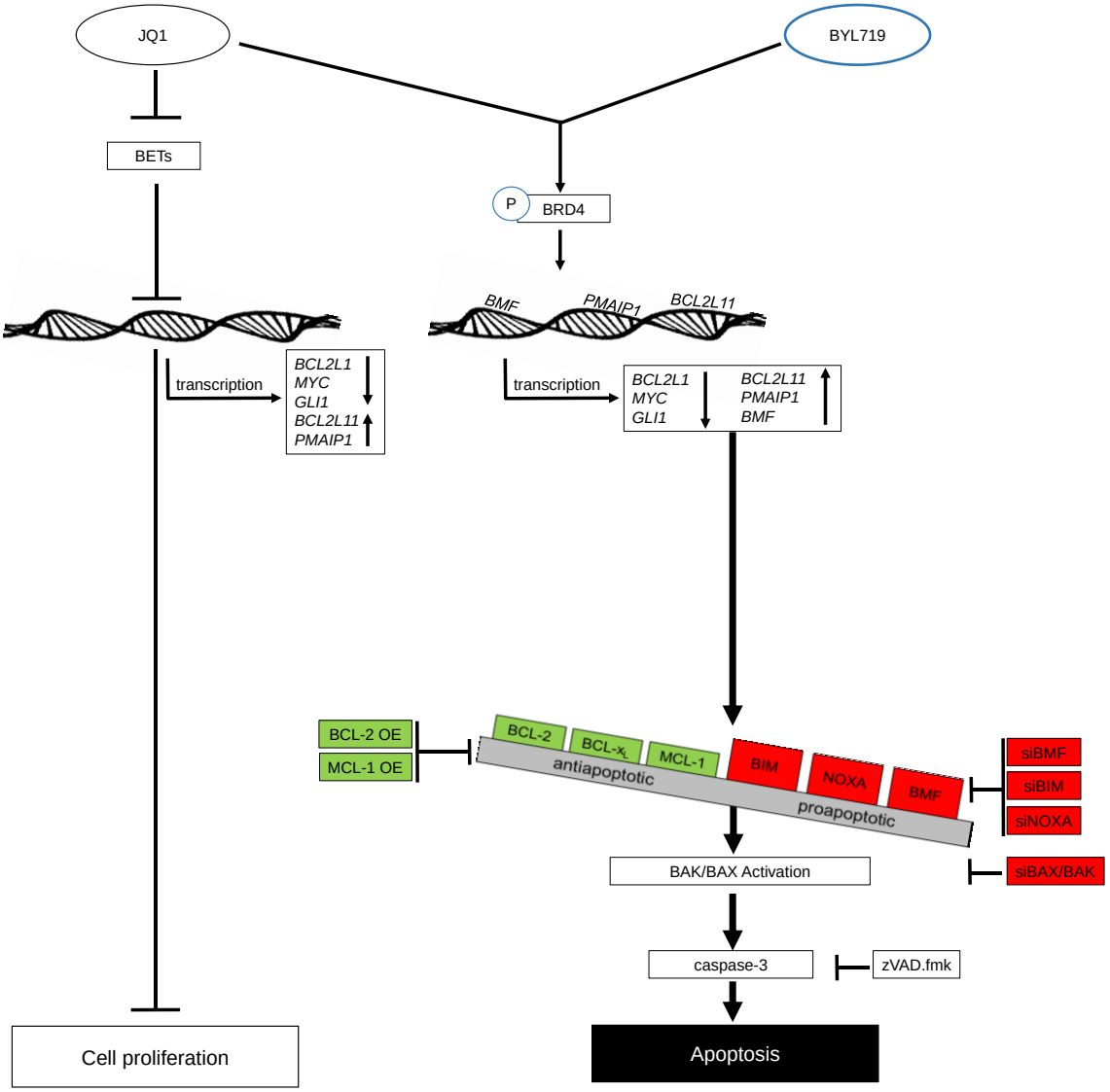

Figure 51: Scheme of the proposed mechanism of JQ1/BYL719-mediated BRD4 regulation and mitochondrial apoptosis.
JQ1 alone inhibits BRD4 binding to chromatin, while addition of BYL719 increases phosphorylation of BRD4 at S484/488 and BRD4 binding to chromatin including BH3-only genes (*BMF, BCL2L11, PMAIP1*) which are transcriptionally regulated: JQ1 alone upregulates *BCL2L11, PMAIP1* and downregulates *BCL2L1*, while the addition of BYL719 increases *BMF* expression. This proapoptotic rebalancing of BCL-2 family members results in BAX/BAK activation and caspase-dependent apoptosis. Individual silencing of BMF, BIM, NOXA, BAX or BAK, overexpression of BCL-2 or MCL-1 or, alternatively, caspase inhibition by zVAD.fmk all prevent JQ1/BYL719-induced cell death. In addition, JQ1 inhibits MYC and Hh signaling (GLI1), which may contribute to inhibition of cell proliferation.

5 JQ1 synergizes with distinct HDAC inhibitors to induce cell death in RMS cells

5.1 JQ1 synergizes with JNJ-26481585, Vorinostat, Entinostat and Panobinostat to induce cell death in RMS cells

To compare the potential of JQ1/BYL719 co-treatment to other common BET inhibitor-based combination therapies, we combined JQ1 with distinct HDAC inhibitors including JNJ-26481585, SAHA (Vorinostat), MS-275 (Entinostat) and LBH-589 (Panobinostat) in RH30 and RD cells (Figure 52, Figure 53) (experiments were partially performed by Julius Enßle). All four combinations synergistically induced cell death as indicated by calculation of CI value (Table 21, Table 22). By comparison, the synergism of all four combinations was minor compared to the synergistic cell death induction of JQ1/BYL719 co-treatment as indicated by lower CI values for JQ1/BYL719 co-treatment, further underlining the potency of combined BET and PI3Kα inhibition in RMS cells (Table 18, Table 21, Table 22).

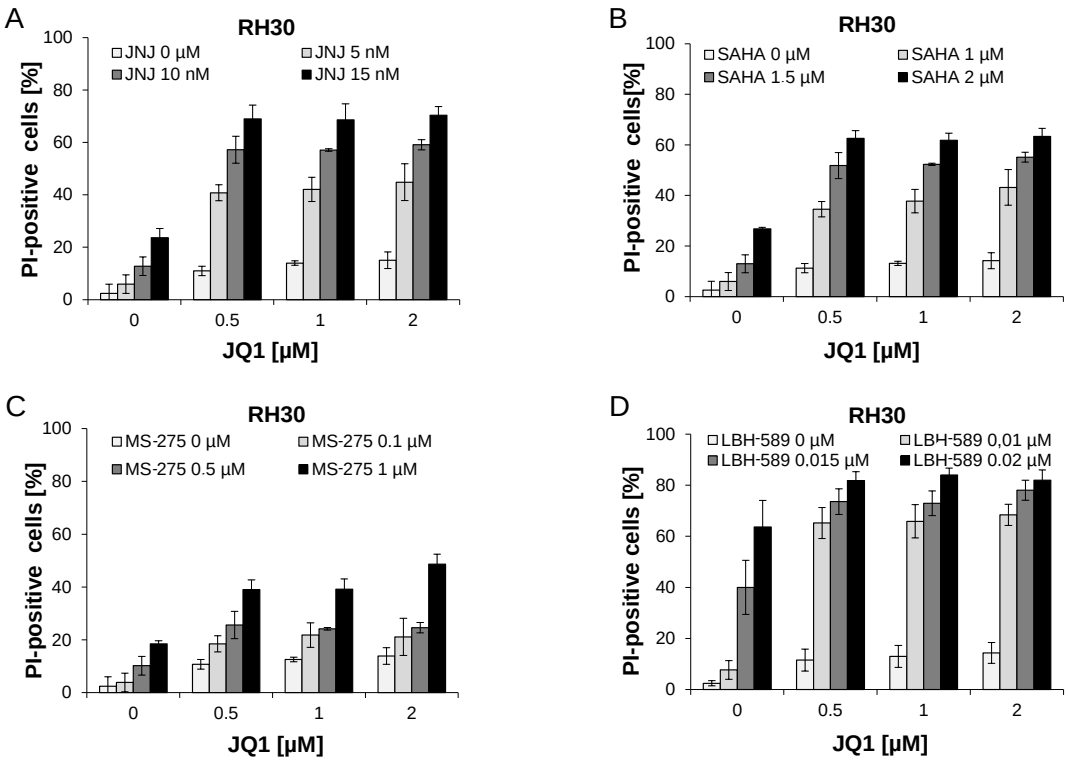

Figure 52: JQ1 synergizes with distinct HDAC inhibitors to induce cell death in RH30 cells
RH30 cells were treated with the indicated concentrations of JQ1 and (A) JNJ-26481585, (B) SAHA, (C) MS-275 or (D) LBH-589 for 72 hours. Cell death was determined by analysis of PI/Hoechst staining and ImageXpress Micro XLS system. Data are shown as mean and SD of at least three independent experiments performed in triplicate.

Table 21: Synergistic induction of PI positive cells by combined BET and HDAC inhibition in RH30 cells

RH30		JQ1 [µM]		
		0.5	1	2
JNJ [nM]	5	0.182	0.177	0.164
	10	0.228	0.229	0.216
	15	0.239	0.242	0.229
SAHA [µM]	1	0.42	0.398	0.363
	1.5	0.473	0.472	0.449
	2	0.529	0.536	0.522
MS 275 [µM]	0.1	0.251	0.215	0.331
	0.5	0.248	0.263	0.264
	1	0.229	0.209	0.155
LBH 589 [nM]	10	0.506	0.502	0.489
	15	0.693	0.699	0.657
	20	0.83	0.802	0.829

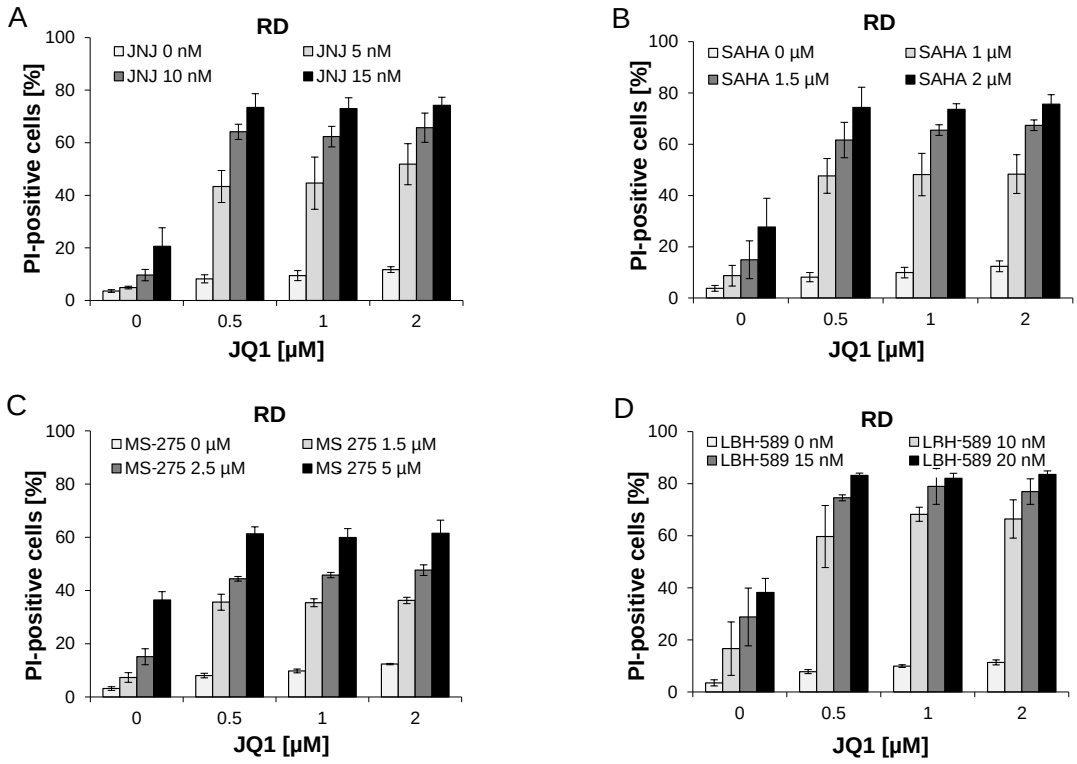

Figure 53: JQ1 synergizes with distinct HDAC inhibitors to induce cell death in RD cells.

RD cells were treated with the indicated concentrations of JQ1 and (A) JNJ-26481585, (B) SAHA, (C) MS-275 or (D) LBH-589 for 72 hours. Cell death was determined by analysis of PI/Hoechst staining and ImageXpress Micro XLS system. Data are shown as mean and SD of at least three independent experiments performed in triplicate.

Table 22: Synergistic induction of PI positive cells by combined BET and HDAC inhibition in RD cells

RD		JQ1 [µM]		
		0.5	1	2
JNJ [nM]	5	0.144	0.14	0.114
	10	0.159	0.168	0.151
	15	0.176	0.178	0.171
SAHA [µM]	1	0.311	0.309	0.31
	1.5	0.349	0.321	0.307
	2	0.344	0.352	0.333
MS 275 [µM]	0.1	0.309	0.316	0.317
	0.5	0.408	0.395	0.38
	1	0.537	0.556	0.535
LBH 589 [nM]	10	0.297	0.237	0.249
	15	0.294	0.252	0.272
	20	0.285	0.3	0.281

5.1.1 JQ1/JNJ co-treatment significantly induces caspase-3 activation in RD cells in CAM tumor model

For comparison of HDAC/BET co-treatment to JQ1/BYL719 co-treatment, we evaluated the synergism of JQ1 with JNJ testing since the combination of JQ1 and JNJ revealed the highest synergism as indicated by lowest CI values beyond the tested HDAC combinations (Table 21). Thus, we treated RD cells in the CAM model with 1 µM JQ1 and 50 or 500 nM JNJ. In result, we could not observe a cooperative effect on caspase-activation in the combination of JQ1 with 50 nM JNJ, since levels of caspase-activation upon JNJ single treatment were similar to levels upon JQ1/JNJ co-treatment. However, upon combination with 500 nM JNJ we observe significantly more activated caspase-3 upon JQ1/JNJ co-treatment compared to single treatments. This combination, revealing 9.9 fold caspase-3 activation relative to the control, included many tumors with necrotic

parts. By comparison, the single treatment with 50 nM JNJ already activates 4.3 fold more caspase-3 compared to control, highlighting the anti-tumor efficiency of JNJ single treatment as monotherapeutic treatment (Figure 54). By further comparison JQ1/BYL719 co-treatment resulted in 5.3 fold caspase-3 activation compared to the control while BYL719 or JQ1 single treatment resulted only in 1 to 2.3 fold more caspase-3 activation compared to the control, highlighting the synergistic effect of JQ1 and BYL719. In summary, JQ1/BYL719 co-treatment shows a stronger synergism, while JQ1/JNJ co-treatment exhibits more caspase-3 activation (Figure 54, Figure 24).

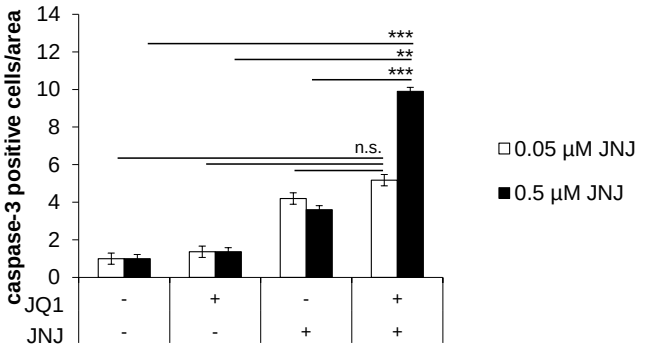

Figure 54: JQ1/JNJ co-treatment significantly induces caspase-3 activation in RD cells in CAM tumor model.
RD cells were seeded on the CAM of fertilized chicken eggs, treated with 1 µM JQ1 and/or 50 or 500 nM JNJ for three days and caspase-3 activation was determined counting caspase-3 positive cells of paraffin sections of the CAM sections stained with cleaved caspase-3 antibody. Representative pictures and quantification of caspase-3 positive tumor cells of at least 10 tumors are shown. Mean and SEM of two independent experiments are shown; **p< 0.01, ***p< 0.001.

6 Discussion

6.1 BET inhibitor JQ1 inhibits cell viability without inducing cell death in RMS cell lines

BET inhibitors have been shown to be cytostatic but not cytotoxic in a number of cancer types [113, 129, 232]. In line with these results, we report inhibition of cell viability at nanomolar concentrations without induction of cell death. Furthermore, several reports show that BET inhibitors suppress MYC or inhibit pathways involved in development including WNT or Hh signaling [113, 114, 125, 130]. In RMS cells, the BET inhibitor JQ1 suppresses MYC and Hh signaling, which is known to modulate responses to chemotherapeutics, differentiation status and motility of RMS cells [113, 130] [14]. In summary, JQ1 single treatment reduces cell viability and inhibits prosurvival pathways in RMS cells highlighting the need for effective combination therapies to trigger cell death in RMS cells [194, 226, 233].

6.2 JQ1/BYL719 co-treatment synergistically induces cell death and reduces cell viability in RMS cell lines

In this study we have exhibited that the BET inhibitor JQ1 and the PI3Kα-selective inhibitor Alpelisib (BYL719) synergistically induce cell death in all tested RMS cell lines as shown by PI/Hoechst staining. This synergism was confirmed by analysis of DNA fragmentation as another cell death assay. Calculation of CI values for both cell death assays confirmed the synergism. In complementary genetic approaches, knockdown of PI3Kα together with JQ1 or silencing of BRD4 combined with BYL719 significantly increased cell death, further confirming the synergism of BET and PI3Kα inhibition. Moreover, JQ1 and BYL719 synergistically induced cell death in primary derived ARMS cells generated from a patient sample. Additionally, JQ1 and BYL719 cooperated to significantly decrease cell density compared to JQ1 or BYL719 single treatment. The synergistic cell death induction of the JQ1/BYL719 co-treatment was superior to the combination with the pan-PI3K/mTOR inhibitor PI-103, highlighting the potential of isoform-specific PI3K inhibitors for combination therapies. The potential of BYL719 in combination therapies in RMS is further highlighted by a previous study showing synergistic cell death induction in NRAS-mutated RMS cells in in combination with MEK inhibition [208]. The synergistic interaction of JQ1 and BYL719 as calculated by CI value was superior to the synergism of JQ1 and distinct HDAC inhibitors, which have previously been reported to synergize with BET inhibitors [136, 150]. The superior synergism of JQ1/BYL719 co-treatment may be explained by the fact, that JQ1/PI-103

co-treatment did not succeed to induce cell death to a similar extent compared to JQ1/BYL719 co-treatment, or in the case of HDAC inhibitors, due to the efficiency of HDAC inhibitors as single treatment in RMS cells [144]. In summary, these results highlight the synergistic potential of combined BET and PI3Kα inhibition in RMS cells.

6.2.1 Combined BET and PI3K inhibition induces DNA fragmentation indicating apoptotic cell death

DNA fragmentation is a typical hallmark of apoptosis [37, 70]. Combination of subtoxic concentration of JQ1 with subtoxic concentrations of BYL719 synergizes to induce DNA fragmentation in a dose and time dependent manner. PI-103 and JQ1 also synergize to induce DNA fragmentation in RMS cells as well. Cell death execution by adheres to previous reports revealing initial priming of RMS cells to undergo apoptosis [234] and identification of apoptosis as main death mechanism induced by BET inhibitors or combination therapies with using BET inhibitors [129, 135, 142].

6.2.2 JQ1/BYL719 co-treatment induces LOMMP in RMS cells

Loss of mitochondrial membrane potential is another typical feature of intrinsic apoptosis and tightly controlled by the balance between pro- and antiapoptotic proteins. If the balance of pro- and antiapoptotic proteins shifts towards the proapoptotic side, the proapoptotic multidomain proteins BAK and BAX mediate disruption of the mitochondrial membrane integrity resulting in LOMMP [235, 236]. Since JQ1/BYL719-mediated cell death induction is relatively slow, loss of mitochondrial potential is not very marked until after 24 hours. To get a better insight into LOMMP during JQ1/BYL719-mediated cell death induction a detailed kinetic measuring LOMMP would be helpful, since low levels of LOMMP might occur over a longer time course. Furthermore, we did not confirm that LOMMP is independent of caspase activation. To assess this, LOMMP measurement in presence of the broad-range caspase inhibitor zVAD.fmk could be conducted. If we observed LOMMP in presence of zVAD.fmk, we could confirm, that LOMMP is activated upstream and independent of caspase activation. However, since the main cell death mechanism mediated by JQ1 and distinct JQ1 co-treatments is described as classical intrinsic apoptosis, which states LOMMP prior to caspase activation, we assume LOMMP to be upstream of caspase activation [88, 128, 237].

6.2.3 JQ1 synergizes with BYL719 to induce caspase-dependent apoptosis in RMS cells

Another typical feature of apoptosis is the activation of caspases at the level of cell death execution. We observed caspase-3/7 activation upon JQ1/BYL719 co-treatment while both single agents had only minor effects on caspase activation. To further underline the relevance of caspase activation for JQ/BYL719-mediated cell death, we used the broad range caspase inhibitor zVAD.fmk. Inhibition of caspases using zVAD.fmk significantly reduced JQ1/BYL719-mediated DNA fragmentation further highlighting that JQ1/BYL719-triggered cell death is mediated by caspase-dependent apoptosis.

6.2.4 JQ1/BYL719 co-treatment shifts the ratio of pro- and antiapoptotic BCL-2 family proteins towards apoptosis

Since intrinsic apoptosis is tightly controlled by the balance of pro- and antiapoptotic proteins, we next investigated the effect of JQ1/BYL719 co-treatment on pro- and antiapoptotic proteins. As we were also interested in the upstream mechanism mediating the shift of the ration of pro- and antiapoptotic BCL-2 proteins, we performed RNA-Sequencing as an unbiased approach using RH30 treated with either JQ1, BYL719 or JQ1/BYL719 co-treatment. Using the RNA-Seq data, we observed an overall shift of pro- and antiapoptotic proteins: while JQ1 alone upregulated mRNA encoding for the proapoptotic proteins BIM, PUMA and NOXA accompanied by the downregulation of mRNA encoding the antiapoptotic protein BCL-x_L, addition of BYL719 induced mRNA of BMF. The effect on the other antiapoptotic proteins such as BCL-2 and MCL-1 was minor and thus not further the focus of this study. QRT-PCR and Western Blot confirmed JQ1-mediated upregulation of proapoptotic BIM and downregulation of antiapoptotic BCL-x_L in RH30 and RD cells. Interestingly upregulation of the short-live protein NOXA could only be confirmed in RH30 cells, while NOXA levels in RD cells remained unchanged at early time points. This difference between RH30 and RD cells in the regulation of pro-apoptotic BCL-2 proteins has previously been reported and explained by selective upregulation of proapoptotic proteins being constitutively low expressed in the respective cell line [143]. Since basal NOXA levels in RD cells are relatively high compared to NOXA levels in RH30 cells this would explain why NOXA is only upregulated in RH30, but not in RD cells. However, in a previous study BIM induction was mainly restricted to RD cells while we observe BIM induction upon treatment in both cell lines [143]. Regarding the fact that BIM induction is of the most frequent reported modulations of BCL-2 proteins upon BET inhibition in various cancer types, it appears less surprising that both, RD and RH30 cells as well, show induction of BIM regardless of basal protein levels [87, 88, 124,

129, 238]. Induction of mRNA encoding PUMA could not be validated by qRT-PCR and knockdown of PUMA did not affect cell death induction, pointing to the fact that PUMA does not play a role in JQ1/BYL719-mediated cell death. Furthermore, JQ1 and BYL719 single treatment slightly induced BMF, which is constitutively very lowly expressed in both cell lines. Upon JQ1/BYL719 co-treatment, BMF levels are massively increased, further shifting the ratio between pro-and antiapoptotic proteins towards apoptosis. Since BIM and NOXA are constitutively bound to antiapoptotic BCL-2 proteins, RMS cells are initially primed to undergo apoptosis [56]. This priming for intrinsic apoptosis is further enhanced by JQ1 because it increases BIM and NOXA levels, however this is still not sufficient to execute apoptosis. Only following BYL719-mediated induction of BMF apoptosis is executed. To this end, it would be interesting to include BMF into immunoprecipitation studies to investigate if BMF is able to displace BIM from antiapoptotic BCL-2 proteins thereby facilitating BIM to directly activate BAK and BAX since the mechanism of direct BIM-mediated BAK/BAX activation has been reported in response to paclitaxel in breast cancer cells [239].

The functional relevance of the ratio of pro- and antiapoptotic BCL-2 proteins in determining the sensitivity to JQ1/BYL719 co-treatment is further confirmed by individual knockdown of BIM, NOXA and BMF significantly rescuing RMS cells from JQ1/BYL719-mediated cell death. By comparison, knockdown of BIM lead to the most prominent rescue from cell death which may be explained by the fact that BIM belongs to the direct activators of proapoptotic multidomain proteins BAK and BAX, thereby playing a more critical role in apoptosis compared to NOXA and BMF which belong to the sensitizers of BAK and BAX [240]. The relevance of the relative ratio of pro- and antiapoptotic BCL-2 proteins in determining the sensitivity to JQ1/BYL719 co-treatment is further emphasized by ectopic expression of murine BCL-2, MCL-1 or non-degradable MCL-1`A1´, which counteracts proapoptotic BCL-2 proteins and significantly reduces JQ1/BYL719-induced apoptosis. Phosphorylation of MCL-1 does not seem to play a role, since the non-degradable phosphor-mutant of MCL-1 rescues JQ1/BYL719-mediated apoptosis similar to MCL-1.

6.2.5 JQ1/BYL719 co-treatment activates the proapoptotic multidomain proteins BAK and BAX

The relative shift in the ratio between pro- and antiapoptotic BCL-2 proteins induces LOMMP by activation of BAK and BAX forming pores in the outer mitochondrial membrane [47, 48]. Thus, we checked for activation of BAK and BAX. JQ1/BYL719 co-treatment resulted in pronounced activation of BAK and BAX, while treatment with JQ1

or BYL719 alone resulted in minor activation of BAK and BAX. The functional relevance of activated BAK and BAX is further confirmed by knockdown of either BAK or BAX significantly rescuing RMS cells from JQ1/BYL719-induced cell death, linking rebalancing of BCL-2 proteins to LOMMP.

6.2.6 JQ1/BYL719 co-treatment induces G1 cell cycle arrest and reduces cell viability

Aside from apoptosis JQ1/BYL719 co-treatment induces G1 cell cycle arrest and inhibits cell viability. JQ1 or BYL719 alone already induce G1 cell cycle arrest. Upon combination G1 arrest is even more pronounced. G1 cell cycle arrest might also explain the reduction in cell viability, which is measured by metabolic activity and cell density since both features are dependent on cell cycle progression. As the dependency of cell cycle and metabolism is not unidirectional, inhibition of metabolic activity might also influence cell cycle arrest thereby enhancing G1 arrest [241]. JQ1-imposed suppression of MYC and Hh signaling may also contribute to its inhibitory effects on cell cycle progression and proliferation since MYC has been reported to regulate metabolism facilitated cell cycle entry [242, 243] and Hh signaling is known to regulate proliferation [244].

6.3 JQ1/BYL719 co-treatment induces reallocation of BRD4 and stimulates BRD4 enrichment at regulatory elements of BH3-only proteins

We identified JQ1/BYL719-mediated transcriptional modulation of BCL-2 family proteins as a key mechanism to synergistically induce intrinsic apoptosis. To gain further insight into the upstream mechanism mediating intrinsic apoptosis, we performed RNA-Seq combined with BRD4 ChIP-Seq analysis. JQ1/BYL719 co-treatment induced transcription of the proapoptotic genes *BMF*, *BCL2L11* (BIM) and *PMAIP1* (NOXA) and reduced transcription of the antiapoptotic gene *BCL2L1* (BCL-x_L). Notably, JQ1/BYL719-stimulated changes in gene expression of these BH3-only genes were accompanied by BRD4 enrichment at transcriptional regulatory elements of these genes. This BRD4 enrichment at some but not all genes, is especially interesting, since JQ1 alone, as expected, reduced BRD4 binding to chromatin. Since JQ1 can induce compensatory BRD4 production, we propose that JQ1 dissociates BRD4 from initial BRD4 binding sites, facilitating newly produced BRD4 to reallocate in a target-specific manner in response to JQ1/BYL719 co-treatment [131]. The functional relevance of BRD4 reallocation to BH3-only genes could also explain why the combined knockdown of BRD4 with BYL719 induced less cell death compared to combination of PI3Kα knockdown and JQ1, since BRD4 knockdown reduces BRD4 levels also at BH3-only genes. The hypothesis of

target-specific BRD4 reallocation is further supported by our observation of increased phosphorylation of BRD4 at S484/488, which has been shown to mediate target-specific binding of BRD4 to other transcription factors in a bromodomain-independent manner [108, 110, 134]. Interestingly this phosphorylation of BRD4 occurs most prominent upon JQ1/BYL719 co-treatment, while the effect of JQ1 or BYL719 alone is minor, further highlighting the cooperative effect of JQ1/BYL719 co-treatment on BRD4. Nevertheless, it remains unclear with transcription factor interacts with phosphorylated BRD4 thereby recruiting BRD4 in a gene-specific manner. p53, FosB, NFκB and MED1 have been reported to interact with phosphorylated BRD4 [108, 109, 134]. Since we expect phosphorylation of BRD4 to promote apoptosis, p53 would be the most promising interaction partner. However, the DNA-binding domain of p53 in RH30 and RD cells is mutated and thus it is unlikely, although not impossible, that p53 mediates BRD4 reallocation in RMS cells in favor of apoptosis [245]. p53 could interact with BRD4, which then could bind in a bromodomain-dependent manner to chromatin, thereby facilitating p53-mediated transcription [99, 108]. If this would be the case, it remains unclear why JQ1 does not reduce BRD4 binding to chromatin upon JQ1/BYL719 co-treatment. Another transcription factor potentially recruiting BRD4 in favor of apoptosis might be FOXO3a, which is a downstream target of PI3K signaling [180, 186]. However, the only study describing direct interaction of BRD4 and FOXO3a states, that the interaction is bromodomain-dependent and subsequently disrupted by addition of JQ1, which does not fit to our observation of increased binding upon JQ1/BYL719 co-treatment [104]. The interaction of BRD4 with transcription factors defines cell identity and thus may differ between cell types [246]. Thus, it could be that BRD4 interacts with FOXO3a in a bromodomain-independent manner in RMS. Alternatively, other members of the FOXO family could be possible interaction partners of BRD4, since FOXO transcription factors have been described to promote transcription of BH3-only genes including *BMF* and *BCL2L11* (BIM) [247, 248]. To provide further insight into the interaction of BRD4 with other transcription factors upon JQ1/BYL719 co-treatment further investigations will be necessary. These studies could include SILAC (stable isotope labeling with amino acids in cell culture)-based proteomic analysis to identify the BRD4-interacting transcription factors followed by Co-IP experiments for validation of the obtained results.

Selective BRD4-dependent regulation of BCL-2 proteins is in line with recent reports showing super-enhancer-mediated regulation of some, but not all BCL-2 protein members in RMS [12, 249]. Super-enhancer-regulated genes enrich BRD4 and are known to be highly dependent on BRD4 [12, 250], thus being especially sensitive to BET inhibition. In ARMS *BMF*, *BCL2L11* (BIM) and *BCL2L1* (BCL-x_L) were among reported

super-enhancer-regulated genes [12], and *BMF* was shown to be super-enhancer-regulated upon MEK inhibition in RAS-mutated ERMS [249]. Thus, we observe regulation of gene expression and accompanied by BRD4 enrichment at exactly those BH3-only genes that are predicted to be BRD4-dependet by former studies [12, 250]. While previous studies focused only on BCL-2 protein expression upon BET inhibition alone or in combination with PI3K inhibition [88, 140, 238, 251, 252], our present study provides for the first time an explanation on the chromatin level for the joint action of BET and PI3Kα inhibition to modulate expression levels of BH3-only proteins.

6.3.1 Specificity of JQ1/BYL719 co-treatment in RMS cells

From the safety perspective, it is essential to examine the effect of JQ1/BYL719 co-treatment on nonmalignant cells. C2C12 cells, a mouse skeletal muscle cell line, represent one of the frequent used control cells for treatments of RMS cells. While showing little effect on induction of PI positive cells, JQ1 and BYL719 cooperate to induce DNA fragmentation in C2C12 cells. However, compared to the effect observed in RMS cells, the effect is less pronounced, pointing to some tumor selectivity of JQ1/BYL719 co-treatment. The efficiency of JQ1/BYL719 co-treatment is further highlighted by the fact that JQ1/BYL719 co-treatment succeeds to induce apoptosis in primary derived RMS cells. The observation, that non-malignant cells are also affected by JQ1/BYL719 co-treatment goes in line with results from clinical studies showing dose-limiting adverse effects in response to treatment of patients with PI3K or BET inhibitors [210, 253].

6.4 Targeting BET proteins in combination with targeted therapy as general approach to treat cancer *in vivo* and in clinics

BET and PI3K inhibitors are both promising anticancer drugs. Several BET inhibitors e.g. OTX015, GSK525762, CPI-0610 or TEN-010 are currently tested in phase I or phase II clinical trials in patients with solid tumors or hematologic malignancies [253, 254]. Single treatment with the BET inhibitor OTX015 has turned out to be very efficient in NUT midline carcinoma (NMC) harboring the BRD4-NUT fusion oncoprotein [122]. *In vivo,* BET inhibitors have been reported to affect AML cells more than normal bone marrow or hematopoetic stem cells, encouraging the advancement of clinical trials with AML patients [114, 255]. However, BET inhibitors have dose limiting adverse effects including thrombocytopenia, nausea, vomiting, diarrhea, GI side-effects, fatigue or low-grade dysgeusia [256]. Furthermore, efficiency of single BET inhibition is limited due to several resistance mechanisms: rebound increase of BET proteins [131], compensatory

upregulation of pro-survival kinases [132], compensatory upregulation of Wnt/β-catenin signaling [133] or decreased activation of the phosphatase PP2A resulting in hyperphosphorylation of BRD4 and interaction with MED1 [134]. However, several preclinical studies highlighted the potential of BET inhibitors in combination therapies with HDAC inhibitors [124, 136, 137], tyrosine kinase inhibitors [129], cell cycle modulating kinase inhibitors [137], BCL-2 inhibitors [138], proteasome inhibitors [139] and immunomodulatory drugs [141]. These results provided a rationale for several clinical trials combining BET inhibitors with other chemotherapeutics including the cytostatic drug fulvestrant (NCT02964507) or the tyrosine kinase inhibitor Ruxolitinib (NCT02308761) in patients with Hormone Receptor-positive (HR+)/Human Epidermal Growth Factor Receptor 2 Negative (HER2), advanced and metastatic breast cancer or acute myeloid leukemia. In addition to combination approaches the use of dual-kinase-bromodomain inhibitors and BET degraders opens new perspectives for BET inhibitions that need to be further evaluated [131, 257]. To date, several BET inhibitors have shown promising results in some clinical trials while in other cases the benefit for patients was minor [233, 254]. The noncancerous relevance of BRD4 [258, 259] as well as development of resistances to BET inhibitors [133] raises concerns regarding the consequences of BET inhibition [254].

PI3K inhibitors including pan-PI3K inhibitors or isoform-specific PI3K inhibitors are under investigation in clinical trials or have been approved by the FDA for several hematologic malogancies (NCT01610284, NCT01219699) [226]. The pan-PI3K inhibitor buparlisib (BKM120) as well as the PI3Kα-selective inhibitor BYL719 have shown potent antitumor activity in preclinical studies as well as tolerable side effects in clinical studies mainly associated with “on-target” effects of PI3K inhibition (NCT02437318). However, single treatment with PI3K inhibitors has resulted in moderate benefit for patients so far, resulting in several clinical trials combining PI3K inhibitors with other chemotherapeutics. Several phase II or III clinical trials have been conducted in solid tumors combining BKM120 with the cytostatic drug paclitaxel, the monoclonal antibody trastuzumab (NCT01816594, NCT01572727) or with capecitabine, trastuzumab and lapatinib (NCT01300962). Currently the use of isoform-specific PI3K inhibitors is under discussion, since targeting of specific isoforms may lead to higher efficiency accompanied by lower toxicity [226]. The PI3Kα-selective BYL719 has been under investigation in combination with other chemotherapeutics including capecitabine (NCT01300962), letrozole (NCT01923168) or tamoxifen and goserelin acetate (NCT02058381). Unfortunately, evaluation of these combination therapies revealed inconsistent efficiency and severe toxicity [260]. Dose-limiting adverse effects of pan-

PI3K-inhibitors as well as isoform-specific PI3K inhibitors were hyperglycemia, nausea, fatigue, rash and gastrointestinal toxicities [210]. Unsurprisingly, considering BYL719 hyperglycemia was the most common dose-limiting adverse event [210]. This is an “on-target” effect since PI3K signaling is interacting with insulin signaling [211, 212].

In summary, BET and PI3K inhibitors seem to be potent anticancer drugs. However, their “on target” adverse effects and resistance mechanisms limit their use in clinics as single agents. Thus, further investigations are needed to determine potent and tolerable combinations for clinical use to exploit the potential of these two inhibitor classes as anti-cancer agents.

7 Outlook

In 2010 the benzotriazolodiazepine I-BET and the thienotriazolodiazepine JQ1 were published as small molecule inhibitors targeting BET proteins [119, 120]. JQ1 and I-BET have been modified for clinical use and tested relatively fast in clinical trials since the dependency of myeloid leucemia on BRD4 and the NUT-BET fusion protein in nut midline carcinoma provided a rationale for clinical use [86, 122]. Ever since then preclinical and clinical studies have tried to exploit the potential of BET inhibitors in various tumor entities and in distinct combinations [135, 137, 138, 142]. Still, there are concerns about resistances and off-target effects of pan-BET inhibitors resulting in the development of bivalent BET inhibitors targeting two bromodomains to increase specificity, dual-kinase-bromodomain inhibitors and BET degraders [131, 257, 261]. Effects of low doses of BET inhibitors have been proved to be not restricted to cancers but to affect macrophages, T-cells, pancreatic β-cells, adipocytes and BRD4-regulated viruses underlining the general importance of BET proteins in transcriptional control [119, 262-264]. Behind this background warnings arise to push BET inhibitors into clinics if the cancers do not lack efficient therapies [254]. Our study is one beyond many others trying to move from description of the downstream effects to understanding how BET inhibitors clamp together with targeted therapies. For future use in clinic it will not be sufficient to describe the execution of apoptosis but to investigate the upstream mechanism to learn more about the complex effects of interfering with the epigenetic landscape. It should be taken into consideration that targeted therapies and standard chemotherapeutics as well might remodel the epigenetic landscape thereby interacting with BET inhibitors, since we showed that the isoform-specific inhibitor BYL719 affects BRD4 binding. Therefore, our results are also relevant for treatment of cancer in a more general way beyond the application of combined BET and PI3K inhibition in RMS. Furthermore, PI3K pathway has been shown to be activated in various cancer types pointing to a potential broader relevance of JQ1/BYL719 co-treatment [166, 210, 230, 265]. To use the potential of BYL719 or JQ1/BYL719 co-treatment for patients, biomarkers should be identified to define patient populations most profiting from specifically targeting PI3Kα [226]. Finally, combining JQ1 and BYL719 to treat RMS cells adheres to the general concept of exploiting synergistic antitumor effects of two drug classes and thus minimizing adverse effects of each single compound.

Nevertheless, our study leaves some open questions. First, as already mentioned, we do not know the transcription factor interacting with BRD4 upon JQ1/BYL719 co-treatment. As previously stated, SILAC-based proteomic analysis followed by BRD4 Co-

IP would be appropriate to identify the BRD4-interacting transcription. Second, BRD4 is reallocated to many other genes. Here the correlation between transcription factor dependent recruitment and transcription should be confirmed. Third, the functional relevance of BRD4 phosphorylation should be further investigated. Therefore, BRD4 phosho-mutants of Ser492/494 could be used followed by BRD4 Co-IP to check for disruption of the interaction with the identified transcription factor as previously described by Wu et al. [108]. Fourth, to really confirm a broader relevance of BRD4 reallocation in response of JQ1/BYL719 co-treatment as mechanism of BCL-2 expression, BRD4 reallocation should be investigated in other tumor entities. Finally, the preclinical evaluation and clinical evaluation of JQ1/BYL719 co-treatment needs to be discussed. Using JQ1 is unlikely since other BET inhibitors have been developed for clinical use including OTX015, GSK525762, CPI-0610 or TEN-010 [89, 122, 141, 253, 254, 266]. Since BYL719 in already tested in clinical trials, BYL719 could be used itself [210]. Besides patient-derived xenografts of RMS, xenograft models with other soft tissue sarcomas would be interesting to explore the antitumor efficiency of combined BET/PI3Kα inhibition *in vivo* evaluating the potential of BET/PI3Kα co-inhibition for clinical trials.

8 Summary (Deutsche Zusammenfassung)

Das Rhabdomyosarkom (RMS) ist das häufigste Weichteilsarkom im Kindesalter und wird histologisch in zwei Subtypen unterteilt – den alveolären Subtyp (ARMS) und den embryonalen Subtyp (ERMS). Neben der histologischen Unterscheidung können beide Subtypen auch durch genetische und epigenetische Veränderungen klassifiziert werden. Der ARMS Subtyp weist typischerweise eine Translokation von Chromosom 13 und Chromosom 2 (13(t(2;13)(q35;q14)) oder 1 (13(t(1;13)(p36;q14)) auf, wodurch das PAX3/7-FOXO Fusionsprotein entsteht. Der ERMS Subtyp besitzt häufig neben einer Deletion auf Chromosom 11p15.5 Mutationen der *RAS*-Onkogene sowie des Tumorsuppressorgens *P53* auf. Sowohl beim ARMS als auch beim ERMS Subtyp sind der Phosphoinositide-3-kinase (PI3K) Signalweg und der Hedgehog (Hh) Signalweg häufig übermäßig aktiviert, was die Prognose verschlechtert. Die Behandlung von Kindern und Jugendlichen mit RMS ist derzeit multimodal und beinhaltet die chirurgische Entfernung des Tumors, Strahlentherapie sowie Chemotherapie, beziehungsweise eine Kombination dieser Therapien. Obwohl genetische und epigenetische Studien in den letzten Jahren Proteine für gezielte Therapien identifiziert haben, besteht die derzeitige Chemotherapie hauptsächlich aus Zytostatika, die unspezifisch das Zellwachstum hemmen. Während die 5-Jahres-Überlebensprognose von ERMS Patienten ohne Metastasen derzeit 70 % beträgt, ist die Prognose für Subgruppen mit ARMS, Metastasen oder Rezidiven mit 25-50 % deutlich schlechter. Für diese Subgruppen mit schlechter Prognose ist die Entwicklung neuer, gezielter Therapien notwendig.

Die meisten derzeitigen Chemotherapien beruhen darauf, in Krebszellen Apoptose, eine Form des programmierten Zelltods, auszulösen. Klassische Apoptose wird in extrinsische (Rezeptor-vermittelte) und intrinsische (mitochondriale) Apoptose unterteilt. Bei der extrinsischen Apoptose erfolgt die Aktivierung der Initiatorcaspase-8 (oder -10) durch die Bindung eines extrazellulären Liganden an einen Rezeptor. Intrinsische Apoptose wird infolge verschiedenster Stressstimuli aktiviert, die zu einer Verschiebung des Gleichgewichts von anti-apoptotischen BCL-2 Proteinen (BCL-2, BCL-x_L, MCL-1) und pro-apoptotischen BCL-2 Proteinen (BIM, BMF, NOXA, PUMA) führt. Dadurch werden die Effektormoleküle BAK und BAX aktiviert, die durch Porenbildung zum Verlust des mitochondrialen Potentials und der Freisetzung mitochondrialer Proteine führen. Hierbei wird unter anderem Cytochrom c freigesetzt, das mit Procaspase-9 das Apoptosom bildet und in der Aktivierung der Initiatorcaspase-9 resultiert. Die jeweiligen Initiatorcaspasen aktivieren die Effektorcaspasen-3 und -7, die apoptotische Zielproteine spalten.

Die funktionelle Identität von Zellen wird maßgeblich durch epigenetische Markierungen bestimmt. Acetylierte Lysine an Histonen gehören zu einer dieser epigenetischen Markierungen. Das Bromodomain und extra-terminal (BET) Protein 4 (BRD4) bindet mittels zweier Bromodomänen an acetylierte Lysine von Histonen oder nukleären Proteinen. Als transkriptioneller Kofaktor dient es als Plattform für die Bindung von Transkriptionsfaktoren und anderen Kofaktoren im Bereich von Promotorregionen, Enhancern und Super-Enhancern (SE). Somit ist BRD4 entscheidend an der tumorspezifischen Transkription, die durch mutierte Transkriptionsfaktoren oder vermehrt aktivierte Signalwege vermittelt wird, beteiligt und stellt ein interessantes Zielprotein für die Tumortherapie dar. BET Inhibitoren (z.B. JQ1) konkurrieren mit acetylierten Lysinen um die Bindestellen der Bromodomänen und hemmen die Interaktion von BRD4 mit acetylierten Histonen, Transkriptionsfaktoren und somit die BRD4-abhängige Genexpression. In vielen Tumorentitäten wirkt BET-Inhibition zytostatisch aber nicht zytotoxisch, zeigt aber in Kombinationstherapien zytotoxisches Potential.

Im Rahmen dieser Arbeit sollte das Potential des BET Inhibitors JQ1 als Einzelsubstanz sowie in Kombination mit PI3K Inhibitoren in RMS Zellen untersucht werden. Neben der Kombination von JQ1 mit dem pan-PI3K/mTOR Inhibitor PI-103, wurde auch die Kombination mit dem PI3Kα-spezifischen Inhibitor BYL719 (Alpelisib) untersucht, da RMS-spezifische Mutationen auf eine vermehrte PI3Kα-Aktivierung hinweisen.

Zunächst wurde der dosisabhängige Effekt von JQ1 auf die metabolische Aktivität und die Zelltodinduktion mittels MTT und PI/Hoechst Assay in einer Konzentrationsreihe in zwei repräsentativen ARMS Zelllinien (RH30, RH41) und zwei repräsentativen ERMS Zelllinien (RD, RH36) untersucht. JQ1 hemmte die metabolische Aktivität der Zellen in nanomolaren Konzentrationen, wohingegen es auch in hohen Konzentrationen von bis zu 20 µM kaum Zelltod (<20 %) induzierte. Außerdem reduzierte JQ1 im subtoxischen Bereich die Expression des Proteins MYC sowie die Aktivität des Hh Signalwegs. Folglich hemmt JQ1 proliferationsfördernde Signalwege sowie die Zellproliferation ohne Zelltod in RMS Zellen auszulösen. Da JQ1 den Hedgehog (Hh) Signalweg hemmt und vorherige Studien die synergistische Zelltodinduktion von Hh Inhibitoren und PI3K Inhibitoren in RMS Zellen gezeigt hatten, testeten wir die Kombination von JQ1 mit PI3K Inhibitoren. Außerdem wurde JQ1 in Kombination mit verschiedenen HDAC Inhibitoren (JNJ-26481585, SAHA, MS-275, LBH-589) untersucht, da die synergistische Zelltodinduktion von BET und HDAC Inhibitoren bereits für andere Tumorentitäten beschrieben wurde. JQ1 induzierte sowohl in Kombination mit subtoxischen

Konzentrationen des pan-PI3K/mTOR Inhibitors PI-103, des PI3Kα Inhibitors BYL719 als auch mit den HDAC Inhibitoren JNJ-26481585, SAHA, MS-275 und LBH-589 Zelltod, der in Form von DNA-Fragmentierung oder Verlust der Membranintegrität gemessen wurde. Die Berechnung des Synergismus nach der Chou-Talalay-Methode ergab für alle Kombinationen eine synergistische Zelltodinduktion, wobei die Kombination mit BYL719 den stärksten Synergismus aufwies. Im Folgenden wurde der Fokus auf die Untersuchung der Kombination von JQ1 und BYL719 gelegt. Vergleichbar mit den RMS Zelllinien, induzierte die Kombination von JQ1 und BYL719 auch in RMS Zellen, die aus einer primären alveolären RMS Probe kultiviert wurden, signifikant mehr Zelltod im Vergleich zu den Einzelsubstanzen. In der nicht-malignen murinen Myoblastenzelllinie C2C12 induzierte die JQ1/BYL719-Kombinationsbehandlung im Vergleich zu RMS Zellen geringeren Zelltod, was auf eine gewisse Tumorspezifität der Behandlung hinweist.

Bei der Untersuchung des Zelltodmechanismus wurde der Fokus auf die Kombination von JQ1 und BYL719 in RH30 und RD Zellen als repräsentativen ARMS und ERMS Zelllinien gelegt. Die JQ1/BYL719-Kombinationsbehandlung induzierte einen G0/G1 Zellzyklusarrest vor Zelltodinduktion und verringerte verglichen mit beiden Einzelbehandlungen signifikant die Zelldichte. Auch das Langzeitüberleben wurde im Vergleich zur Kontrolle signifikant verringert. Des Weiteren zeigten RH30 und RD Zellen infolge der JQ1/BYL719-Kombinationsbehandlung charakteristische Merkmale intrinsischer (mitochondrialer) Apoptose. Die Caspase-Abhängigkeit des Zelltods zeigte sich in Form von kooperativer Caspase-3/-7-Aktivierung infolge der JQ1/BYL719-Kombinationsbehandlung. Die zusätzliche Behandlung mit dem Caspase-Inhibitor zVAD.fmk verringerte sowohl die Caspase-3/-7-Aktivierung als auch die JQ1/BYL719-vermittelte DNA-Fragmentierung signifikant. Auch im Chorion-Allantois-Membran (CAM)-Modell in Hühnereiern, einem etablierten *in vivo* Modell zur Substanztestung, zeigten RD Zellen signifikante Caspase-3-Aktivierung im Vergleich zu den Einzelbehandlungen und der Kontrolle, was zudem auf die *in vivo* Aktivität der JQ1/BYL719-Kombinationsbehandlung hindeutet. Weiterhin konnte der partielle Verlust des mitochondrialen Membranpotentials infolge der JQ1/BYL719-Kombinationsbehandlung beobachtet werden. Zur weiteren Untersuchung des Zelltodmechanismus wurde eine RNA-Seq in RH30 Zellen mit Einzel- und Kombinationsbehandlung vor Eintritt des Zelltods durchgeführt. Die genauere Analyse ergab, dass die Einzelbehandlung mit JQ1 oder in Kombination mit BYL719 zu einer signifikanten Zunahme der Genexpression von *BCL2L11* (BIM), *PMAIP1* (NOXA) und *BBC3* (PUMA) führte, während die Genexpression von *BCL2L1* (BCL-x_L) signifikant

reduziert wurde (log2 FC>2). BYL719 oder die Kombination mit JQ1 führte zu einer signifikanten Zunahme der *BMF* Expression (log2 FC>2). Die Effekte der Behandlungen auf die Genexpression anderer BCL-2 Proteine waren gering (log2 FC<1). Die Zunahme der Genexpression von *BCL2L11, PMAIP1, BMF* sowie die Abnahme von *BCL2L1* konnte mittels qRT-PCR validiert werden, wohingegen die erhöhte Expression von *BBC3* nicht bestätigt werden konnte. In Übereinstimmung mit den Genexpressionsdaten nahm die Proteinexpression der proapoptotischen Proteine BIM und BMF zu und die des antiapoptotischen Proteins BCL-x_L ab. Die Proteinlevel des kurzlebigen Proteins NOXA waren nach 6 h nur in RH30 Zellen unter Behandlung von JQ1 und JQ1/BYL719 erhöht, wohingegen es nach 20 h in beiden Zellen zu einer Reduktion von NOXA infolge der Behandlungen kam. Die Co-Immunopräzipitation von BCL-2, BCL-x_L und MCL-1 ergab, dass RMS Zellen bereits für intrinsische Apoptose geprimt sind, da sie konstitutiv BIM binden, was durch vermehrte Bindung von BIM infolge der Kombinationsbehandlung verstärkt wird. Die JQ1/BYL719-vermittelte Verschiebung des Gleichgewicht pro- und antiapoptotischer BCL-2 Proteine aktivierte BAK und BAX, was ein entscheidender Schritt mitochondrialer Apoptose ist. Die funktionelle Relevanz der Verschiebung des Gleichgewichts pro- und antiapoptotischer Proteine für den Zelltod wurde durch Knockdown der proapoptotischen Proteine BIM, BMF, NOXA, BAK und BAX oder der Überexpression der antiapoptotischen Proteine BCL-2 und MCL-1 unterstrichen, die zu einer signifikanten Verringerung des Zelltodes führten.

Um zu untersuchen inwieweit die beobachteten transkriptionellen Veränderungen BRD4-vermittelt sind, wurde neben der RNA-Seq eine BRD4 ChIP-Seq in RH30 Zellen durchgeführt. Während die Einzelbehandlung mit JQ1 die globale Bindung von BRD4 an Chromatin verringerte, führte die JQ1/BYL719-Kombinationsbehandlung zur Rekonstitution der globalen BRD4 Bindung. Weitere Analysen zeigten, dass sich BRD4 infolge der Kombinationstherapie umlagerte, was in 1707 neuen BRD4 Peaks sowie einer Anreicherung von BRD4 im Bereich von Promotorregionen resultierte. Anschließend konzentrierten wir uns auf die zuvor von Gryder *et al.* beschriebenen transkriptionellen regulatorischen Elemente der BH3-only Proteine, die veränderte Genexpression zeigten [12]. Im Zuge der Umlagerung reicherte sich BRD4 im Bereich des *BMF* SEs sowie des SEs, Enhancers und Promotors von *BCL2L11* (BIM) und des *PMAIP1* (NOXA) Promoters an, während es an anderen genomischen Regionen (z.B. *PTORQ, CDH6*, *ARFGEF3)* zu keiner Anreicherung kam. Die Hypothese der Gen-spezifischen BRD4 Umlagerung wird durch die Zunahme phosphorylierten BRD4s infolge der Kombinationsbehandlung unterstützt, da phospho-BRD4$^{S484/488}$ im Zusammenhang mit Transkriptionsfaktor-spezifischem BRD4-Recruitment beschrieben

wurde. Die Integration von RNA-Seq und ChIP-Seq Daten zeigte 773 BRD4 Peaks mit veränderter Genexpression (log2 FC>I0.58I) infolge der Kombinationsbehandlung von denen 677 *de novo* BRD4 Promotor Peaks waren. Gene Ontology (GO) “Molecular Function“ dieser BRD4 Promotor Peaks ergab nur für die Kombination eine signifikante Anreicherung von GO Gensets, die vor allem transkriptionelle Kontrolle von RNA Polymerase II beinhalteten, was die funktionelle Relevanz der BRD4 Promotor Peaks unterstreicht. Folglich führt die Kombination von JQ1 und BYL719 zu einer transkriptionell relevanten Umlagerung von BRD4, welche die Anreicherung an transkriptionell regulatorischen Elementen von BH3-only Genen und deren vermehrte Genexpression beinhaltet. Wir schlagen einen Mechanismus vor, bei dem initial gebundenes BRD4 durch JQ1 vom Chromatin gelöst wird und sich infolge der Kombinationsbehandlung durch Phosphorylierung genspezifisch umlagert. Diese Hypothese wird durch vorangegangene Arbeiten unterstützt, die kompensatorische BRD4 Produktion infolge von BET Inhibition sowie die genspezifische Anreicherung von BRD4 gezeigt haben. Die selektive Regulation von BCL-2 Proteinen ist durch deren unterschiedliche transkriptionelle Regulation zu erklären, da insbesondere SE und Enhancer regulierte Gene durch BET Inhibition moduliert werden. Die Anreicherung an Promotorregionen von BH3-only Genen zeigt, dass die JQ1/BYL719-vermittelte transkriptionelle Regulation nicht nur auf SE-regulierte Gene beschränkt ist und eröffnet eine breitere therapeutische Relevanz dieser Kombinationstherapie.

In der vorliegenden Arbeit konnten wir damit erstmals zeigen, dass der BET Inhibitor JQ1 und der PI3Kα Inhibitor BYL719 synergistisch mitochondriale Apoptose in RMS Zellen auslösen. Hierbei wird das initiale Priming der RMS Zellen, durch mitochondriale Apoptose zu sterben, ausgenutzt. Während vorangegangene Studien BET Inhibitoren mit pan-PI3K Inhibitoren kombinierten, zeigt diese Arbeit, dass BET-Inhibition in Kombination mit PI3Kα-Inhibition einen stärkeren Synergismus aufweist als in Kombination mit dem pan-PI3K/mTOR Inhibitor PI-103. Dies könnte mitunter an der Eigenschaft von BET Inhibitoren liegen, adaptive Feedbackloops, wie zum Beispiel die kompensatorische Hochregulation anderer PI3K Isoformen, zu inhibieren, die häufig die Effektivität von isoform-spezifischen PI3K Inhibitoren limitieren. Im Vergleich zu vorangegangenen Studien beschränkt sich diese Arbeit nicht auf Untersuchung der Zelltodinduktion, sondern zeigt auch die kooperativen Effekte von BET- und PI3Kα-Inhibition auf Chromatinebene. Damit liefert diese Arbeit neue Einblicke in den Wirkmechanismus kombinierter BET- und PI3Kα-Inhibition und zeigt das Potential dieser Kombination als zukünftige Behandlungsoption für das Rhabdomyosarkom auf.

9 References

1. Saab, R., S.L. Spunt, and S.X. Skapek, *Myogenesis and rhabdomyosarcoma the Jekyll and Hyde of skeletal muscle.* Curr Top Dev Biol, 2011. **94**: p. 197-234.
2. Drummond, C.J. and M.E. Hatley, *A Case of mistaken identity: Rhabdomyosarcoma development from endothelial progenitor cells.* Mol Cell Oncol, 2018. **5**(4): p. e1448246.
3. Nitzki, F., et al., *Hedgehog/Patched-associated rhabdomyosarcoma formation from delta1-expressing mesodermal cells.* Oncogene, 2016. **35**(22): p. 2923-31.
4. Ognjanovic, S., et al., *Trends in childhood rhabdomyosarcoma incidence and survival in the United States, 1975-2005.* Cancer, 2009. **115**(18): p. 4218-26.
5. De Giovanni, C., et al., *Molecular and cellular biology of rhabdomyosarcoma.* Future Oncol, 2009. **5**(9): p. 1449-75.
6. Dagher, R. and L. Helman, *Rhabdomyosarcoma: an overview.* Oncologist, 1999. **4**(1): p. 34-44.
7. Hayes-Jordan, A. and R. Andrassy, *Rhabdomyosarcoma in children.* Curr Opin Pediatr, 2009. **21**(3): p. 373-8.
8. Pappo, A.S., et al., *Survival after relapse in children and adolescents with rhabdomyosarcoma: A report from the Intergroup Rhabdomyosarcoma Study Group.* J Clin Oncol, 1999. **17**(11): p. 3487-93.
9. Visser, M., et al., *Allelotype of pediatric rhabdomyosarcoma.* Oncogene, 1997. **15**(11): p. 1309-14.
10. Minniti, C.P., et al., *Insulin-like growth factor II overexpression in myoblasts induces phenotypic changes typical of the malignant phenotype.* Cell Growth Differ, 1995. **6**(3): p. 263-9.
11. Zhang, M., C.M. Linardic, and D.G. Kirsch, *RAS and ROS in rhabdomyosarcoma.* Cancer Cell, 2013. **24**(6): p. 689-91.
12. Gryder, B.E., et al., *PAX3-FOXO1 Establishes Myogenic Super Enhancers and Confers BET Bromodomain Vulnerability.* Cancer Discov, 2017. **7**(8): p. 884-899.
13. Petricoin, E.F., 3rd, et al., *Phosphoprotein pathway mapping: Akt/mammalian target of rapamycin activation is negatively associated with childhood rhabdomyosarcoma survival.* Cancer Res, 2007. **67**(7): p. 3431-40.
14. Satheesha, S., et al., *Targeting hedgehog signaling reduces self-renewal in embryonal rhabdomyosarcoma.* Oncogene, 2016. **35**(16): p. 2020-30.
15. Crist, W.M., et al., *Intergroup rhabdomyosarcoma study-IV: results for patients with nonmetastatic disease.* J Clin Oncol, 2001. **19**(12): p. 3091-102.
16. Breneman, J.C., et al., *Prognostic factors and clinical outcomes in children and adolescents with metastatic rhabdomyosarcoma--a report from the Intergroup Rhabdomyosarcoma Study IV.* J Clin Oncol, 2003. **21**(1): p. 78-84.
17. Arndt, C.A., et al., *Vincristine, actinomycin, and cyclophosphamide compared with vincristine, actinomycin, and cyclophosphamide alternating with vincristine, topotecan, and cyclophosphamide for intermediate-risk rhabdomyosarcoma: children's oncology group study D9803.* J Clin Oncol, 2009. **27**(31): p. 5182-8.
18. Pappo, A.S., et al., *Biology and therapy of pediatric rhabdomyosarcoma.* J Clin Oncol, 1995. **13**(8): p. 2123-39.

19. Breitfeld, P.P., et al., *Ifosfamide and etoposide are superior to vincristine and melphalan for pediatric metastatic rhabdomyosarcoma when administered with irradiation and combination chemotherapy: a report from the Intergroup Rhabdomyosarcoma Study Group.* J Pediatr Hematol Oncol, 2001. **23**(4): p. 225-33.

20. Wyllie, A.H., J.F. Kerr, and A.R. Currie, *Cell death: the significance of apoptosis.* Int Rev Cytol, 1980. **68**: p. 251-306.

21. Dixon, S.J., et al., *Ferroptosis: an iron-dependent form of nonapoptotic cell death.* Cell, 2012. **149**(5): p. 1060-72.

22. Shimizu, S., et al., *Autophagic cell death and cancer.* Int J Mol Sci, 2014. **15**(2): p. 3145-53.

23. Fulda, S. and K.M. Debatin, *Extrinsic versus intrinsic apoptosis pathways in anticancer chemotherapy.* Oncogene, 2006. **25**(34): p. 4798-811.

24. Hengartner, M.O., *The biochemistry of apoptosis.* Nature, 2000. **407**: p. 770.

25. Meier, P., A. Finch, and G. Evan, *Apoptosis in development.* Nature, 2000. **407**(6805): p. 796-801.

26. Fulda, S. and K.M. Debatin, *Targeting apoptosis pathways in cancer therapy.* Curr Cancer Drug Targets, 2004. **4**(7): p. 569-76.

27. Hanahan, D. and R.A. Weinberg, *The hallmarks of cancer.* Cell, 2000. **100**(1): p. 57-70.

28. Wachtel, M. and B.W. Schafer, *Targets for cancer therapy in childhood sarcomas.* Cancer Treat Rev, 2010. **36**(4): p. 318-27.

29. Kischkel, F.C., et al., *Cytotoxicity-dependent APO-1 (Fas/CD95)-associated proteins form a death-inducing signaling complex (DISC) with the receptor.* EMBO J, 1995. **14**(22): p. 5579-88.

30. Park, Y.H., M.S. Jeong, and S.B. Jang, *Death domain complex of the TNFR-1, TRADD, and RIP1 proteins for death-inducing signaling.* Biochem Biophys Res Commun, 2014. **443**(4): p. 1155-61.

31. Ashkenazi, A. and V.M. Dixit, *Death receptors: signaling and modulation.* Science, 1998. **281**(5381): p. 1305-8.

32. Walczak, H. and P.H. Krammer, *The CD95 (APO-1/Fas) and the TRAIL (APO-2L) apoptosis systems.* Exp Cell Res, 2000. **256**(1): p. 58-66.

33. Sayers, T.J., *Targeting the extrinsic apoptosis signaling pathway for cancer therapy.* Cancer Immunol Immunother, 2011. **60**(8): p. 1173-80.

34. Ashkenazi, A., *Targeting the extrinsic apoptosis pathway in cancer.* Cytokine Growth Factor Rev, 2008. **19**(3-4): p. 325-31.

35. Luo, X., et al., *Bid, a Bcl2 interacting protein, mediates cytochrome c release from mitochondria in response to activation of cell surface death receptors.* Cell, 1998. **94**(4): p. 481-90.

36. Yin, X.M., et al., *Bid-deficient mice are resistant to Fas-induced hepatocellular apoptosis.* Nature, 1999. **400**(6747): p. 886-91.

37. Galluzzi, L., et al., *Molecular definitions of cell death subroutines: recommendations of the Nomenclature Committee on Cell Death 2012.* Cell Death Differ, 2012. **19**(1): p. 107-20.

38. Westphal, D., et al., *Apoptotic pore formation is associated with in-plane insertion of Bak or Bax central helices into the mitochondrial outer membrane.* Proc Natl Acad Sci U S A, 2014. **111**(39): p. E4076-85.

39. Halestrap, A.P., *The C Ring of the F1Fo ATP Synthase Forms the Mitochondrial Permeability Transition Pore: A Critical Appraisal.* Front Oncol, 2014. **4**: p. 234.

40. Brentnall, M., et al., *Caspase-9, caspase-3 and caspase-7 have distinct roles during intrinsic apoptosis.* BMC Cell Biol, 2013. **14**: p. 32.

41. Huang, Y., et al., *Structural basis of caspase inhibition by XIAP: differential roles of the linker versus the BIR domain.* Cell, 2001. **104**(5): p. 781-90.

42. Cande, C., et al., *Apoptosis-inducing factor (AIF): a novel caspase-independent death effector released from mitochondria.* Biochimie, 2002. **84**(2-3): p. 215-22.

43. Li, L.Y., X. Luo, and X. Wang, *Endonuclease G is an apoptotic DNase when released from mitochondria.* Nature, 2001. **412**(6842): p. 95-9.

44. Vaux, D.L., S. Cory, and J.M. Adams, *Bcl-2 gene promotes haemopoietic cell survival and cooperates with c-myc to immortalize pre-B cells.* Nature, 1988. **335**(6189): p. 440-2.

45. Gross, A., J.M. McDonnell, and S.J. Korsmeyer, *BCL-2 family members and the mitochondria in apoptosis.* Genes Dev, 1999. **13**(15): p. 1899-911.

46. Czabotar, P.E., et al., *Control of apoptosis by the BCL-2 protein family: implications for physiology and therapy.* Nat Rev Mol Cell Biol, 2014. **15**(1): p. 49-63.

47. Chipuk, J.E. and D.R. Green, *How do BCL-2 proteins induce mitochondrial outer membrane permeabilization?* Trends Cell Biol, 2008. **18**(4): p. 157-64.

48. Edlich, F., *The great migration of Bax and Bak.* Mol Cell Oncol, 2015. **2**(3): p. e995029.

49. Boyd, J.M., et al., *Bik, a novel death-inducing protein shares a distinct sequence motif with Bcl-2 family proteins and interacts with viral and cellular survival-promoting proteins.* Oncogene, 1995. **11**(9): p. 1921-8.

50. Youle, R.J. and A. Strasser, *The BCL-2 protein family: opposing activities that mediate cell death.* Nature Reviews Molecular Cell Biology, 2008. **9**: p. 47.

51. Taylor, R.C., S.P. Cullen, and S.J. Martin, *Apoptosis: controlled demolition at the cellular level.* Nature Reviews Molecular Cell Biology, 2008. **9**: p. 231.

52. Dlugosz, P.J., et al., *Bcl-2 changes conformation to inhibit Bax oligomerization.* EMBO J, 2006. **25**(11): p. 2287-96.

53. Murphy, K.M., et al., *Bcl-2 inhibits Bax translocation from cytosol to mitochondria during drug-induced apoptosis of human tumor cells.* Cell Death Differ, 2000. **7**(1): p. 102-11.

54. Willis, S.N., et al., *Proapoptotic Bak is sequestered by Mcl-1 and Bcl-xL, but not Bcl-2, until displaced by BH3-only proteins.* Genes Dev, 2005. **19**(11): p. 1294-305.

55. Gavathiotis, E., et al., *BH3-triggered structural reorganization drives the activation of proapoptotic BAX.* Mol Cell, 2010. **40**(3): p. 481-92.

56. Heinicke, U., et al., *BCL-2 selective inhibitor ABT-199 primes rhabdomyosarcoma cells to histone deacetylase inhibitor-induced apoptosis.* Oncogene, 2018. **37**(39): p. 5325-5339.

57. Chen, L., et al., *Differential targeting of prosurvival Bcl-2 proteins by their BH3-only ligands allows complementary apoptotic function.* Mol Cell, 2005. **17**(3): p. 393-403.

58. Hubner, A., et al., *Functional cooperation of the proapoptotic Bcl2 family proteins Bmf and Bim in vivo.* Mol Cell Biol, 2010. **30**(1): p. 98-105.

59. Willis, S.N., et al., *Apoptosis initiated when BH3 ligands engage multiple Bcl-2 homologs, not Bax or Bak.* Science, 2007. **315**(5813): p. 856-9.

60. Kuwana, T., et al., *BH3 domains of BH3-only proteins differentially regulate Bax-mediated mitochondrial membrane permeabilization both directly and indirectly.* Mol Cell, 2005. **17**(4): p. 525-35.

61. Certo, M., et al., *Mitochondria primed by death signals determine cellular addiction to antiapoptotic BCL-2 family members.* Cancer Cell, 2006. **9**(5): p. 351-65.

62. Merino, D., et al., *The role of BH3-only protein Bim extends beyond inhibiting Bcl-2-like prosurvival proteins.* J Cell Biol, 2009. **186**(3): p. 355-62.

63. Yamamoto, K., H. Ichijo, and S.J. Korsmeyer, *BCL-2 Is Phosphorylated and Inactivated by an ASK1/Jun N-Terminal Protein Kinase Pathway Normally Activated at G₂/M.* Molecular and Cellular Biology, 1999. **19**(12): p. 8469-8478.

64. Fang, X., et al., *Regulation of BAD phosphorylation at serine 112 by the Ras-mitogen-activated protein kinase pathway.* Oncogene, 1999. **18**: p. 6635.

65. Hubner, A., et al., *Multisite phosphorylation regulates Bim stability and apoptotic activity.* Mol Cell, 2008. **30**(4): p. 415-25.

66. Walsh, J.G., et al., *Executioner caspase-3 and caspase-7 are functionally distinct proteases.* Proceedings of the National Academy of Sciences, 2008. **105**(35): p. 12815-12819.

67. Fischer, U., R.U. Janicke, and K. Schulze-Osthoff, *Many cuts to ruin: a comprehensive update of caspase substrates.* Cell Death Differ, 2003. **10**(1): p. 76-100.

68. Enari, M., et al., *A caspase-activated DNase that degrades DNA during apoptosis, and its inhibitor ICAD.* Nature, 1998. **391**(6662): p. 43-50.

69. Coleman, M.L., et al., *Membrane blebbing during apoptosis results from caspase-mediated activation of ROCK I.* Nature Cell Biology, 2001. **3**: p. 339.

70. Taylor, R.C., S.P. Cullen, and S.J. Martin, *Apoptosis: controlled demolition at the cellular level.* Nat Rev Mol Cell Biol, 2008. **9**(3): p. 231-41.

71. Holliday, R., *The inheritance of epigenetic defects.* Science, 1987. **238**(4824): p. 163-70.

72. Holliday, R. and J.E. Pugh, *DNA modification mechanisms and gene activity during development.* Science, 1975. **187**(4173): p. 226-32.

73. Riggs, A.D., *X inactivation, differentiation, and DNA methylation.* Cytogenet Cell Genet, 1975. **14**(1): p. 9-25.

74. Brehm, A., et al., *Retinoblastoma protein recruits histone deacetylase to repress transcription.* Nature, 1998. **391**(6667): p. 597-601.

75. Filippakopoulos, P. and S. Knapp, *Targeting bromodomains: epigenetic readers of lysine acetylation.* Nat Rev Drug Discov, 2014. **13**(5): p. 337-56.

76. Handy, D.E., R. Castro, and J. Loscalzo, *Epigenetic modifications: basic mechanisms and role in cardiovascular disease.* Circulation, 2011. **123**(19): p. 2145-56.

77. Durrin, L.K., et al., *Yeast histone H4 N-terminal sequence is required for promoter activation in vivo.* Cell, 1991. **65**(6): p. 1023-31.

78. Tse, C., et al., *Disruption of higher-order folding by core histone acetylation dramatically enhances transcription of nucleosomal arrays by RNA polymerase III.* Mol Cell Biol, 1998. **18**(8): p. 4629-38.

79. Buurman, R., et al., *Histone deacetylases activate hepatocyte growth factor signaling by repressing microRNA-449 in hepatocellular carcinoma cells.* Gastroenterology, 2012. **143**(3): p. 811-820 e15.

80. Nebbioso, A., et al., *c-Myc Modulation and Acetylation Is a Key HDAC Inhibitor Target in Cancer.* Clin Cancer Res, 2017. **23**(10): p. 2542-2555.

81. Bolden, J.E., M.J. Peart, and R.W. Johnstone, *Anticancer activities of histone deacetylase inhibitors.* Nature Reviews Drug Discovery, 2006. **5**: p. 769.

82. Scuto, A., et al., *The novel histone deacetylase inhibitor, LBH589, induces expression of DNA damage response genes and apoptosis in Ph- acute lymphoblastic leukemia cells.* Blood, 2008. **111**(10): p. 5093-100.

83. Tamkun, J.W., et al., *brahma: a regulator of Drosophila homeotic genes structurally related to the yeast transcriptional activator SNF2/SWI2.* Cell, 1992. **68**(3): p. 561-72.

84. Zhao, Y., et al., *Histone acetylation regulates both transcription initiation and elongation of hsp22 gene in Drosophila.* Biochem Biophys Res Commun, 2005. **326**(4): p. 811-6.

85. Jenuwein, T. and C.D. Allis, *Translating the histone code.* Science, 2001. **293**(5532): p. 1074-80.

86. Zuber, J., et al., *RNAi screen identifies Brd4 as a therapeutic target in acute myeloid leukaemia.* Nature, 2011. **478**(7370): p. 524-8.

87. Li, G.Q., et al., *Suppression of BRD4 inhibits human hepatocellular carcinoma by repressing MYC and enhancing BIM expression.* Oncotarget, 2016. **7**(3): p. 2462-74.

88. Hogg, S.J., et al., *BET Inhibition Induces Apoptosis in Aggressive B-Cell Lymphoma via Epigenetic Regulation of BCL-2 Family Members.* Mol Cancer Ther, 2016. **15**(9): p. 2030-41.

89. Berenguer-Daize, C., et al., *OTX015 (MK-8628), a novel BET inhibitor, displays in vitro and in vivo antitumor effects alone and in combination with conventional therapies in glioblastoma models.* Int J Cancer, 2016. **139**(9): p. 2047-55.

90. Josling, G.A., et al., *The role of bromodomain proteins in regulating gene expression.* Genes (Basel), 2012. **3**(2): p. 320-43.

91. Dhalluin, C., et al., *Structure and ligand of a histone acetyltransferase bromodomain.* Nature, 1999. **399**(6735): p. 491-6.

92. Filippakopoulos, P., et al., *Histone recognition and large-scale structural analysis of the human bromodomain family.* Cell, 2012. **149**(1): p. 214-31.

93. Yang, Z., et al., *Recruitment of P-TEFb for stimulation of transcriptional elongation by the bromodomain protein Brd4.* Mol Cell, 2005. **19**(4): p. 535-45.

94. Miller, T.C., et al., *A bromodomain-DNA interaction facilitates acetylation-dependent bivalent nucleosome recognition by the BET protein BRDT.* Nat Commun, 2016. **7**: p. 13855.

95. Bhagwat, A.S., et al., *BET Bromodomain Inhibition Releases the Mediator Complex from Select cis-Regulatory Elements.* Cell Rep, 2016. **15**(3): p. 519-530.

96. Zippo, A., et al., *PIM1-dependent phosphorylation of histone H3 at serine 10 is required for MYC-dependent transcriptional activation and oncogenic transformation.* Nat Cell Biol, 2007. **9**(8): p. 932-44.

97. Su, J., et al., *The Functional Analysis of Histone Acetyltransferase MOF in Tumorigenesis.* Int J Mol Sci, 2016. **17**(1).

98. Zippo, A., et al., *Histone crosstalk between H3S10ph and H4K16ac generates a histone code that mediates transcription elongation.* Cell, 2009. **138**(6): p. 1122-36.

99. Wu, S.Y. and C.M. Chiang, *The double bromodomain-containing chromatin adaptor Brd4 and transcriptional regulation.* J Biol Chem, 2007. **282**(18): p. 13141-5.

100. Marshall, N.F. and D.H. Price, *Purification of P-TEFb, a transcription factor required for the transition into productive elongation.* J Biol Chem, 1995. **270**(21): p. 12335-8.

101. Benedikt, A., et al., *The leukemogenic AF4-MLL fusion protein causes P-TEFb kinase activation and altered epigenetic signatures.* Leukemia, 2011. **25**(1): p. 135-44.

102. Price, D.H., *P-TEFb, a cyclin-dependent kinase controlling elongation by RNA polymerase II.* Mol Cell Biol, 2000. **20**(8): p. 2629-34.

103. Chiba, K., et al., *Promoter-proximal pausing and its release: molecular mechanisms and physiological functions.* Exp Cell Res, 2010. **316**(17): p. 2723-30.

104. Liu, J., et al., *Targeting the BRD4/FOXO3a/CDK6 axis sensitizes AKT inhibition in luminal breast cancer.* Nat Commun, 2018. **9**(1): p. 5200.

105. Huang, B., et al., *Brd4 coactivates transcriptional activation of NF-kappaB via specific binding to acetylated RelA.* Mol Cell Biol, 2009. **29**(5): p. 1375-87.

106. Wu, T., Y.F. Kamikawa, and M.E. Donohoe, *Brd4's Bromodomains Mediate Histone H3 Acetylation and Chromatin Remodeling in Pluripotent Cells through P300 and Brg1.* Cell Rep, 2018. **25**(7): p. 1756-1771.

107. Rahman, S., et al., *The Brd4 extraterminal domain confers transcription activation independent of pTEFb by recruiting multiple proteins, including NSD3.* Mol Cell Biol, 2011. **31**(13): p. 2641-52.

108. Wu, S.Y., et al., *Phospho switch triggers Brd4 chromatin binding and activator recruitment for gene-specific targeting.* Mol Cell, 2013. **49**(5): p. 843-57.

109. Chiang, C.M., *Phospho-BRD4: transcription plasticity and drug targeting.* Drug Discov Today Technol, 2016. **19**: p. 17-22.

110. Wang, R., et al., *Uncovering BRD4 hyperphosphorylation associated with cellular transformation in NUT midline carcinoma.* Proc Natl Acad Sci U S A, 2017. **114**(27): p. E5352-E5361.

111. Suarez-Alvarez, B., et al., *BET Proteins: An Approach to Future Therapies in Transplantation.* Am J Transplant, 2017. **17**(9): p. 2254-2262.

112. Bradner, J.E., D. Hnisz, and R.A. Young, *Transcriptional Addiction in Cancer.* Cell, 2017. **168**(4): p. 629-643.

113. Bid, H.K., et al., *The Bromodomain BET Inhibitor JQ1 Suppresses Tumor Angiogenesis in Models of Childhood Sarcoma.* Mol Cancer Ther, 2016. **15**(5): p. 1018-28.

114. Delmore, J.E., et al., *BET bromodomain inhibition as a therapeutic strategy to target c-Myc.* Cell, 2011. **146**(6): p. 904-17.

115. Alekseyenko, A.A., et al., *The oncogenic BRD4-NUT chromatin regulator drives aberrant transcription within large topological domains.* Genes Dev, 2015. **29**(14): p. 1507-23.

116. Schuijers, J., et al., *Transcriptional Dysregulation of MYC Reveals Common Enhancer-Docking Mechanism.* Cell Rep, 2018. **23**(2): p. 349-360.

117. Loven, J., et al., *Selective inhibition of tumor oncogenes by disruption of super-enhancers.* Cell, 2013. **153**(2): p. 320-34.

118. Zanconato, F., et al., *Transcriptional addiction in cancer cells is mediated by YAP/TAZ through BRD4.* Nat Med, 2018. **24**(10): p. 1599-1610.

119. Nicodeme, E., et al., *Suppression of inflammation by a synthetic histone mimic.* Nature, 2010. **468**(7327): p. 1119-23.

120. Filippakopoulos, P., et al., *Selective inhibition of BET bromodomains.* Nature, 2010. **468**(7327): p. 1067-73.

121. Whitfield, J.R., M.E. Beaulieu, and L. Soucek, *Strategies to Inhibit Myc and Their Clinical Applicability.* Front Cell Dev Biol, 2017. **5**: p. 10.

122. Stathis, A., et al., *Clinical Response of Carcinomas Harboring the BRD4-NUT Oncoprotein to the Targeted Bromodomain Inhibitor OTX015/MK-8628.* Cancer Discov, 2016. **6**(5): p. 492-500.

123. Beesley, A.H., et al., *Comparative drug screening in NUT midline carcinoma.* Br J Cancer, 2014. **110**(5): p. 1189-98.

124. Enssle, J.C., et al., *Co-targeting of BET proteins and HDACs as a novel approach to trigger apoptosis in rhabdomyosarcoma cells.* Cancer Lett, 2018. **428**: p. 160-172.

125. Alghamdi, S., et al., *BET protein inhibitor JQ1 inhibits growth and modulates WNT signaling in mesenchymal stem cells.* Stem Cell Res Ther, 2016. **7**: p. 22.

126. Hensel, T., et al., *Targeting the EWS-ETS transcriptional program by BET bromodomain inhibition in Ewing sarcoma.* Oncotarget, 2016. **7**(2): p. 1451-63.

127. Baltz, N.J., et al., *JQ1, a Potential Therapeutic Molecule for Myeloid Leukemia with PTEN Deficiency.* Blood, 2016. **128**(22): p. 5899-5899.

128. Lee, D.H., et al., *Synergistic effect of JQ1 and rapamycin for treatment of human osteosarcoma.* Int J Cancer, 2015. **136**(9): p. 2055-64.

129. Fiskus, W., et al., *BET protein antagonist JQ1 is synergistically lethal with FLT3 tyrosine kinase inhibitor (TKI) and overcomes resistance to FLT3-TKI in AML cells expressing FLT-ITD.* Mol Cancer Ther, 2014. **13**(10): p. 2315-27.

130. Tang, Y., et al., *Epigenetic targeting of Hedgehog pathway transcriptional output through BET bromodomain inhibition.* Nat Med, 2014. **20**(7): p. 732-40.

131. Lu, J., et al., *Hijacking the E3 Ubiquitin Ligase Cereblon to Efficiently Target BRD4.* Chem Biol, 2015. **22**(6): p. 755-63.

132. Kurimchak, A.M., et al., *Resistance to BET Bromodomain Inhibitors Is Mediated by Kinome Reprogramming in Ovarian Cancer.* Cell Rep, 2016. **16**(5): p. 1273-86.

133. Fong, C.Y., et al., *BET inhibitor resistance emerges from leukaemia stem cells.* Nature, 2015. **525**(7570): p. 538-42.

134. Shu, S., et al., *Response and resistance to BET bromodomain inhibitors in triple-negative breast cancer.* Nature, 2016. **529**(7586): p. 413-417.

135. Zanellato, I., D. Colangelo, and D. Osella, *JQ1, a BET inhibitor, synergizes with cisplatin and induces apoptosis in highly chemoresistant malignant pleural mesothelioma cells.* Curr Cancer Drug Targets, 2017.

136. Holscher, A.S., et al., *Combined inhibition of BET proteins and class I HDACs synergistically induces apoptosis in urothelial carcinoma cell lines.* Clin Epigenetics, 2018. **10**: p. 1.

137. Gerlach, D., et al., *The novel BET bromodomain inhibitor BI 894999 represses super-enhancer-associated transcription and synergizes with CDK9 inhibition in AML.* Oncogene, 2018. **37**(20): p. 2687-2701.

138. Kim, S.R., et al., *BET inhibition in advanced cutaneous T cell lymphoma is synergistically potentiated by BCL2 inhibition or HDAC inhibition.* Oncotarget, 2018. **9**(49): p. 29193-29207.

139. Moros, A., et al., *Synergistic antitumor activity of lenalidomide with the BET bromodomain inhibitor CPI203 in bortezomib-resistant mantle cell lymphoma.* Leukemia, 2014. **28**(10): p. 2049-59.

140. Tinsley, S., et al., *Synergistic induction of cell death in haematological malignancies by combined phosphoinositide-3-kinase and BET bromodomain inhibition.* Br J Haematol, 2015. **170**(2): p. 275-8.

141. Diaz, T., et al., *The BET bromodomain inhibitor CPI203 improves lenalidomide and dexamethasone activity in in vitro and in vivo models of multiple myeloma by blockade of Ikaros and MYC signaling.* Haematologica, 2017.

142. Stratikopoulos, E.E., et al., *Kinase and BET Inhibitors Together Clamp Inhibition of PI3K Signaling and Overcome Resistance to Therapy.* Cancer Cell, 2015. **27**(6): p. 837-51.

143. Haydn, T., et al., *Concomitant epigenetic targeting of LSD1 and HDAC synergistically induces mitochondrial apoptosis in rhabdomyosarcoma cells.* Cell Death Dis, 2017. **8**(6): p. e2879.

144. Heinicke, U., J. Kupka, and S. Fulda, *JNJ-26481585 primes rhabdomyosarcoma cells for chemotherapeutics by engaging the mitochondrial pathway of apoptosis.* Oncotarget, 2015. **6**(35): p. 37836-51.

145. Seto, E. and M. Yoshida, *Erasers of histone acetylation: the histone deacetylase enzymes.* Cold Spring Harb Perspect Biol, 2014. **6**(4): p. a018713.

146. Chen, L., et al., *Dual role of Zn2+ in maintaining structural integrity and suppressing deacetylase activity of SIRT1.* J Inorg Biochem, 2010. **104**(2): p. 180-5.

147. Landry, J., et al., *The silencing protein SIR2 and its homologs are NAD-dependent protein deacetylases.* Proc Natl Acad Sci U S A, 2000. **97**(11): p. 5807-11.

148. Garnock-Jones, K.P., *Panobinostat: first global approval.* Drugs, 2015. **75**(6): p. 695-704.

149. Mann, B.S., et al., *FDA approval summary: vorinostat for treatment of advanced primary cutaneous T-cell lymphoma.* Oncologist, 2007. **12**(10): p. 1247-52.

150. Fiskus, W., et al., *Highly active combination of BRD4 antagonist and histone deacetylase inhibitor against human acute myelogenous leukemia cells.* Mol Cancer Ther, 2014. **13**(5): p. 1142-54.

151. Bhadury, J., et al., *BET and HDAC inhibitors induce similar genes and biological effects and synergize to kill in Myc-induced murine lymphoma.* Proc Natl Acad Sci U S A, 2014. **111**(26): p. E2721-30.

152. West, A.C. and R.W. Johnstone, *New and emerging HDAC inhibitors for cancer treatment.* J Clin Invest, 2014. **124**(1): p. 30-9.

153. Arts, J., et al., *JNJ-26481585, a novel "second-generation" oral histone deacetylase inhibitor, shows broad-spectrum preclinical antitumoral activity.* Clin Cancer Res, 2009. **15**(22): p. 6841-51.

154. Vivanco, I. and C.L. Sawyers, *The phosphatidylinositol 3-Kinase AKT pathway in human cancer.* Nat Rev Cancer, 2002. **2**(7): p. 489-501.

155. Vadas, O., et al., *Molecular determinants of PI3Kgamma-mediated activation downstream of G-protein-coupled receptors (GPCRs).* Proc Natl Acad Sci U S A, 2013. **110**(47): p. 18862-7.

156. McGlade, C.J., et al., *SH2 domains of the p85 alpha subunit of phosphatidylinositol 3-kinase regulate binding to growth factor receptors.* Mol Cell Biol, 1992. **12**(3): p. 991-7.

157. Songyang, Z., et al., *SH2 domains recognize specific phosphopeptide sequences.* Cell, 1993. **72**(5): p. 767-78.

158. Manning, B.D. and L.C. Cantley, *AKT/PKB signaling: navigating downstream.* Cell, 2007. **129**(7): p. 1261-74.

159. Klippel, A., et al., *A specific product of phosphatidylinositol 3-kinase directly activates the protein kinase Akt through its pleckstrin homology domain.* Mol Cell Biol, 1997. **17**(1): p. 338-44.

160. Alessi, D.R., et al., *Characterization of a 3-phosphoinositide-dependent protein kinase which phosphorylates and activates protein kinase Balpha.* Curr Biol, 1997. **7**(4): p. 261-9.

161. Vanhaesebroeck, B., et al., *The emerging mechanisms of isoform-specific PI3K signalling.* Nat Rev Mol Cell Biol, 2010. **11**(5): p. 329-41.

162. Denley, A., et al., *Requirement of phosphatidylinositol(3,4,5)trisphosphate in phosphatidylinositol 3-kinase-induced oncogenic transformation.* Mol Cancer Res, 2009. **7**(7): p. 1132-8.

163. Cantley, L.C. and B.G. Neel, *New insights into tumor suppression: PTEN suppresses tumor formation by restraining the phosphoinositide 3-kinase/AKT pathway.* Proc Natl Acad Sci U S A, 1999. **96**(8): p. 4240-5.

164. Weng, L.P., et al., *PTEN suppresses breast cancer cell growth by phosphatase activity-dependent G1 arrest followed by cell death.* Cancer Res, 1999. **59**(22): p. 5808-14.

165. Cully, M., et al., *Beyond PTEN mutations: the PI3K pathway as an integrator of multiple inputs during tumorigenesis.* Nat Rev Cancer, 2006. **6**(3): p. 184-92.

166. Weigelt, B., et al., *PI3K pathway dependencies in endometrioid endometrial cancer cell lines.* Clin Cancer Res, 2013. **19**(13): p. 3533-44.

167. Sarbassov, D.D., et al., *Phosphorylation and regulation of Akt/PKB by the rictor-mTOR complex.* Science, 2005. **307**(5712): p. 1098-101.

168. Stephens, L., et al., *Protein kinase B kinases that mediate phosphatidylinositol 3,4,5-trisphosphate-dependent activation of protein kinase B.* Science, 1998. **279**(5351): p. 710-4.

169. Cross, D.A., et al., *Inhibition of glycogen synthase kinase-3 by insulin mediated by protein kinase B.* Nature, 1995. **378**(6559): p. 785-9.

170. Brunet, A., et al., *Akt promotes cell survival by phosphorylating and inhibiting a Forkhead transcription factor.* Cell, 1999. **96**(6): p. 857-68.

171. Scheid, M.P. and V. Duronio, *Dissociation of cytokine-induced phosphorylation of Bad and activation of PKB/akt: involvement of MEK upstream of Bad phosphorylation.* Proc Natl Acad Sci U S A, 1998. **95**(13): p. 7439-44.

172. Alliouachene, S., et al., *Inactivation of the Class II PI3K-C2beta Potentiates Insulin Signaling and Sensitivity.* Cell Rep, 2015. **13**(9): p. 1881-94.

173. Dong, X.P., et al., *PI(3,5)P(2) controls membrane trafficking by direct activation of mucolipin Ca(2+) release channels in the endolysosome.* Nat Commun, 2010. **1**: p. 38.

174. Tassa, A., et al., *Class III phosphoinositide 3-kinase--Beclin1 complex mediates the amino acid-dependent regulation of autophagy in C2C12 myotubes.* Biochem J, 2003. **376**(Pt 3): p. 577-86.

175. Yip, C.K., et al., *Structure of the human mTOR complex I and its implications for rapamycin inhibition.* Mol Cell, 2010. **38**(5): p. 768-74.

176. Pearce, L.R., et al., *Identification of Protor as a novel Rictor-binding component of mTOR complex-2.* Biochem J, 2007. **405**(3): p. 513-22.

177. Liu, P., et al., *Targeting the phosphoinositide 3-kinase pathway in cancer.* Nat Rev Drug Discov, 2009. **8**(8): p. 627-44.

178. Sun, S.Y., et al., *Activation of Akt and eIF4E survival pathways by rapamycin-mediated mammalian target of rapamycin inhibition.* Cancer Res, 2005. **65**(16): p. 7052-8.

179. Breuleux, M., et al., *Increased AKT S473 phosphorylation after mTORC1 inhibition is rictor dependent and does not predict tumor cell response to PI3K/mTOR inhibition.* Mol Cancer Ther, 2009. **8**(4): p. 742-53.

180. Chandarlapaty, S., et al., *AKT inhibition relieves feedback suppression of receptor tyrosine kinase expression and activity.* Cancer Cell, 2011. **19**(1): p. 58-71.

181. Wan, X., et al., *Rapamycin induces feedback activation of Akt signaling through an IGF-1R-dependent mechanism.* Oncogene, 2007. **26**(13): p. 1932-40.

182. Altomare, D.A., et al., *AKT and mTOR phosphorylation is frequently detected in ovarian cancer and can be targeted to disrupt ovarian tumor cell growth.* Oncogene, 2004. **23**(34): p. 5853-7.

183. Stewart, E., et al., *Identification of Therapeutic Targets in Rhabdomyosarcoma through Integrated Genomic, Epigenomic, and Proteomic Analyses.* Cancer Cell, 2018. **34**(3): p. 411-426 e19.

184. Fruman, D.A. and C. Rommel, *PI3K and cancer: lessons, challenges and opportunities.* Nat Rev Drug Discov, 2014. **13**(2): p. 140-56.

185. Guertin, D.A., et al., *mTOR complex 2 is required for the development of prostate cancer induced by Pten loss in mice.* Cancer Cell, 2009. **15**(2): p. 148-59.

186. Zhang, X., et al., *Akt, FoxO and regulation of apoptosis.* Biochim Biophys Acta, 2011. **1813**(11): p. 1978-86.

187. Garcia-Echeverria, C. and W.R. Sellers, *Drug discovery approaches targeting the PI3K/Akt pathway in cancer.* Oncogene, 2008. **27**(41): p. 5511-26.

188. Engelman, J.A., *Targeting PI3K signalling in cancer: opportunities, challenges and limitations.* Nat Rev Cancer, 2009. **9**(8): p. 550-62.

189. Malek, M., et al., *PTEN Regulates PI(3,4)P2 Signaling Downstream of Class I PI3K.* Mol Cell, 2017. **68**(3): p. 566-580 e10.

190. Hayakawa, M., et al., *Synthesis and biological evaluation of pyrido[3',2':4,5]furo[3,2-d]pyrimidine derivatives as novel PI3 kinase p110alpha inhibitors.* Bioorg Med Chem Lett, 2007. **17**(9): p. 2438-42.

191. Graab, U., H. Hahn, and S. Fulda, *Identification of a novel synthetic lethality of combined inhibition of hedgehog and PI3K signaling in rhabdomyosarcoma.* Oncotarget, 2015. **6**(11): p. 8722-35.

192. Al-Saffar, N.M., et al., *The phosphoinositide 3-kinase inhibitor PI-103 downregulates choline kinase alpha leading to phosphocholine and total choline decrease detected by magnetic resonance spectroscopy.* Cancer Res, 2010. **70**(13): p. 5507-17.

193. Yap, T.A., et al., *First-in-man clinical trial of the oral pan-AKT inhibitor MK-2206 in patients with advanced solid tumors.* J Clin Oncol, 2011. **29**(35): p. 4688-95.

194. Brana, I. and L.L. Siu, *Clinical development of phosphatidylinositol 3-kinase inhibitors for cancer treatment.* BMC Med, 2012. **10**: p. 161.

195. O'Brien, C., et al., *Predictive biomarkers of sensitivity to the phosphatidylinositol 3' kinase inhibitor GDC-0941 in breast cancer preclinical models.* Clin Cancer Res, 2010. **16**(14): p. 3670-83.

196. Rodon, J., et al., *Development of PI3K inhibitors: lessons learned from early clinical trials.* Nature Reviews Clinical Oncology, 2013. **10**: p. 143.

197. Renshaw, J., et al., *Dual blockade of the PI3K/AKT/mTOR (AZD8055) and RAS/MEK/ERK (AZD6244) pathways synergistically inhibits rhabdomyosarcoma cell growth in vitro and in vivo.* Clin Cancer Res, 2013. **19**(21): p. 5940-51.

198. Samuels, Y., et al., *High frequency of mutations of the PIK3CA gene in human cancers.* Science, 2004. **304**(5670): p. 554.

199. Huang, C.H., et al., *The structure of a human p110alpha/p85alpha complex elucidates the effects of oncogenic PI3Kalpha mutations.* Science, 2007. **318**(5857): p. 1744-8.

200. Burke, J.E., et al., *Oncogenic mutations mimic and enhance dynamic events in the natural activation of phosphoinositide 3-kinase p110alpha (PIK3CA).* Proc Natl Acad Sci U S A, 2012. **109**(38): p. 15259-64.

201. Hao, Y., et al., *Gain of interaction with IRS1 by p110alpha-helical domain mutants is crucial for their oncogenic functions.* Cancer Cell, 2013. **23**(5): p. 583-93.

202. Mandelker, D., et al., *A frequent kinase domain mutation that changes the interaction between PI3Kalpha and the membrane.* Proc Natl Acad Sci U S A, 2009. **106**(40): p. 16996-7001.

203. Zhao, J.J., et al., *The p110alpha isoform of PI3K is essential for proper growth factor signaling and oncogenic transformation.* Proc Natl Acad Sci U S A, 2006. **103**(44): p. 16296-300.

204. Foukas, L.C., et al., *Critical role for the p110alpha phosphoinositide-3-OH kinase in growth and metabolic regulation.* Nature, 2006. **441**(7091): p. 366-70.

205. Jia, S., et al., *Essential roles of PI(3)K-p110beta in cell growth, metabolism and tumorigenesis.* Nature, 2008. **454**(7205): p. 776-9.

206. Bohnacker, T., et al., *PI3Kgamma adaptor subunits define coupling to degranulation and cell motility by distinct PtdIns(3,4,5)P3 pools in mast cells.* Sci Signal, 2009. **2**(74): p. ra27.

207. Saudemont, A., et al., *p110gamma and p110delta isoforms of phosphoinositide 3-kinase differentially regulate natural killer cell migration in health and disease.* Proc Natl Acad Sci U S A, 2009. **106**(14): p. 5795-800.

208. Dolgikh, N., et al., *NRAS-Mutated Rhabdomyosarcoma Cells Are Vulnerable to Mitochondrial Apoptosis Induced by Coinhibition of MEK and PI3Kalpha.* Cancer Res, 2018. **78**(8): p. 2000-2013.

209. Vora, S.R., et al., *CDK 4/6 inhibitors sensitize PIK3CA mutant breast cancer to PI3K inhibitors.* Cancer Cell, 2014. **26**(1): p. 136-49.

210. Juric, D., et al., *Phosphatidylinositol 3-Kinase alpha-Selective Inhibition With Alpelisib (BYL719) in PIK3CA-Altered Solid Tumors: Results From the First-in-Human Study.* J Clin Oncol, 2018. **36**(13): p. 1291-1299.

211. Zhu, W., et al., *MicroRNA-503 regulates hypoxia-induced cardiomyocytes apoptosis through PI3K/Akt pathway by targeting IGF-1R.* Biochem Biophys Res Commun, 2018. **506**(4): p. 1026-1031.

212. Yu, T., et al., *Insulin promotes macrophage phenotype transition through PI3K/Akt and PPAR-gamma signaling during diabetic wound healing.* J Cell Physiol, 2018.

213. Martinelli, S., et al., *RAS signaling dysregulation in human embryonal Rhabdomyosarcoma.* Genes Chromosomes Cancer, 2009. **48**(11): p. 975-82.

214. Bhagwat, A.S. and C.R. Vakoc, *Targeting Transcription Factors in Cancer.* Trends Cancer, 2015. **1**(1): p. 53-65.

215. Yohe, M.E., et al., *MEK inhibition induces MYOG and remodels super-enhancers in RAS-driven rhabdomyosarcoma.* Sci Transl Med, 2018. **10**(448).

216. Zibat, A., et al., *Activation of the hedgehog pathway confers a poor prognosis in embryonal and fusion gene-negative alveolar rhabdomyosarcoma.* Oncogene, 2010. **29**(48): p. 6323-30.

217. Rahl, P.B., et al., *c-Myc regulates transcriptional pause release.* Cell, 2010. **141**(3): p. 432-45.

218. Sabo, A. and B. Amati, *BRD4 and MYC-clarifying regulatory specificity.* Science, 2018. **360**(6390): p. 713-714.

219. Blee, A.M., et al., *BET bromodomain-mediated interaction between ERG and BRD4 promotes prostate cancer cell invasion.* Oncotarget, 2016. **7**(25): p. 38319-38332.

220. Segatto, M., et al., *Epigenetic targeting of bromodomain protein BRD4 counteracts cancer cachexia and prolongs survival.* Nature Communications, 2017. **8**(1): p. 1707.

221. Zawistowski, J.S., et al., *Enhancer Remodeling during Adaptive Bypass to MEK Inhibition Is Attenuated by Pharmacologic Targeting of the P-TEFb Complex.* Cancer Discov, 2017. **7**(3): p. 302-321.

222. Wyce, A., et al., *MEK inhibitors overcome resistance to BET inhibition across a number of solid and hematologic cancers.* Oncogenesis, 2018. **7**(4): p. 35.

223. Fulda, S., *Tumor resistance to apoptosis.* Int J Cancer, 2009. **124**(3): p. 511-5.

224. Carracedo, A., et al., *Inhibition of mTORC1 leads to MAPK pathway activation through a PI3K-dependent feedback loop in human cancer.* J Clin Invest, 2008. **118**(9): p. 3065-74.

225. Vanhaesebroeck, B., et al., *The emerging mechanisms of isoform-specific PI3K signalling.* Nature Reviews Molecular Cell Biology, 2010. **11**: p. 329.

226. Massacesi, C., et al., *PI3K inhibitors as new cancer therapeutics: implications for clinical trial design.* Onco Targets Ther, 2016. **9**: p. 203-10.

227. Chou, T.C., *Drug combination studies and their synergy quantification using the Chou-Talalay method.* Cancer Res, 2010. **70**(2): p. 440-6.

228. Stratikopoulos, E.E. and R.E. Parsons, *Molecular Pathways: Targeting the PI3K Pathway in Cancer-BET Inhibitors to the Rescue.* Clin Cancer Res, 2016. **22**(11): p. 2605-10.

229. Costa, C., et al., *Measurement of PIP3 levels reveals an unexpected role for p110beta in early adaptive responses to p110alpha-specific inhibitors in luminal breast cancer.* Cancer Cell, 2015. **27**(1): p. 97-108.

230. Rodon, J., et al., *Development of PI3K inhibitors: lessons learned from early clinical trials.* Nat Rev Clin Oncol, 2013. **10**(3): p. 143-53.

231. Schwartz, S., et al., *Feedback suppression of PI3Kalpha signaling in PTEN-mutated tumors is relieved by selective inhibition of PI3Kbeta.* Cancer Cell, 2015. **27**(1): p. 109-22.

232. Da Costa, D., et al., *BET inhibition as a single or combined therapeutic approach in primary paediatric B-precursor acute lymphoblastic leukaemia.* Blood Cancer J, 2013. **3**: p. e126.

233. Odore, E., et al., *Phase I Population Pharmacokinetic Assessment of the Oral Bromodomain Inhibitor OTX015 in Patients with Haematologic Malignancies.* Clin Pharmacokinet, 2016. **55**(3): p. 397-405.

234. Heinicke, U., et al., *Critical role of mitochondria-mediated apoptosis for JNJ-26481585-induced antitumor activity in rhabdomyosarcoma.* Oncogene, 2016. **35**(28): p. 3729-41.

235. Saelens, X., et al., *Toxic proteins released from mitochondria in cell death.* Oncogene, 2004. **23**(16): p. 2861-74.

236. Bratton, S.B. and G.S. Salvesen, *Regulation of the Apaf-1-caspase-9 apoptosome.* J Cell Sci, 2010. **123**(Pt 19): p. 3209-14.

237. Tan, Z., et al., *Arsenic sulfide amplifies JQ1 toxicity via mitochondrial pathway in gastric and colon cancer cells.* Drug Des Devel Ther, 2018. **12**: p. 3913-3927.

238. Xu, Z., et al., *BET inhibition represses miR17-92 to drive BIM-initiated apoptosis of normal and transformed hematopoietic cells.* Leukemia, 2016. **30**(7): p. 1531-41.

239. Kutuk, O. and A. Letai, *Displacement of Bim by Bmf and Puma rather than increase in Bim level mediates paclitaxel-induced apoptosis in breast cancer cells.* Cell Death Differ, 2010. **17**(10): p. 1624-35.

240. Del Gaizo Moore, V., et al., *Chronic lymphocytic leukemia requires BCL2 to sequester prodeath BIM, explaining sensitivity to BCL2 antagonist ABT-737.* J Clin Invest, 2007. **117**(1): p. 112-21.

241. Kaplon, J., L. van Dam, and D. Peeper, *Two-way communication between the metabolic and cell cycle machineries: the molecular basis.* Cell Cycle, 2015. **14**(13): p. 2022-32.

242. Morrish, F., et al., *The oncogene c-Myc coordinates regulation of metabolic networks to enable rapid cell cycle entry.* Cell Cycle, 2008. **7**(8): p. 1054-66.

243. Morrish, F., et al., *c-Myc activates multiple metabolic networks to generate substrates for cell-cycle entry.* Oncogene, 2009. **28**(27): p. 2485-91.

244. Detmer, K., et al., *Hedgehog signaling and cell cycle control in differentiating erythroid progenitors.* Blood Cells Mol Dis, 2005. **34**(1): p. 60-70.

245. Hosoi, H., et al., *Rapamycin causes poorly reversible inhibition of mTOR and induces p53-independent apoptosis in human rhabdomyosarcoma cells.* Cancer Res, 1999. **59**(4): p. 886-94.

246. Lee, T.I. and R.A. Young, *Transcriptional regulation and its misregulation in disease.* Cell, 2013. **152**(6): p. 1237-51.

247. Hornsveld, M., et al., *Restraining FOXO3-dependent transcriptional BMF activation underpins tumour growth and metastasis of E-cadherin-negative breast cancer.* Cell Death Differ, 2016. **23**(9): p. 1483-92.

248. Gilley, J., P.J. Coffer, and J. Ham, *FOXO transcription factors directly activate bim gene expression and promote apoptosis in sympathetic neurons.* J Cell Biol, 2003. **162**(4): p. 613-22.

249. Yohe, M.E., et al., *MEK inhibition induces MYOG and remodels super-enhancers in RAS-driven rhabdomyosarcoma.* Sci Transl Med, 2018. **10**: p. 448.

250. Zuber, V., et al., *Bromodomain protein 4 discriminates tissue-specific super-enhancers containing disease-specific susceptibility loci in prostate and breast cancer.* BMC Genomics, 2017. **18**(1): p. 270.

251. Swerev, T.M., T. Wirth, and A. Ushmorov, *Activation of oncogenic pathways in classical Hodgkin lymphoma by decitabine: A rationale for combination with small molecular weight inhibitors.* Int J Oncol, 2017. **50**(2): p. 555-566.

252. Wu, X., et al., *Inhibition of BRD4 Suppresses Cell Proliferation and Induces Apoptosis in Renal Cell Carcinoma.* Cell Physiol Biochem, 2017. **41**(5): p. 1947-1956.

253. Bhattacharya, S., S. Piya, and G. Borthakur, *Bromodomain inhibitors: what does the future hold?* Clin Adv Hematol Oncol, 2018. **16**(7): p. 504-515.

254. Andrieu, G., A.C. Belkina, and G.V. Denis, *Clinical trials for BET inhibitors run ahead of the science.* Drug Discov Today Technol, 2016. **19**: p. 45-50.

255. Ward, P.S., et al., *The common feature of leukemia-associated IDH1 and IDH2 mutations is a neomorphic enzyme activity converting alpha-ketoglutarate to 2-hydroxyglutarate.* Cancer Cell, 2010. **17**(3): p. 225-34.

256. Doroshow, D.B., J.P. Eder, and P.M. LoRusso, *BET inhibitors: a novel epigenetic approach.* Ann Oncol, 2017. **28**(8): p. 1776-1787.

257. Ciceri, P., et al., *Dual kinase-bromodomain inhibitors for rationally designed polypharmacology.* Nat Chem Biol, 2014. **10**(4): p. 305-12.

258. Bolden, J.E., et al., *Inducible in vivo silencing of Brd4 identifies potential toxicities of sustained BET protein inhibition.* Cell Rep, 2014. **8**(6): p. 1919-1929.

259. Liu, W., et al., *BRD4 regulates Nanog expression in mouse embryonic stem cells and preimplantation embryos.* Cell Death Differ, 2014. **21**(12): p. 1950-60.

260. Criscitiello, C., et al., *Profile of buparlisib and its potential in the treatment of breast cancer: evidence to date.* Breast Cancer (Dove Med Press), 2018. **10**: p. 23-29.

261. Waring, M.J., et al., *Potent and selective bivalent inhibitors of BET bromodomains.* Nat Chem Biol, 2016. **12**(12): p. 1097-1104.

262. Mele, D.A., et al., *BET bromodomain inhibition suppresses TH17-mediated pathology.* J Exp Med, 2013. **210**(11): p. 2181-90.

263. Wu, S.Y., et al., *BRD4 Phosphorylation Regulates HPV E2-Mediated Viral Transcription, Origin Replication, and Cellular MMP-9 Expression.* Cell Rep, 2016. **16**(6): p. 1733-1748.

264. Wang, F., et al., *Brd2 disruption in mice causes severe obesity without Type 2 diabetes.* Biochem J, 2009. **425**(1): p. 71-83.

265. Soler, A., et al., *Therapeutic Benefit of Selective Inhibition of p110alpha PI3-Kinase in Pancreatic Neuroendocrine Tumors.* Clin Cancer Res, 2016. **22**(23): p. 5805-5817.

266. Seal, J., et al., *Identification of a novel series of BET family bromodomain inhibitors: binding mode and profile of I-BET151 (GSK1210151A).* Bioorg Med Chem Lett, 2012. **22**(8): p. 2968-72.

10 Related Publications

The main part of the results is depicted from the manuscript

“Co-inhibition of BET proteins and PI3Kα reallocates BRD4 to transcriptional regulatory elements of BH3-only proteins and triggers mitochondrial apoptosis”,

which is currently under review in Oncogene.

Additional part of the results is depicted from the publication

“Co-targeting of BET proteins and HDACs as a novel approach to trigger apoptosis in rhabdomyosarcoma cells“,

which was published in Cancer Letters in 2018.

11 Acknowledgements

After more than four years of work, I finally want to say thank you. First of all, I would like to thank my direct supervisor Prof. Simone Fulda for providing me with the opportunity to complete my PhD thesis at her lab. Thanks for the constant support, guidance and encouragement during the years.

Furthermore, I want to thank Prof. Rolf Marschalek from the Institute of Phamaceutical Biology at the Fachbereich 14 for being my internal supervisor as well as for helpful discussions and advice.

Many thanks goes to Prof. Michal Schweiger and Michelle Hussong from the Center for Molecular Medicine Cologne for their great collaboration.

In addition, I want to thank Prof. Stefan Knapp and Marek Wanior from the Insitute of Pharmaceutical Chemistry for providing me JQ1 as well as sharing their knowledge about BET inhibitors with me.

Thanks goes also to all the present and past members of the AG Fulda, who were truly reliable colleagues or even became friends throughout the years. Thanks for sharing your knowledge, always being willing to help, making coffee, sharing lunch, chocolate, frustration and happiness. Thank you Michael Meister and Julius Enßle for the nice companionship during the years in our ‘girls lab’ and thank you ‘BCL-2 family girls’ for a fantastic time.

I am very grateful for the technical support with the FACS and CAM assay provided by Daniela Bücher. Many thanks goes to Christina Hugenberg for providing assistance with all the bureaucratic issues and always being helpful and supporting.

Finally, I would like to express my gratitude to my mother, extended family and near friends. Thanks for your patience with me, motivation, enthusiasm and for your steadily, committed support during the past years. Thank you for everything …we finally made it!

12 Eidesstattliche Erklärung

Ich erkläre hiermit an Eides Statt, dass ich die vorgelegte Dissertation mit dem Titel “Combined inhibition of BET proteins and PI3Kα reallocates BRD4 to transcriptional regulatory elements of BH3-only proteins and triggers mitochondrial apoptosis**“** selbstständig angefertigt und mich anderer Hilfsmittel als der in ihr angegebenen nicht bedient habe, insbesondere, dass alle Entlehnungen aus anderen Schriften mit Angabe der betreffenden Schrift gekennzeichnet sind.

Ich versichere, nicht die Hilfe einer kommerziellen Promotionsvermittlung in Anspruch genommen, sowie die Grundsätze der guten wissenschaftlichen Praxis beachtet zu haben.

Frankfurt, den _____ *Cathinka Boedicker*